Biodegradation rates of petroleum in contaminated aquifers: a comparison of radiocarbon correction methods for determining source zone natural attenuation.

Anne Wozney

A thesis submitted to the Faculty of Graduate and Postdoctoral Studies
in partial fulfillment of the requirements for the degree of

MASTER OF SCIENCE

in Earth and Environmental Science

Ottawa–Carleton Geoscience Center
University of Ottawa
Ottawa, Canada

March 2017

Author:
Anne Wozney
Department of Earth Sciences
University of Ottawa
Advanced Research Complex
25 Templeton Street
Ottawa Ontario
K1N 5N5

Under the direction of:

1. Dr. Ian Clark
   idclark@uottawa.ca
   Department of Earth and Environmental Sciences
   University of Ottawa

2. Dr. K. Ulrich Mayer
   umayer@eos.ubc.ca
   Department of Earth, Ocean and Atmospheric Sciences
   University of British Columbia

Abstract

Recently, a novel approach using surficial CO_2 efflux surveys has been used to delineate hydrocarbon source zones in contaminated aquifers and provide estimates of hydrocarbon biodegradation rates. This approach requires accurately distinguishing between petroleum–derived CO_2 respiration and background natural soil respiration. Radiocarbon can be used to distinguish ^{14}C–depleted CO_2 of hydrocarbon sources from ^{14}C–enriched CO_2 of natural soil respiration to quantify the contribution of each source to total CO_2 efflux. In this study radiocarbon was sampled from soil gas monitoring wells, soil gas probes, static chambers and dynamic closed chambers during CO_2 efflux studies. Isotopic corrections for quantifying contribution of petroleum–derived CO_2 efflux to total soil respiration using these methods are compared at a historical pipeline rupture site in Bemidji, MN and a de–commissioned oil refinery. Results confirmed that survey CO_2 efflux measurements can be used to delineate subsurface contaminant source zones and the study showed that radiocarbon obtained from static chambers and soil probe methods give large CO_2 sample yields that provide representative contaminant CO_2 efflux measurements.

Abstract

Récemment, une nouvelle approche utilisant l'évaluation d'efflux de CO_2 dans le sol a été utilisée pour délimiter les sources d'hydrocarbures dans des aquifères contaminés et pour estimer les taux de biodégradation de ces hydrocarbures. Cette approche nécessite une distinction précise entre la respiration de CO_2 dérivée du pétrole et de la respiration naturelle du sol. Pour ce faire, l'utilisation du radiocarbone est nécessaire afin de distinguer le CO_2 appauvri en ^{14}C des sources d'hydrocarbures de la respiration naturelle qui est enrichie en ^{14}C. Cette distinction permet alors de quantifier la contribution de chaque source à l'efflux total de CO_2. Dans ce cas-ci, le radiocarbone a été échantillonné pendant la surveillance de l'efflux de CO_2 à partir de puits de contrôle, de sondes de vapeur de sol, de chambres statiques et de chambres fermées dynamiques. Les corrections isotopiques pour quantifier la contribution des hydrocarbures et de la respiration naturelle du sol à l'efflux total de CO_2 ont été calculées en comparant les sites d'un déversement pétrolier à Bemidji, MN et d'une raffinerie de pétrole désaffectée. Finalement, les résultats ont confirmé que les mesures d'évaluation d'efflux de CO_2 peuvent être utilisées pour délimiter des panaches de contamination souterraine en plus d'affirmer que les méthodes de la chambre statique et de la sonde de vapeur du sol offre les résultats les plus représentatifs du flux de CO_2 réel à la surface du sol.

Acknowledgements

This project could not have been completed without the help and support of countless individuals and organizations. Firstly, I want to thank the outstanding support from my co–supervisors; Dr. Ian Clark and Dr. Ulrich Mayer. Ian fostered a fantastic environment for developing my growth as a scientist and Uli provided strong direction and advice for navigating the challenges of this project. I am thankful to have had such amazing scientific role models to guide me throughout this project, and provide incredible support.

This work would not be possible without the financial and technical support of the U.S.G.S and the amazing group of scientists investigating Bemidji, MN. This includes Jarod Trost, Barbara Bekins, Ean Warren and Geoff Delin and the rest of the August 2015 field season team! I want to especially thank all the work of Jarod and Barbara in organizing the 2015 field season and ensuring we had access to the field equipment and resources. Without them, this project would not have been possible.

I would also like to thank Natasha Sihota and her team at Chevron for not only their financial support, but also their technical knowledge and counselling. Natasha started this work during her PhD and I was grateful for her wisdom throughout this project. I would like to give a tremendous thank you to the team at Trihydro including Ben MacAlexander and Alysha Hakala for their participation and work in our field program.

I am grateful to the team at Golder Associates led by Cameron McNaughton, for their field support and assistance during this project. Their logistical support and

enthusiasm towards this project was vital to executing and developing this field program.

I have to thank the countless hours of help and technical support from the lab technicians at the University of Ottawa. Thank–you for the amazing patience and help of the A.E Lalonde radiocarbon girls; Carley Crann and Sarah Murseli. I am so grateful for your enthusiasm and technical help! I would also like to thank my lab assistant Alex Hardy– Mercure for his assistance and contribution to this project. I also need to thank Gilles St Jean for being the handiest man I've ever met, able to provide a solution to any sort of problem that arises.

I am so grateful to have been part of the MAGNET program during this experience. Thank you to Diane Hanano and Dominique Weis for allowing me to be part of such an amazing and inspiring group of geochemists. I feel so blessed to have had the opportunities I have had through the MAGNET program.

A special thank you to Keelin Scully for her help in the field and Olenka Forde for her ever encouraging support and edits. Thanks to my Father for his diligent edits providing unconditional support and advice and my Mom for all her positivity. Finally I want to thank the countless Earth Science Grad students, both at UBC and UOttawa for being my home away from home.

TABLE OF CONTENTS

List of Tables

CHAPTER 5

APPENDIX

List of Figures

List of Acronyms

BTEX	Benzene, toluene, ethyl benzene, and xylene
BGS	Below ground surface
BGC	Background correction method
BD	Below detection
CSR	Contaminant soil respiration
DCC	Directly sampled from dynamic closed chamber
$F^{14}C$	Fraction of radiocarbon
F_{CSR}	Fraction contaminant soil respiration
F_{NSR}	Fraction natural soil respiration
IRGA	Infrared Gas Analyzer (for CO_2 concentration)
J_{TSR}	Total soil respiration CO_2 efflux
J_{CSR}	Contaminant soil respiration CO_2 efflux
LNAPL	Light non-aqueous phase liquid
NSR	[Background] natural soil respiration
Napth	Naphthalene
PHC	Petroleum hydrocarbon
RCC	Radiocarbon correction
SC	Static chamber
SP	Soil probe
SZNA	Source zone natural attenuation
TSR	Total soil respiration
MW	Monitoring well

Chapter 1

1. Introduction

1.1. Literature Review

The release of petroleum hydrocarbon (PHC) contaminants into the environment through pipeline ruptures, leakage from storage units or production spills is a major source of environmental contamination in industrialized nations. In Canada, PHC contaminated sites make up ~52% of federally owned contaminated sites, many of which resulted from contamination events that occurred prior to implementation of present Standards for industrial regulation (CCME, 2008). Regulations require that groundwater be returned to drinking water Standards. Remediation of contaminated sites poses both a health concern for human exposure to contaminants, as well as an immense financial implication. In 2007 the Canadian Council of Ministers for the Environment (CCME) estimated that remediation of federally owned contaminated sites would cost approximately $40.6 billion dollars to clean up over a 30 year period (CCME, 2008).

Traditionally remediation has been attempted through excavation and conventional 'pump and treat' methods, however optimizing natural processes have been utilized in more recent contaminated site reclamation programs (NRC, 1994). Natural attenuation is a remediation approach defined by the Environmental Protection Agency as 'physical, chemical, or biological processes that reduce contaminant mass, toxicity, mobility, volume, or concentration in soil or groundwater' (EPA, 1999). Ongoing monitoring of contaminated sites has indicated that under certain conditions natural

attenuation may be a viable remediation strategy (Mulligan and Yong, 2004). Natural attenuation includes *in situ* processes such as sorption, chemical transformation or biodegradation of contaminants, which limit exposure of humans to contaminants during clean-up and potentially decrease remediation costs (NRC, 1994, Bekins et al, 2001, Johnson et al. 2006, Sihota and Mayer, 2012).

Natural attenuation via biodegradation is facilitated by microbial communities through metabolic processes (EPA, 1999). Biodegradation refers to microbial degradation of contaminants into benign end–member products (Aelion et al. 2010). However, in order to implement natural attenuation as a remediation strategy evidence that source zone natural attenuation is occurring and accurate estimates of source zone natural attenuation rates are required (Johnson et al, 2006).

At PHC contaminated sites, dissolution, volatilization and biodegradation act to decrease the concentration of contaminants (Baedecker et al. 1993, Johnston et al, 2006). Dissolution and volatilization of source zones can be observed by monitoring dissolved and vapour phase hydrocarbon concentrations of the groundwater and soil gas respectively (Johnson et al. 2006, Chaplin 2002).

Microbially mediated biodegradation of hydrocarbons is influenced by the availability of terminal electron acceptors such as O_2, NO_3^-, Mn–oxides, Fe– oxides and SO_4^{2-} (Baedecker et al. 1993). Evidence for verifying the biodegradation of PHCs include observing decreasing concentrations of electron acceptors (O_2, NO_3^- SO_4^{2-}) (Lundegard and Johnson, 2006), increased production of aerobic and anaerobic degradation products (Amos et al 2011, Chaplin 2002), increased Mn^{2+} and Fe^{2+} concentrations down gradient (Baedecker et al. 1993, Tuccillo et al, 1999) and

monitoring microbial populations (Bekins et al. 1999).

During biodegradation of hydrocarbons, longer–chain petroleum hydrocarbon constituents are broken down into carbon dioxide (CO_2) and methane (CH_4) as a result of anaerobic and aerobic microbial processes (Aelion et al, 2010). In shallow aquifers aerobic biodegradation is an important mechanism to degrade light non aqueous NAPL (Aelion et al. 2010, Sihota and Mayer, 2012). As aerobic degradation depletes O_2 concentrations, the center of the hydrocarbon plume often shifts to anaerobic conditions (Baedecker et al. 1993). Under anaerobic conditions methanogenesis often becomes the dominant biodegradation pathway, generating CH_4 (Baedecker et al. 1993). CH_4 production as a result of methanogenesis cause increased concentrations of CH_4 near the source (Amos,et al, 2005). This CH_4 is transported towards the ground surface following a concentration gradient, where it may be oxidized by ingressing O_2 to CO_2 within the shallow vadose zone (Amos et al. 2011). Therefore, increased CO_2 may be measured at the surface overlying a hydrocarbon contaminant plume undergoing aerobic and anaerobic biodegradation (Sihota et al. 2011)

Recently, a novel approach has been developed by Sihota et al. (2011) to monitor biodegradation by measuring the increased CO_2 efflux overlying hydrocarbon contaminant plumes (Sihota et al. 2011). This technique uses a LI–8100A survey dynamic closed chamber to measure increased CO_2 efflux at hydrocarbon biodegradation sites (LICOR, Biosciences, Lincoln, NE). Using these surface measurements, carbon dioxide efflux has been correlated to high subsurface microbial concentrations and increased hydrocarbon loss (Warren et al. 2014). To adequately quantify natural attenuation processes at contaminated sites using this method, CO_2

derived from petroleum biodegradation must be distinctly identified compared to CO_2 derived from natural soil respiration (Sihota et al. 2011).

Isotopic analysis of product CO_2 may be used to verify the source of measured CO_2 and improve the ability to confirm *in situ* biodegradation (Suchomel et al.1990; Aggarwal and Hinchee, 1991; Revesz et al. 1995; Landmeyer et al. 1996; Sihota and Mayer, 2012). Previously, stable carbon isotope ($\delta^{13}C$) studies have been used to distinguish the natural processes from those associated with petroleum degradation (Revesz et al. 1995, Landmeyer et al. 1996, Aggarwal and Hinchee, 1991). stable isotope fractionation can be described by (Clark, 2015):

$$(\delta^{13}C)_{sample} = \frac{\frac{^{13}C}{^{12}C}_{sample} - \frac{^{13}C}{^{12}C}_{standard}}{\frac{^{13}C}{^{12}C}_{standard}} \cdot 1000 \qquad \text{[EQ 1.1]}$$

where $\delta^{13}C$ is the ratio of ^{13}C to ^{12}C isotope of the CO_2 sample compared to the standard Vienna powdered calcite reference material (Vienna Pee Dee Belemnite), which resembles the ratio of ^{13}C to ^{12}C of the original Pee Dee Belemnite in South Carolina (Clark, 2015). The stable carbon signature of petroleum products is less than $\delta^{13}C$ −33 ‰, whereas the signature for modern day plants is $\delta^{13}C$ –24‰ to –33‰ due to more enrichment in ^{13}C isotope (Clark, 2015).

However, anaerobic degradation of oil spills can cause ambiguous stable carbon isotopes results. Under anaerobic conditions CO_2 products can be up to 20‰ more enriched in ^{13}C than the substrate, and the coexisting CH_4 pair will be 20‰ more depleted (Conrad et al. 1997). Significant isotopic shift of the $\delta^{13}C$ signature of the CO_2

product in anaerobic biodegradation can cause overlap with stable isotopic signatures of decaying biomass (Sihota and Mayer, 2012, Revesz et al, 1995, Conrad et al, 1997). Thus, stable carbon isotopes alone may have ambiguous results and thus be insufficient for verifying hydrocarbon degradation (Revesz et al. 1995). The advancement of accelerator mass spectrometry (AMS) technology has enabled trace measurements of the radioactive isotope of carbon, ^{14}C to be a definitive tool for tracing PHC degradation (Conrad et al 1997, Sihota and Mayer, 2012). In recent studies, the use of this radio isotope has proven superior for verifying hydrocarbon biodegradation and natural attenuation (Conrad et al 1997, Sihota and Mayer, 2012, Coffin et al. 2008).

Using Radiocarbon as a petroleum hydrocarbon tracer

Radiocarbon isotopes may be used as a tracer for hydrocarbon biodegradation (Conrad et al. 1997, Sihota and Mayer, 2012). Radiocarbon (^{14}C) is the radioactive isotope of carbon. Its utility as a hydrocarbon contaminant tracer relies on it's half–life of 5730 years (Godwin, 1962), which causes it to decay to levels below detection after ~60,000 years (Crann et al, 2016). Therefore carbon derived from petroleum sources are essentially ^{14}C–free, which is distinct from modern sources with detectable ^{14}C isotope.

Radiocarbon is present in the environment in trace amounts (Table1.1). For every mole of radiocarbon in the environment there are $1.76x10^{12}$ moles of stable ^{12}C, which requires ^{14}C to be measured by low background instruments such as by accelerator mass spectrometry (AMS) (Clark and Fritz, 1997, Crann et al, 2016).

Radiocarbon measurements are reported in the literature as fraction of modern carbon ($F^{14}C$) as defined by the following formula (Stenström et al. 2011)):

$$F^{14}C = \frac{\left(\frac{^{14}C}{^{13}C}\right)_{S[-25]}}{0.9558\left(\frac{^{14}C}{^{13}C}\right)_{OXII[-19]}} \qquad \text{[EQ 1.2]}$$

where modern carbon is identified as 95% of the ^{14}C concentration of the standard Natural Bureau of Standards (NBS) Oxalic Acid II (Olsson, 1970, Crann et al, 2016).

Radiocarbon is produced naturally in the upper atmosphere through the conversion of the stable ^{14}N isotope to ^{14}C by n–p reactions from secondary neutrons created by the interaction of high energy cosmic rays on atmospheric gases(Anderson and Libby, 1947). Radiocarbon enters the biosphere as $^{14}CO_2$ through photosynthesis, and thus living organisms' ^{14}C signature reflects the concentrations in the modern atmosphere (Anderson and Libby, 1947).

Unlike the initial assumptions by Anderson and Libby (1947) radiocarbon has not remained constant in the atmosphere over time. Fluctuations in the ^{14}C concentrations over time have been well documented by cataloguing programs using tree rings, speleothems and varves (Reimer et al. 2013, Stuiver et al. 1998). Today, global atmosphere has an average of $F^{14}C$ 1.07 (Aelion et al. 2010). In North America findings from the Maple leaf project indicate these atmospheric averages are closer to 1.028 and 1.023 in 2015 and 2016 respectively (Crann, 2016 personal communication). During the onset of the industrial revolution, the rising importance of fossil fuels for energy and infrastructure led to a slight decrease in atmospheric levels of ^{14}C (Stuiver et al.

1998). This was a result of dilution of modern ^{14}C with increased ^{14}C- free CO_2 from fossil fuel emissions (Seuss and Urey, 1956). However, in the 1960s the 'bomb spike' occurred which refers to an increase in ^{14}C concentrations in the atmosphere as a result of above ground nuclear testing (Stuiver et al. 1998). Nuclear explosions increase the concentration of ^{14}C in the atmosphere by initiating excited neutrons to collide with ^{14}N in the same reactions which occur naturally in the upper atmosphere (Stuiver et al. 1998, Aelion et al. 2010). Increase in radiocarbon input peaked in ~1965, and since the late 1960s concentrations in the atmosphere have been declining towards background levels due to uptake into long term reservoirs and isotopic decay (Stuiver et al, 1998, Reimer et al, 2013). Global reservoirs have distinctly different $F^{14}C$ ratios as described in Table1.2. In order to use radiocarbon effectively as a tool for tracing contamination it is important to understand the natural ^{14}C content in these different sources. $^{14}CO_2$ in groundwater and vadose zone gas can be affected by inputs from multiple reservoirs (Figure 1.2) including; natural background soil respiration (NSR) from plant matter and carbonate dissolution, and contaminant soil respiration (CSR) from petroleum biodegradation.

Microbial biodegradation of petroleum hydrocarbons to CO_2 is derived from organics with no detectable radiocarbon ($F^{14}C$ 0.00), whereas plant and soil respired CO_2 is attributed solely to atmospheric exchange of $^{14}CO_2$ ($F^{14}C$ 1.02) (Aelion et al. 2010; Dörr and Münnich, 1986).). Therefore plant and soil CO_2 produced from biodegradation of biomass is clearly discernable from CO_2 derived from hydrocarbons (below detection) (Aelion et al. 2010, Clark and Fritz, 1997, Conrad et al. 1997, Cowie et al. 2010). These distinct $F^{14}C$ signatures can be used to trace petroleum derived CO_2

in surface CO_2 efflux surveys for monitoring biodegradation of PHCs (Sihota and Mayer, 2012).

1.2. RESEARCH OBJECTIVE

Sihota and Mayer (2012) used the radioisotope of carbon from gas samples collected from soil gas monitoring wells overlying a hydrocarbon contaminant plume to distinguish petroleum derived CO_2 from natural soil gas CO_2 in the subsurface. They estimated contaminant soil respiration CO_2 efflux (J_{CSR}) using the fraction of ancient carbon quantified from the uppermost subsurface radiocarbon samples collected from soil gas monitoring wells (MW) (Sihota and Mayer 2012). However, it is unknown to what degree using subsurface samples to correct surface CO_2 flux chambers induced a bias regarding the contribution of J_{CSR} measured at the surface. If this assessment approach is to be practiced at contaminated sites in the future, an investigation into the sampling procedure must be conducted to determine the most effective way to correct for surface CO_2 measurements to reduce both temporal and spatial bias when quantifying biodegradation rates. Furthermore, a study has not been previously conducted to evaluate whether or not ancient $^{14}CO_2$ from PHC sources has an effect on the radiocarbon signature of modern plant biomass overlying historically contaminated sources areas. Therefore an investigation into the radiocarbon signature of plant biomass is required to validate the assumption of a modern $^{14}CO_2$ signature of background natural soil respiration CO_2 efflux (J_{NSR}) overlying historical PHC contamination. The purpose of this study is to compare four methods of collecting radiocarbon, and to determine the most effective way to correct the total soil

respiration CO_2 efflux (J_{TSR}) measurements. These methods include sampling: i) directly from the dynamic closed CO_2 chamber (DCC), ii) from a surface static chamber (SC) iii) using a soil gas probe (SP) iv) using an existing soil gas monitoring well (MW) network. This study aims to develop a standard method to assess contaminated sites for biodegradation and quantify natural attenuation of the contaminants.

Therefore the objectives of this study are:

- To examine four different field sampling methods for collecting and analyzing radiocarbon samples
- To identify the method(s) most suitable to determine biodegradation rates at contaminated sites
- To evaluate whether the assumption of plant respiration having a modern radiocarbon signature is justified
- To optimize the method by Sihota and Mayer (2012) of using CO_2 efflux surveys and radiocarbon isotopes to determine biodegradation rates at petroleum contamination sites

1.3. RESEARCH APPROACH

To investigate the best method for using ^{14}C isotopes to correct CO_2 efflux measurements in order to determine surficial CO_2 efflux associated with petroleum hydrocarbon degradation, two detailed CO_2 efflux surveys were conducted at a:

1. Point source pipeline rupture site at U.S.G.S National Crude Oil Spill Fate and Natural Attenuation Research Site in Bemidji, MN in August 2015

2. Historical contamination at an industrial oil refinery site in North Eastern USA in September 2015

CO_2 efflux measurements were conducted using an LI– 8100A dynamic closed CO_2 flux chamber survey system with an infrared gas analyzer control unit (LICOR Inc, Lincoln NE). To identify the contribution of CO_2 derived from petroleum hydrocarbon degradation radiocarbon samples were collected using four different methods:

1. ***Dynamic closed chamber (DCC) sampling–*** Gas samples for radiocarbon analysis were collected directly from the LI–8100A dynamic closed chamber system using a T–fitting in the chamber hosing. Two samples were taken at each location; the first was taken prior to the flux measurement to record the ambient radiocarbon concentration and the second was taken immediately after the CO_2 efflux measurement to determine the radiocarbon attributed to the CO_2 efflux over the 90 second measurement interval.

2. Static chamber (SC) sampling – A single air sample for radiocarbon analysis was collected from a cylindrical PVC Static chambers inserted at DCC collar locations. The chambers are placed for 24 hours to allow gases to collect.

3. Soil gas probe (SP) sampling– Air samples were collected from soil gas probes inserted 30 cm b.g.s and allowed to equilibrate with the soil for 30 minutes. The soil gas probes were located within 1m of the existing soil gas monitoring wells and dynamic closed chamber collars. Air samples were brought to surface by pumping the tubing with the sampling syringe. This method increased concentrations of CO_2, reducing the

sampling volume needed for analytical processing.

4.Soil gas monitoring well (MW) sampling – Gas samples were collected from multi–level soil gas monitoring wells using a peristaltic pump (GeoPump, Geotech Environmental Equipment Inc. Denver, CO). Samples were collected from the top port of each monitoring well which is approximately 0.6 m.b.g.s . While there is a spatial difference between the CO_2 efflux measurement and ^{14}C sample, this method allows for increased concentrations of CO_2 to be obtained, reducing the sample volume required for laboratory radiocarbon analysis. In previous studies, this method was used to characterize the vadose zone gases at the U.S.G.S National Crude Oil Spill Fate and Natural Attenuation Research Site in Bemidji, MN (Sihota and Mayer, 2012, Amos et al. 2005).

Chapter 1 Tables

Table 1. 1 Relative proportions of the three isotopes of carbon in the environment.

Isotope	Protons	Neutrons	Proportions
^{12}C	6	6	99%
^{13}C	6	7	1%
^{14}C	6	8	$1.76x\ 10^{-12}$

Table 1. 2 Average stable carbon isotopes and radiocarbon values of carbon sources (Modified from: Clark and Fritz. 1997, Aelion et al. 2010)

Source	Formula	$\delta^{13}C$ (‰)	$F^{14}C$)
Atmosphere	CO_2	–8	1.07
Atmosphere	CH_4	–47	1.22
Living Biomass	CH_2O	–27	1.00
Soil Biomass	CH_2O	–27	0.95
Shallow Marine	DIC	0	1.10
Shallow Marine	DOC	–30	1.10
Deep Marine	DIC	0	0.75
Carbonate rocks	$Ca(Mg)CO_3$	0	0.0
Coal	C	–27	0.0
Oil and bitumen	$C_xH_{2x}0_x$	–33	0.0
Gas (recoverable)	CH_4	–45	0.0

Table 1. 3 Carbon dioxide stable carbon isotope and radiocarbon isotope data of contaminants collected from previous studies of biodegradation of petroleum contaminants recorded in the literature.

$\delta^{13}C$ (‰) CO_2	$F^{14}C$ CO_2	Reference
–13.9 — –36.8	0.032 — 0.459	*Sihota and Mayer 2012*
+6.45 — –17.70	–	*Revesz et al 1995*
–23.27— –24.70	0.077—0.086	*Suchomel et al 1990*
–12.4 — –28.1	0.14 — 0.32	*Conrad et al 1997*
–27.9 — –29.5	0.245— 0.62	*Kirtland et al 2000*
–22.0 — –35.9	0.159 — 0.477	*Aelion et al 1997*
+8.3 6 — –30.9	0.003 — 0.2.8	*Coffin et al 2008*
–21.1 — –30.1	–	*Aggarwal and Hinchee 1990*
–28 — +11.9	–	*Landmeyer et al 1996*

Chapter 1 Figures

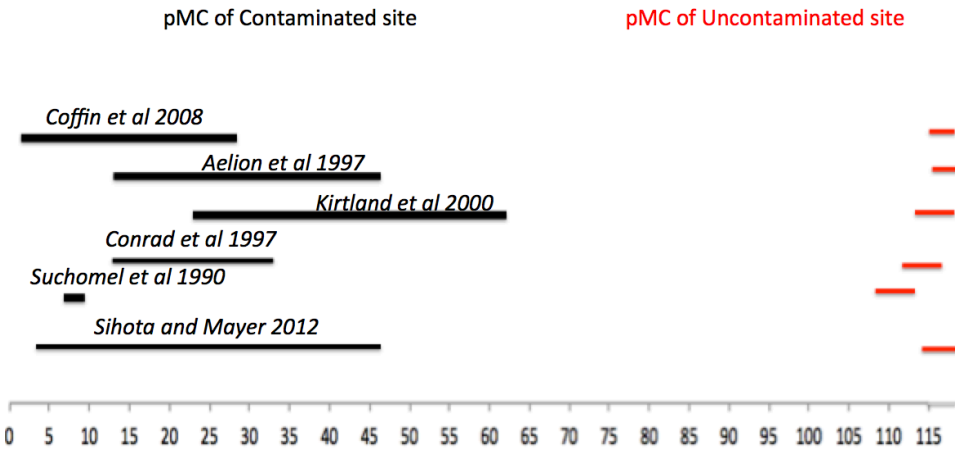

Figure 1. 1 Range of $F^{14}C$ of contaminated and corresponding uncontaminated sites from six studies of petroleum biodegradation using radiocarbon as a tracer.

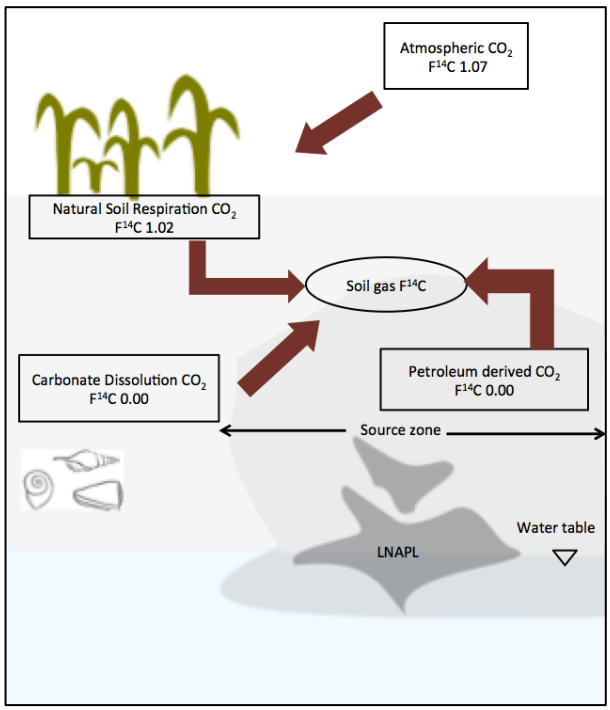

Figure 1. 2 Schematic of contribution of carbon sources to soil gas CO_2. (adapted from Sihota et al, 2011 and Conrad et al, 1997).

Chapter 2

2. METHODS FOR USING RADIOCARBON CORRECTION TO IDENTIFY THE CONTRIBUTION OF PETROLEUM HYDROCARBON DEGREDATION TO THE TOTAL CO_2 EFFLUX

2.1. INTRODUCTION

Quantifying carbon loss at hydrocarbon contaminated sites allows for the assessment of depth- integrated hydrocarbon degradation via natural attenuation processes (Sihota and Mayer 2012). A novel approach for monitoring natural attenuation has been developed which measures the gaseous products of subsurface biodegradation after they diffuse through the vadose zone and are detected at the ground surface (Sihota et al. 2011).

Non–invasive, surficial CO_2 efflux can be measured overlying hydrocarbon contaminant plumes using dynamic closed chamber LI–8100A technology (Licor Biosciences, Lincoln, Nebraska). Therefore, identifying CO_2 efflux attributed to contaminant– related soil respiration can be correlated to carbon loss via contaminant mineralization (Warren et al. 2014, Sihota and Mayer, 2012).

The use of LI–8100A CO_2 efflux system, analyzes the total soil respiration (J_{TSR}) that is emitted from the ground surface overlying a contaminant plume (Sihota et al, 2011). To identify the petroleum–derived contaminant soil respiration contribution to J_{TSR}, previous studies have used a background correction (BGC) method where the background natural soil respiration (NSR) is quantified using the mean value of an unaffected background site and the contaminant soil respiration (CSR) of the elevated CO_2 efflux sites overlying the contaminant source zone is calculated from the following

equation (Sihota et al. 2011):

$$J_{CSR} = J_{TSR} - J_{NSR} \qquad \text{[EQ 2.1]}$$

Subsequent CO_2 efflux investigations used radiocarbon correction (RCC) to identify the contribution of J_{CSR} to J_{TSR} measurements. While both the BGC method and RCC method showed reasonably good agreement with mass loss rates, the BGC method was unable to identify CSR below the mean background NSR value (Sihota et al. 2011, Sihota and Mayer, 2012). The RCC method was more sensitive to spatial variability of a site and able to quantify location specific SZNA rates as well as identify hotspots of hydrocarbon degradation (Sihota, 2014). Sihota and Mayer, (2012) established that ^{14}C isotopes can effectively trace CO_2 gas derived from petroleum sources at biodegradation sites, however a consistent sampling approach for RCC has not yet been determined. Investigation conducted by Sihota and Mayer, (2012) at a historical pipeline rupture site in Bemidji, MN obtained samples from soil gas monitoring wells, whereas samples obtained from a de-commissioned refinery site by Sihota, (2014) collected two samples directly from the dynamic closed chamber; both prior to the dynamic closed chamber measurement and immediately after. A standard method for radiocarbon correction of CO_2 efflux surveys is still required to implement CO_2 efflux surveys for evaluation of SZNA and assessment of source zone longevity at contaminated sites. Therefore, a comparison of radiocarbon sampling methods was conducted at the well–characterized U.S.G.S National Crude Oil Spill Research Site in Bemidji, MN in August 2015 and a de–commissioned oil refinery site in the North Eastern United states in September 2015.

2.2. METHOD FOR CO_2 EFFLUX SURVEYS

Surficial CO_2 efflux measurements

CO_2 efflux measurements were conducted using an LI–8100A dynamic closed CO_2 flux 20cm survey chamber with an infrared gas analyzer calibrated by the manufacturer [0–20 000ppm] (LICOR Inc, Lincoln, NE). Each flux chamber measurement was taken on a 20 cm ID by 10cm height PVC soil collar (Figure 2.1) that was inserted at least 24 hours prior to chamber measurement due minimize soil disturbance effects according to the manufacturer's recommendations (LICOR Biosciences Inc, Lincoln, NE). Chamber offset (ranging from ~5–8 cm) was averaged using 3 height measurements and inputted into the LI–8100A Soil Flux Pro software (LICOR Biosciences Inc, Lincoln, NE). Survey CO_2 efflux measurements were taken for 1.5 minutes to limit the artificial effects of the surface chamber on J_{TSR} (Sihota et al, 2011). The LICOR system calculated CO_2 efflux using the following formula:

$$J_{TSR} = \frac{10VP_0\left(1-\frac{W_0}{1000}\right)\partial C}{RA(T_0+273.15)\partial t} \qquad \text{[EQ 2.2]}$$

where J_{TSR} is the flux in μmol·m^{-2} s^{-1} , W_0 is the initial water content in the chamber (mmol ·mol $^{-1}$), T_0 is the initial chamber temperature (°C), V is the total volume of the chamber, tubing and soil collar (cm^3), $P_0$is the initial pressure (kPa), A is the soil surface area (cm^2), R is the gas constant (8.314 Pa· m^3 K^{-1} ·mol^{-1}), $\frac{\partial c}{dt}$ is the change in dry air CO_2 concentration in the chamber over the measurement time period (μmol· mol^{-1} s^{-1}). The exponential fit of the concentration over this time period was calculated using the Soil Flux pro software and CO_2 efflux results were recorded.

Bemidji CO_2 efflux survey Aug 14–19 2015

CO_2 efflux survey measurements were conducted from August 14 to August 19 2015, overlying the North Pool LNAPL source zone at Bemidji, MN (Figure 2.3). Collar locations were approximately 5–15m apart in a grid network (See appendix for grid GPS locations). Measurements at 20 select locations along the North Pool transect were taken three times a day over three days. The measurements were taken from ~9:00–12:00, 12:00–15:00, and 15:00–18:00, respectively. The average of the ~9 CO_2 efflux measurements at each location were calculated and are referred to as the mean J_{TSR} for each transect location. The extended CO_2 efflux survey included 3 measurements taken from the 40 grid locations in the morning, afternoon and evening time intervals. These 3 measurements were averaged to calculate the mean J_{TSR} at each location on the grid.

De-commissioned refinery site surficial CO_2 efflux survey September 14–30 2015

The CO_2 efflux survey was conducted from September 14 to 30 2015 at 40 soil collar locations located on a grid as shown in Figure 2.4. CO_2 efflux measurements were conducted by Alysha Hakala at Trihydro Engineering and environmental consultants, using an LI– 8100A dynamic closed CO_2 flux survey chamber as described above. The replicates at each location were averaged to determine a total soil respiration CO_2 efflux for each location (mean J_{TSR}).

2.3. RADIOCARBON SAMPLING METHODS

To assess the contribution of J_{CSR} to J_{TSR}, ^{14}C isotopes were analyzed from gas samples collected using four different field sampling methods:

I. Directly from the LI–8100A dynamic closed CO_2 chamber (DCC)

II. Static chamber (SC)

III. Soil gas probe (SP)

IV. Existing soil gas monitoring wells (MW)

At the USA de–commissioned refinery site, ^{14}C samples were obtained using only methods I,II and III, because an existing monitoring network was not in place.
A detailed description of each field sampling method is described below:

I. Dynamic closed CO_2 chamber (DCC) sampling

Two gas samples for radiocarbon analysis were taken at each location. The initial sample was taken prior to CO_2 survey measurement to assess ambient radiocarbon content over the collar area and the second was taken after the CO_2 survey measurement to assess the radiocarbon content over the measurement time interval and is attributed to the radiocarbon from the CO_2 efflux. The radiocarbon samples were taken from a T–fitting with septa (LI–8100–664 trace gas adapter) that was inserted into the LI–8100A 'air in' chamber hosing (LICOR, Inc, Lincoln NE). The initial 400mL gas sample was collected from the LI–8100–664 trace gas adapter using a 100mL luer lock gas tight syringe (Hamilton 1000 series) immediately prior to survey flux measurement (before the chamber closed). The sample was inserted into a pre–

evacuated 250mL Wheaton bottle. The LI–8100A CO_2 efflux measurement was initiated, and after 1.5minutes a second 400mL sample was extracted using a 100mL Luer lock gas tight syringe from the LI–8100–664 trace gas adapter and inserted into a pre–evacuated 250mL Wheaton bottle. The total length of chamber closure was 5 minutes at Bemdji, MN and this time interval was lengthened to seven minutes at the USA refinery site. At the USA refinery site, the sample volumes were 2x 250mL samples for the ambient air gas sample and 1x 250mL sample for the second sample due industrial site safety restrictions.

II. Static chamber (SC) sampling

Cylindrical PVC Static chambers 20 cm ID and 20 cm high were constructed and the top was sealed. Static chambers were inserted at DCC collar locations 24 hours prior to sampling to allow settling of disturbed soil. A mallet was used to drive chambers 5–6cm into the ground. A 100mL Luer lock gas tight syringe was used to draw a sample out of a septa in the center of the lid (Figure 2.1II) and insert into pre–evacuated Wheaton bottles. 300mL gas samples were inserted into 200mL Wheaton bottles and 250mL samples in 250mL Wheaton bottles at Bemidji and the USA refinery site, respectively.

III. Soil gas probe (SP) sampling

A soil gas probe was driven into the ground 30 cm b.g.s and allowed to equilibrate with the soil for 30 minutes. The SP was located within 1m of the existing monitoring well. A 100 mL gas tight syringe attached with tygon tubing was used to

purge 3 line volumes and then extract gas for insertion into a pre–evacuated Wheaton bottles. 300mL volume gas samples were inserted into 200mL Wheaton bottles and 250mL samples in 250mL Wheaton bottles at Bemidji and the USA refinery site, respectively.

IV. Soil gas monitoring well (MW) sampling

Gas samples were collected from multi–level monitoring wells constructed from 3.2mm tubing with 10cm long 6.4mm outer diameter stainless steel screens (Hult and Grabbe, 1988). Sampling was conducted from the top port of each monitoring well, which averaged 0.6m b.g.s. A peristaltic pump (GeoPump, Geotech Environmental Equipment Inc. Denver, CO) was used to bring the samples to the surface at 1.5L/min flow rate (Sihota and Mayer, 2012). Three line volumes were purged from each port before sampling. 300mL gas samples were collected by filling a 100mL Luer lock, gas tight syringe and inserting the sample into 200mL pre–evacuated Wheaton bottles (Sihota and Mayer, 2012).

2.4. Radiocarbon Analysis

2.4.1 CO_2 extraction and purification from gas mixtures

CO_2 was extracted from gas samples using the multi–purpose vacuum extraction line (10^{-5} kPa) at the G.G HATCH lab (University of Ottawa). Wheaton sample bottles were flushed with a helium carrier gas at 250mL/ minute for ten minutes and the CO_2 was

cryogenically trapped using liquid nitrogen (−196° C) on sequential U–traps. The first U-trap contained silver wire to increase surface area within the trap to avoid sample loss. After ten minutes, excess He was pumped away, and the sample was transferred to a second liquid nitrogen trap in preparation for water removal. In order to cryogenically trap water and liberate the CO_2, the liquid nitrogen trap was swapped for an ethanol liquid nitrogen slurry at −80° C. The CO_2 was then transferred to a calibrated volume and sample yield was measured on the pressure transducer and recorded before transferring the sample into a 6mm O.D. pyrex break seal and torch sealed.

For 8 select locations with low samples yields at the USA refinery site, an ancient carbon CO_2 standard (Luxfer $F^{14}C$ 0.0005 ± 0.0001) was added to increase the sample volume for measurement on the AMS before sealing into the breakseal. Luxfer addition volumes and mass balance calculations can be found in the appendix. All CO_2 break seals contained 6–8 grains silvered cobaltus and were baked overnight at 200° C to scrub out any remaining sulphur impurities (Palstra and Meijer, 2014).

Sample yields

The CO_2 yield was measured on the pressure transducer on the multi–purpose extraction vacuum line for all methods. The corresponding carbon content for SC samples ranged from 0.19 to 0.94 mg C. The mean sample yield was 0.43 mg which is within the range of recommended sample size for precise analytical measurement on the AMS (~0.5 mg C). Sufficient sample sizes enabled consistently low error which ranged from $F^{14}C$ ± 0.0029 to 0.0093.

The average sample yield for radiocarbon collected using soil probes was 0.24 mg C. There was a larger range in sample size from as small as 0.03 to 0.47mg. However the error was similar to SC measurements and ranged from $F^{14}C$ ± 0.0021 to 0.0961.

The mean sample yield using the MW method was 0.85 mg C. This exceeds the recommended sample size for increased precision on the AMS. Thus there was lower error on ^{14}C measurements ranging from $F^{14}C$ ±0.0008 to 0.0095.

Sample yields for samples collected directly from the LI–8100A DCC chamber ranged from 0.05 to 0.08 mg C per sample with a mean sample size of 0.06 mg C. This is only 10% of the recommended 0.5mgC sample volume for acceptable analytical precision on the AMS. There was a greater range of error on the AMS from as low as $F^{14}C$ ±0.0009 to 0.0692.

2.4.2 CO_2 extraction and purification from plant and soil samples

Ten locations from each site were selected for radiocarbon analysis of vegetation and soil to characterize the modern soil respiration radiocarbon signature.

Soil samples were collected from inside the 20cm soil collar area and transported back to University of Ottawa for ^{14}C analysis. All samples were sieved to less than 200μm grain size prior to acid treatment to remove carbonates. Samples were acid washed with 1N HCl and then triple rinsed with MilliQ deionized water, centrifuged and decanted (Brock et al. 2010). Acid washed samples were combusted on a Thermo 1112 flash elemental analyzer and isolated into pure CO_2, and then sealed into 6 mm O.D. pyrex break seals. Samples with less than 1% carbon measured during the

combustion stage could not be analyzed.

Plant samples were collected from inside the 20 cm collar area and air dried before being sent to the University of Ottawa for ^{14}C analysis. Vegetation samples were freeze dried over night at –50°C before undergoing direct combustion on the Thermo 1112 flash elemental analyzer and isolated into pure CO_2 and sealed into 6mm O.D. pyrex break seals.

2.4.3 Graphitization

Purified CO_2 from the gas, soil, and vegetation samples was converted into elemental carbon in the presence of 5.0mg of pre–conditioned iron catalysts through the following high temperature Bosch hydrogen– reduction:

$$CO_2 + 2H_2 \xrightarrow{Fe} C + 2H_2$$

[EQ 2.3]

First, iron powder was pre conditioned through an oxidation step at 520° C for 20 minutes to remove any contaminant carbon (Equation 2.4) and subsequent hydrogen reduction step (Equation 2.5) at 520° C for 30 minutes to return it to elemental iron (St–Jean et al. 2016).

$$2Fe + 2C + 3O_2 \rightarrow 2FeO + 2CO_2$$

[EQ 2.4]

$$FeO + H_2 \rightarrow Fe + H_2O$$

[EQ 2.5]

The graphitization system was kept under 10^{-5} kPa high vacuum (Pfeiffer Hi–Cube 80 eco). After iron conditioning and pumping for 1 hour, CO_2 was released from break

seals and reduced to elemental carbon through a 3 hours graphitization step at 650°C (St–Jean et al. 2016). Water was removed from system with a −40° C ethanol water trap.

Graphitized samples were removed from the graphitization line, homogenized and pressed into targets using a press module with a pure copper pin. All press equipment used was sterilized with a double sonication bath for ten minutes (Crann et al. 2016).

2.4.4 Analysis by Accelerator Mass Spectrometer

Pressed targets were run on the A.E Lalonde 3.0MV accelerator mass spectrometer equipped with a 200 sample ion source and 2 channel gas ionization detector (Kieser et al. 2015). Results were fractionation corrected using the online $\delta^{13}C$ value and normalized to the Oxalic Acid II standard ($F^{14}C$= 1.34) (Crann et al. 2016).

2.5. Radiocarbon Correction Methods

To estimate the contribution of contaminant soil respiration CO_2 efflux J_{CSR} to total CO_2 efflux J_{TSR} measured by the LI–8100A chamber, it is commonly assumed that radiocarbon can be used as a direct measure of the fraction contaminant soil respired CO_2 (F_{CSR}) (Sihota and Mayer 2012, Conrad et al. 1997).

Directly from LI–8100A

To estimate the contribution of J_{CSR} to J_{TSR} the results of $F^{14}C$ determined from AMS from DCC samples collected before and after the chamber measurement were used in the following equations.

$$F_{CSR}^{DCC} = \frac{\left(1 - F^{14}C_{final}\right) \cdot \left[CO_2\right]_{final} - \left(1 - F^{14}C_{initial}\right) \cdot \left[CO_2\right]_{initial}}{\left[CO_2\right]_{final} - \left[CO_2\right]_{initial}}$$

[EQ 2.6]

$$J_{CSR}^{DCC} = F_{CSR}^{DCC} \cdot J_{TSR}^{DCC}$$

[EQ 2.7]

Where F_{CSR}^{DCC} is the fraction of contaminant respired CO_2 calculated using DCC method, $F^{14}C_{initial}$ is the radiocarbon initial sample measured on the AMS collected prior to chamber closure and $F^{14}C_{final}$ is the radiocarbon sample measured on the AMS collected after the CO_2 efflux measurement (at t= 90s to t=final). The initial $F^{14}C_{initial}$ reflects proportion of ancient carbon present before the CO_2 efflux was taken. The change of $F^{14}C$ over the measurement interval is attributed to the $F^{14}C$ of the CO_2 flux.

Therefore, F_{CSR}^{DCC} is calculated using Equation(2.6) where the prior to chamber closure and after measurement radiocarbon values are multiplied by their respective CO_2 concentrations. $[CO_2]_{initial}$ is the concentration CO_2 in the chamber at t=0 and $[CO_2]_{final}$ is the representative concentration of CO_2 during sample collection. For the Bemidji site, $[CO_2]_{final}$ was the concentration of CO_2 at t=195s which is the concentration half way through the sampling time interval. Thus the Δt was 195s. At the USA refinery site, $[CO_2]_{final}$ was the concentration of CO_2 at t=255s and therefore Δt was 255s . The F_{CSR}^{DCC} is then used as a correction factor for the J_{TSR} measurement taken at the time of sampling.

Using SP, SC and MW methods, fraction of contaminant soil respiration (F_{CSR}) was related directly to fraction of ^{14}C to quantify the petroleum–derived CO_2 efflux using the simplification equation (2.10). For the SC method, the initial CO_2 concentration when the chamber was placed was hypothesized to be negligible based on increased CO_2 concentrations collected by the static chamber.

The petroleum–derived CO_2 efflux (J_{CSR}) calculated from ^{14}C samples obtained using SP, SC and MW methods are as follows:

$$F_{NSR} = \frac{F^{14}C_{sample}}{F^{14}C_{BG}} \qquad \text{[EQ 2.8]}$$

$$F_{CSR} = 1 - F_{NSR} \qquad \text{[EQ 2.9]}$$

$$J_{CSR} = F_{CSR} \cdot J_{TSR} \qquad \text{[EQ 2.10]}$$

where $F^{14}C_{sample}$ is the radiocarbon measured from the collected sample, $F^{14}C_{BG}$ is the fraction of radiocarbon measured at the background site(s), F_{NSR} is the fraction of background natural soil respiration, J_{TSR} is the average total soil CO_2 efflux measured by the LI–8100A flux chamber over ~9 measurements, and J_{CSR} is the calculated petroleum– derived contaminant soil respiration CO_2 efflux.

Stable isotope analysis

Ten locations at USGS National Crude Oil Spill research site were selected for stable carbon isotopic analysis. 20mL samples of gas were collected from the top port (~0.6m b.g.s) of monitoring wells (as described in section 2.3 IV) using a 10mL gas

tight Hamilton syringe and injected into 12mL pre–evacuated exetainers. Sample were analyzed using a 1 Thermo DeltaV+ (with dual inlet & 10 ports) Isotope ratio mass spectrometer (IRMS) at the University of Ottawa G.G Hatch stable Isotope Laboratory.

Gas compositional analysis

Gas samples for compositional analysis were collected in 12mL exetainers at the same time as radiocarbon sample collection for SC, SP, and MW. These samples were analyzed for N_2, O_2, CH_4 and CO_2 using SRI Gas chromotograph (GC) with flamie ionization detector (FID) and thermal conductivity detector (TCD) at the University of Ottawa G.G Hatch stable isotope laboratory (1000 to 10 000 ppm). For precise CO_2 compositions of lower concentration DCC samples, the concentrations were analyzed *insitu* using the LI–8100A IRGA gas analyzer control unit calibrated by the manufacturer (0– 20 000ppm CO_2) (LICOR Biosciences INC, Lincoln NE).

Chapter 2 Figures

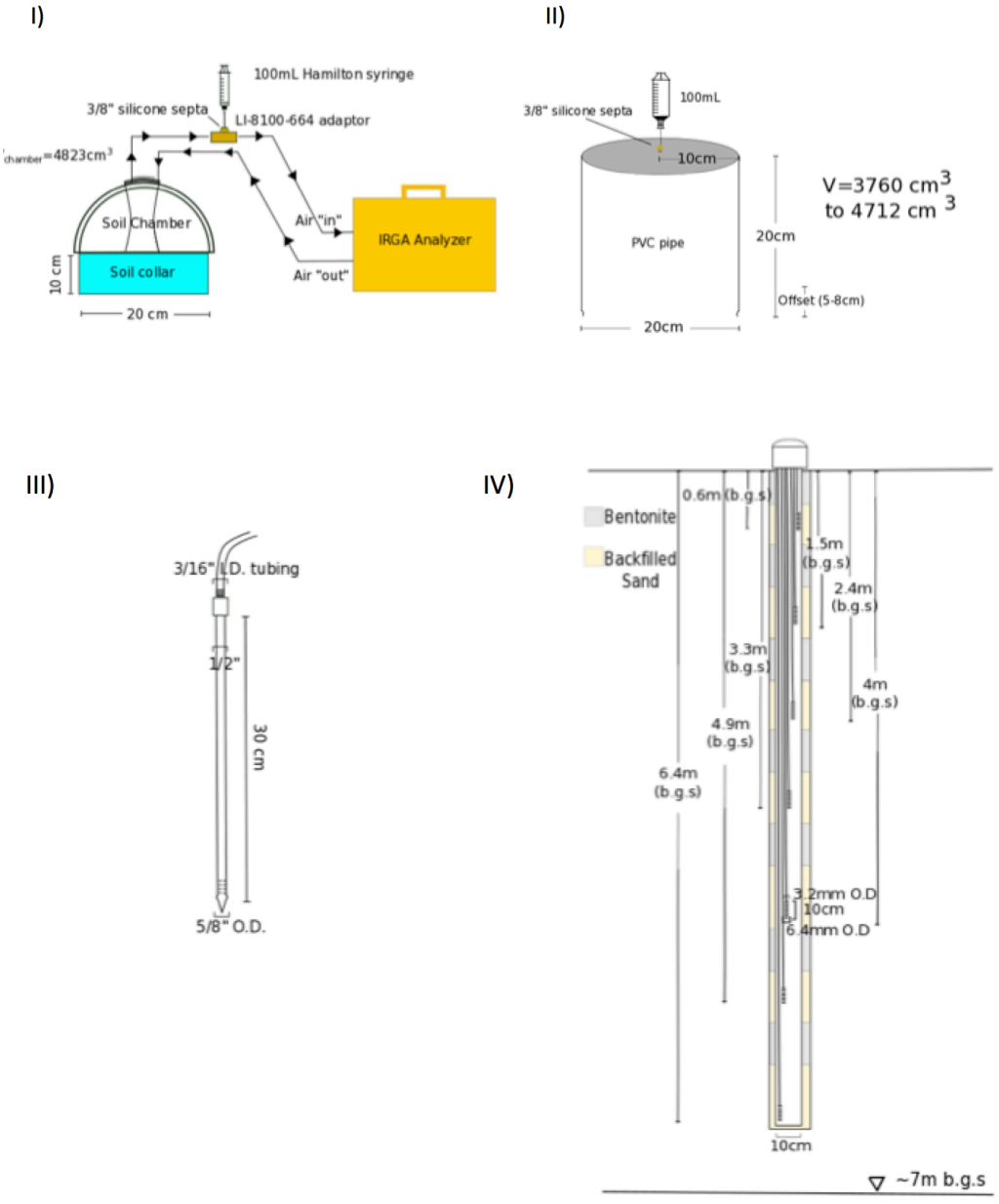

Figure 2. 1 Schematic diagram of the four field sampling methods using a 100mL Hamilton syringe; I) Sampling directly from the LI–8100A dynamic closed CO_2 chamber (DCC) from a T–septa (LI–8100–664 adapter) II) From a septa port in the top of a static Chamber (SC) III) Soil probe (SP) attached to tubing and IV) The top port of monitoring wells (MW) which bring sample to surface using a peristaltic pump

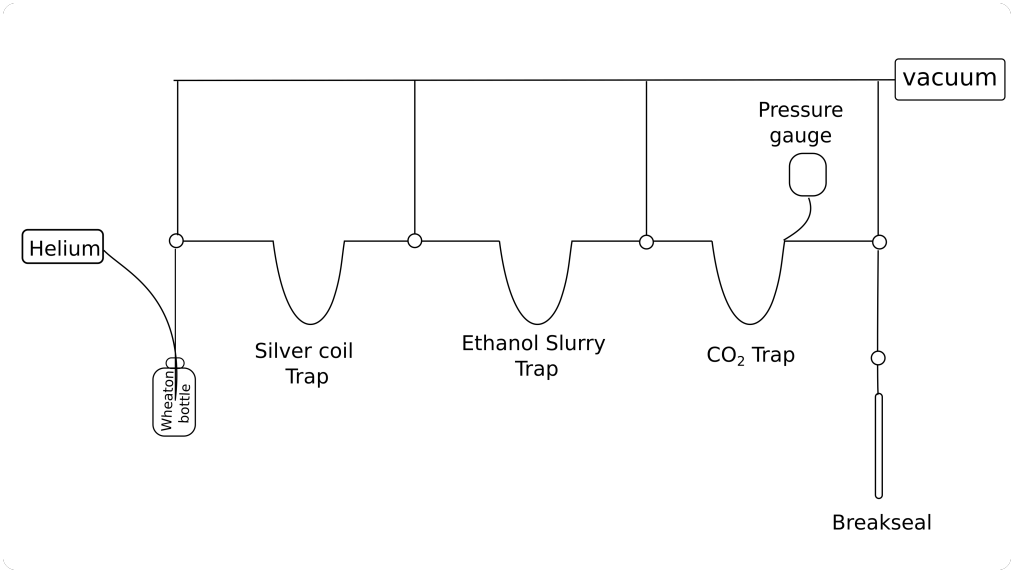

Figure 2. 2 Extraction of air sample to pure CO_2 in a breakseal using successive traps. The sample is flushed with helium carrier gas at 250mL/minute for ten minutes, then transported through a i) a silver coil using a liquid nitrogen trap ii)Second Liquid Nitrogen trap iii) Ethanol slurry trap to remove excess water and iv) a final liquid Nitrogen trap . The CO_2 sample yield is read off a pressure gauge and recorded before transferring into a breakseal using liquid nitrogen.

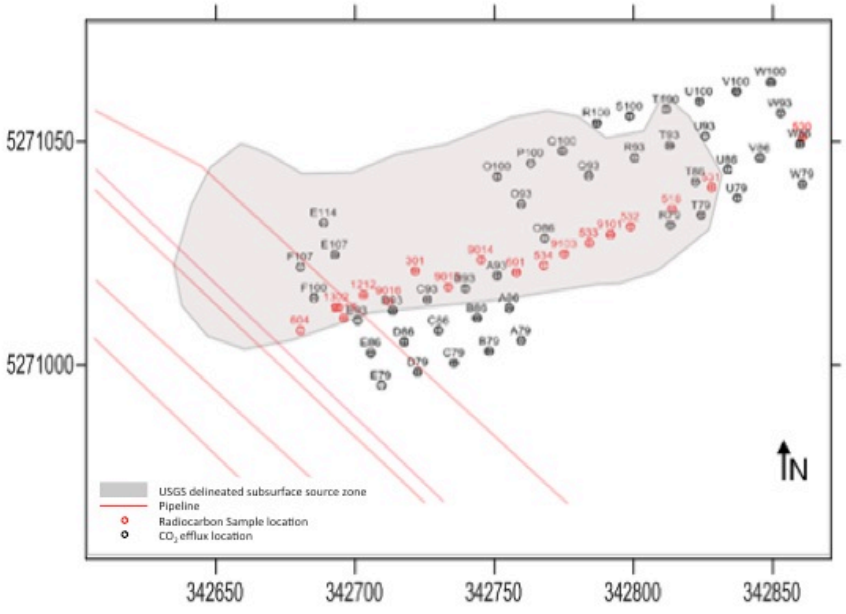

Figure 2. 3 The locations of the 60 collar locations at the National Crude Oil Spill Fate and Natural Attenuation Research Site Bemidji, MN. The 20 locations along the North Pool transect selected for radiocarbon analysis are shown in red. The remaining North Pool grid locations are shown in black.

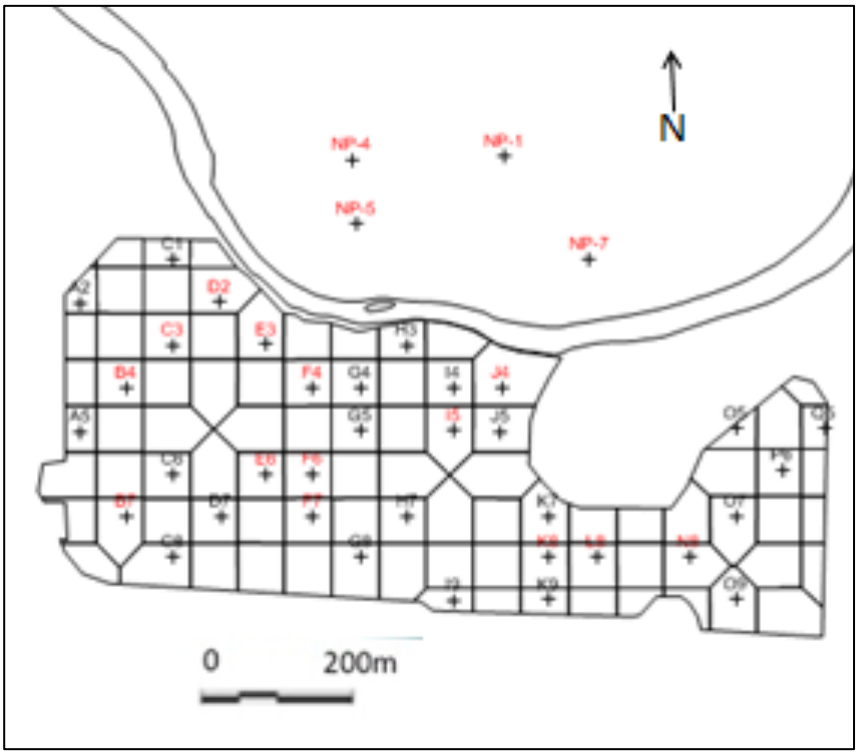

Figure 2. 4 A map of the 40 locations at the USA refinery site for CO_2 efflux measurement using the LI–8100A. The selected locations for ^{14}C sampling are shown in red.

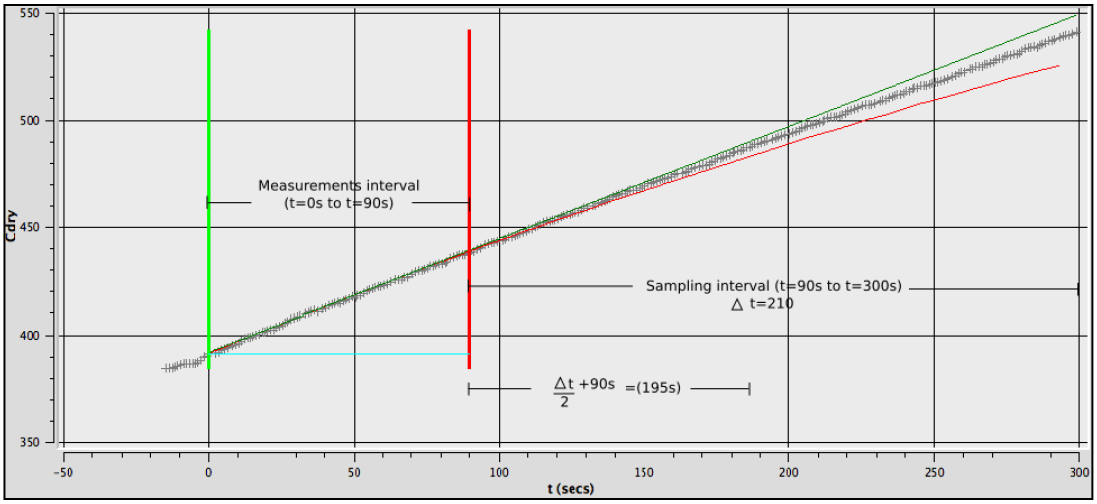

Figure 2. 5 Measured output of the $[CO_2]$ over time measured by the LI–8100A dynamic CO_2 flux chamber survey system measured at well 9017 at Bemidji, MN. The 90s measurement interval is shown from t=0s to t=90s. The sampling interval occurred from t=90s to t=300s (Δt= 210s time interval). Therefore, Equation 2.8 assumes that the $[CO_2]_b$ occurs at t=Δt/2 +90 =195s which is used to calculate $\boldsymbol{J}_{\boldsymbol{CO2\ DCC}}$. Conversely, at the de–commissioned refinery site, the sampling interval occurs from t=90s to t=420s. Thus $[CO_2]_b$ in Equation 2.8 corresponds to t=255s.

Chapter 3

3. RADIOCARBON CORRECTED CO_2 EFFLUX TO DETERMINE PETROLEUM DERIVED CO_2 EFFLUX (J_{CSR}) RATES AT BEMIDJI, MN

3.1. INTRODUCTION

To compare sampling methods for radiocarbon a field investigation using the four methods described in chapter 2 was conducted at the USGS National Crude Oil Spill Research Site in Bemidji, MN. The research site is ideal for method development due to extensive characterization of the subsurface aquifer, and previous studies investigating surface CO_2 efflux overlying the contaminant plume (Sihota et al. 2011, Sihota and Mayer 2012, Warran et al. 2014, Sihota et al. 2016).

3.2. SITE HISTORY

This study was conducted at the USGS National Crude Oil Spill Research Site near Bemidji, MN (latitude 47°34'23", longitude 95°05'33") (Figure 3.1). In 1979, a pipeline rupture released ~1.7 x 10^6 L of crude oil into the environment. Initial clean–up efforts removed ~75% of the released product, however an estimated 400 000L infiltrated into the underlying aquifer, where it accumulated in the unsaturated zone and at the water table, which lies 6–8m below ground surface (b.g.s). The groundwater flows NE towards Unamed lake, with minor backflow towards a local wetland. The residual oil is predominantly in two main pools; the North Pool which has been extensively characterized and is the focus of this study, and the smaller South Pool which accumulated to the south west of the pipeline rupture (Delin et al. 1998).

The ~20m thick aquifer consists of predominantly glacial outwash and is a mixture of sands, gravel and lacustrine silts (Franzi, 1988). On–going site investigation has indicated the occurrence of microbial biodegradation of the contaminant plume, where iron reducing and methanogenic bacteria predominate (Bekins et al. 2001). The presence of fermenters and methanogen microbial populations (Bekins et al. 1999), reducing conditions in groundwater (Cozzarelli et al. 2001), and compositional gas data (Amos et al. 2005) support stable methanogenic conditions at the Bemidji site. The sustained methanogenic conditions are due limited oxygen ingress from the atmosphere and significant rates of methane generation in the smear zone and directly above the water table (Molins et al. 2010). Methane produced from microbial degradation diffuses up through the vadose zone and reacts with oxygen 2–4 m b.g.s creating an active methanotrophic zone (Amos et al. 2005).

Previous studies of *n–alkanes* have identified different rates of biodegradation from the up–gradient and down gradient zones (Bekins et al. 2005). The excavation of contaminated material during initial clean–up has left a local depression (430m a.s.l)) which acts to accumulate recharge during storm events and increase recharge over the up–gradient wells by almost 2 times that of the down–gradient (433m a.s.l.) part of the plume (Bekins et al. 2005).

Previous research conducted at the site has investigated transport of the gaseous phase contaminant plume through the vadose zone to the subsurface (Amos et al. 2005, Sihota and Mayer, 2012, Molins et al. 2010). The investigations of Sihota et al. (2011) measured the efflux of CO_2 transported to ground surface, and found average surficial CO_2

efflux over the source area at Bemidji, are almost double that of background locations. Furthermore, the use of CO_2 effluxes was found to adequately delineate the shallow subsurface plume by finding a strong correlation between increased vadose zone CO_2 concentrations and increased CO_2 efflux measurements (Sihota et al. 2011). Warren et al. (2014) correlated surface CO_2 efflux to concentrations of microbes and hydrocarbon loss, and suggested that a one month temporal difference existed between subsurface production of degradation products and surficial efflux detection at Bemidji. This was attributed to diffusion rates and transport times of gases to surface (Warren et al. 2014).

Previous isotopic analysis of CO_2 from soil gas monitoring wells (Figure 2.1IV) revealed $\delta^{13}C$ ranged from –13.2‰ − –36.8 ‰ across the Bemidji site (Sihota and Mayer, 2012). Areas of greatest local depletion of ^{12}C isotope in the vadose zone ($\delta^{13}C$–13.2‰ to –16.2 ‰) were located 6–8 m b.g.s. and had corresponding high methane concentrations, indicative of the methanogenic zone (Sihota and Mayer, 2012). High methane concentrations associated with more enriched rather than depleted ^{12}C isotopic data at Bemidji, demonstrates the ambiguity of using stable carbon isotopes to trace biodegradation processes occurring under anoxic conditions that are often present at contaminant sites (Conrad et al. 1997, Revesz et al. 1995).

Therefore, initial radiocarbon analysis was conducted using the soil gas monitoring well network at Bemidji, MN in August 2009 (Sihota and Mayer, 2012). The ^{14}C content of CO_2 surveyed at Bemidji from vadose zone monitoring wells in August 2009 ranged from the oldest CO_2 ($F^{14}C$ 0.062) found 11.8 m downgradient of the center of the oil plume at 7.9 m

b.g.s, and the youngest CO_2 ($F^{14}C$ 0.926) found 92.9m downgradient at 1.5 m.b.g.s (Sihota and Mayer 2012). The average radiocarbon collected in the source zone in 2009 was $F^{14}C$ 0.159 and was found to be as high as $F^{14}C$ 0.459 (Sihota and Mayer 2012). The results of the 2009 study showed ^{14}C isotopes could be effectively used to distinguish petroleum sourced and naturally sourced CO_2 in the vadose zone of a contaminated aquifer under anoxic conditions (Sihota and Mayer, 2012).

The shallow soil gas monitoring wells were again used to measure $^{14}CO_2$ values in a seasonal CO_2 efflux study at Bemidji, MN from 2011– 2013 (Sihota et al. 2016). In this study F_{CSR} was quantified using the shallow soil gas monitoring wells and found that 63 to 93% CO_2 measured in the shallow subsurface overlying the source zone locations was petroleum – derived (Sihota et al. 2016). However, the radiocarbon samples collected in 2009, 2012 and 2013 related subsurface $^{14}CO_2$ concentration to correct surface $^{14}CO_2$ efflux rates. This spatial discrepancy between radiocarbon values in the shallow subsurface and surface efflux measurements has not been considered in previous studies, and was therefore examined in this study to optimize the radiocarbon correction method and its application to surface CO_2 efflux surveys.

3.3. RESULTS

Summary of Bemidji Results

Total Efflux Measurements

The total soil respiration CO_2 efflux (J_{TSR}) across the site from survey measurements along the North Pool Transect and North Grid locations ranged from 1.2 μmol· $m^{-2}s^{-1}$ to 12.2 μmol· $m^{-2}s^{-1}$ (Figure 3.2). The minimum CO_2 efflux was measured at background

site 310, 200m up gradient from the center of the oil body, while the maximum measured CO_2 efflux was measured at location A86, located south of well North Pool Transect well 9015 (2m from the center of the oil body). The mean J_{TSR}, calculated from the average of repeat efflux measurements at each location, ranged from 1.9 μmol· $m^{-2}s^{-1}$ at W100 to 9.3 μmol· $m^{-2}s^{-1}$ at O100. O100 lies north of the North Pool transect between well 9015 and 9014. Collar location W100 lies north of well 531 which is along the North Pool Transect 68.4m down gradient from the center of the oil plume.

Total Efflux Measurements along North Pool Transect

Total efflux measurements obtained from 20 locations along the North Pool transect (Shown in red in Figure 2.3) were averaged from ~9 measurements from each location. Background location, 310 had an J_{TSR} of 2.7 μmol· $m^{-2}s^{-1}$. The lowest J_{TSR} measured along the North Pool transect was 2.8 μmol· $m^{-2}s^{-1}$ at location 9103, 30.2 m down gradient of the contaminant plume. The J_{TSR} at down gradient locations; 533, 9101, 532, 518, and 531 ranged from 3.7 μmol· $m^{-2}s^{-1}$ to 4.7 μmol· $m^{-2}s^{-1}$. These locations lie 36.6, 42.0, 47.1, 57.7 and 68.4 m down gradient of the center of the plume, respectively. The furthest measurement, 92.9m down gradient of the center of the source zone, was 5.1 μmol· $m^{-2}s^{-1}$ at location 530. The mean J_{TSR} measured at the down gradient locations was 4.1 μmol· $m^{-2}s^{-1}$.

Location 603 is located in the spray zone 118.4m up gradient of the center of the contaminant plume. This area contains hydrophobic soils, as well as increased vegetation in comparison to locations further down the transect. The average J_{TSR} in this location was 5.7 μmol· $m^{-2}s^{-1}$.

The source zone is the area that lies from well 1302 (24.0 m up gradient)and 1402 (26.6 m down gradient of the center of the plume) along the North Pool transect. The mean J_{TSR} ranges from 4.1 μmol· $m^{-2}s^{-1}$ at location 1212 to 7.4 μmol· $m^{-2}s^{-1}$ at 9015, 2.0m up gradient of the center of the oil body. The average mean J_{TSR} over the source area is 5.2 μmol•$m^{-2}s^{-1}$.

Total efflux measurements across grid

The J_{TSR} measured from 40 locations on the North Pool Grid (shown in black on Figure 2.3) were averaged from three measurements at each locations. The locations with the highest mean J_{TSR} were O100, A86, O86 and A93 with 9.3, 9.1, 8.2 and 7.9 μmol· $m^{-2}s^{-1}$, respectively. These locations lie in the center of the source zone area as shown by red contours in Figure 3.2.

Down gradient survey locations (Q–W) had average J_{TSR} ranging from to 1.9 μmol· $m^{-2}s^{-1}$ to 4.2 μmol· $m^{-2}s^{-1}$. Up gradient survey locations (B–F) had average J_{TSR} ranging from 2.00 μmol· $m^{-2}s^{-1}$ to 6.5 μmol· $m^{-2}s^{-1}$.

Carbon Isotopes Analysis

Stable Isotopes

Analysis of stable carbon isotopes ranged from $\delta^{13}C$ −10.4 to −24.1‰ across the site. Down gradient wells 9014 and 533 were more enriched in ^{12}C despite being within close proximity of the source zone. Well location 9016 was anomalously enriched with $\delta^{13}C$ −12.4‰.

Radiocarbon Isotopes

Static Chamber (SC)

The ^{14}C collected from 20 static chambers along the North Pool transect ranged from a maximum of $F^{14}C$ 1.036 ± 0.0041 at location 531, 68.40m down gradient from the center of the contaminant plume to a minimum of $F^{14}C$ 0.572± 0.0031 at 9017, 23.3m up gradient from the center of the oil plume.

The $F^{14}C$ increased with distance away from the center of the contaminant plume. Locations with a modern $F^{14}C$ signature included 531, 530 and background location 310. These SCs provided gas samples with $F^{14}C$ 1.036± 0.0041 , $F^{14}C$ 1.025 ± 0.0041 and 1.000 ± 0.0061 respectively.

The most depleted $F^{14}C$ air samples were collected from SCs at location 9017(23.3m up gradient), 1302 (23.9m up gradient) and 301 (3.41m up gradient) with $F^{14}C$ 0.572 ± 0.0031, $F^{14}C$ 0.650 ± 0.0030 , $F^{14}C$ 0.660± 0.0030, respectively.

Soil Gas Probe (SP)

^{14}C collected from 20 SP along the North Pool transect ranged from a maximum of $F^{14}C$ 0.994 ± 0.0052 at location 531, 68.4m down gradient of the oil center to a minimum of $F^{14}C$ 0.475 ± 0.0023 at 9017, 23.9 m up gradient from the center of the oil body.

The background site, 310, had a $F^{14}C$ 0.948 ± 0.0117. The SP samples with the most modern signature were down gradient locations; 531 ($F^{14}C$ 0.994 ± 0.0052) , 530 ($F^{14}C$ 0.978 ± 0.0079) and 518 ($F^{14}C$ 0.966 ± 0.0057) .

The most depleted SP radiocarbon samples were obtained from locations 301($F^{14}C$ 0.597± 0.0021) , 604($F^{14}C$ 0.539 ± 0.0034), 9015($F^{14}C$ 0.529 ± 0.0021), 9017 ($F^{14}C$ 0.475 ± 0.0023). These locations were 2.0 to 34.0 m up gradient of the contaminant plume.

Monitoring Wells (MW)

The ^{14}C collected from the top port(~0.6m b.g.s) of 17 monitoring wells along the North Pool transect ranged from a maximum of $F^{14}C$ 1.011 ± 0.0046 at 530, 92.86 up gradient of the oil center to a minimum of $F^{14}C$ 0.122 ± 0.0008 at 9015, 3.41 m up gradient from the oil center.

The background site, 310, had a relatively modern signature of $F^{14}C$ 0.964 ± 0.0070.

The radiocarbon values decreased with decreasing distance away from the center of the oil body, excluding location 603 (118.4m up gradient) which was in the spray zone and had $F^{14}C$ 0.802 ± 0.0095.

Locations in the source zone show a trend of depleted radiocarbon values. Locations 9017, (23.3m up gradient) 9014(11.8m down gradient), and 1302 (23.9m up gradient) had low radiocarbon values of; $F^{14}C$ 0.351 ± 0.0026, $F^{14}C$ 0.319 ± 0.0025, $F^{14}C$ 0.300 ± 0.0014, respectively.

However, locations 9016 (12.2m up gradient) and 1212 (16.9 m up gradient) showed anomalously higher ^{14}C isotope values compared to the above samples despite their close proximity to the center of the oil body. These two locations were enriched in ^{14}C compared to other source zone samples by approximately $F^{14}C$ 0.25.

Samples from soil gas monitoring wells became more enriched in radiocarbon downgradient from the center of the oil body. Locations 601 and 534 (18.0 m and 24.7m down gradient) had $F^{14}C$ 0.607 ± 0.0025 and $F^{14}C$ 0.569 ± 0.0026. Soil gas monitoring well 9101 and 532, 42.0 m and 47.1 m down gradient of the center of the oil body had $F^{14}C$ 0.609 ± 0.0024 and $F^{14}C$ 06551 ± 0.0028, respectively. Location 518 (57.7m down gradient from the center of the oil body) had $F^{14}C$ 0.795 ± 0.0032. Up gradient location 531 (68.4m) had a high fraction of radiocarbon, $F^{14}C$ 0.907 ± 0.0036.

Dynamic Closed Chambers (DCC)

The results of the radiocarbon analysis collected directly from the LI–8100A dynamic closed flux chamber prior to CO_2 efflux measurements ranged from a maximum $F^{14}C$ 1.022 ± 0.0013 at location 9016 to a minimum of $F^{14}C$ 0.930 ± 0.0177 at location 1402. All sites had a considerably modern ^{14}C signature, and there was no apparent correlation between distance and depletion of ^{14}C isotope.

The results of the radiocarbon analysis collected from the dynamic closed flux chamber after chamber closure from 1.5 minute to 5 minutes, ranged from a a minimum $F^{14}C$ 0.900 ± 0.0134 at locations 9017 to a maximum $F^{14}C$ 1.022 **±** 0.0010 at down gradient location 9101.

The most ^{14}C depleted samples collected after chamber measurement, were found in the source zone at 9017 (23.3 m up gradient), 9015 (2.0 m up gradient) and 301 (3.4 m up gradient), which all had ~$F^{14}C$ 0.90. The average radiocarbon ratio measured from locations in the source zone after the efflux measurement was $F^{14}C$ 0.93**±** 0.011.

Samples taken prior to chamber measurement were more enriched with ^{14}C isotopes than the sample taken after CO_2 flux measurement, with the exception of four down gradient locations; 9101, 533, 532 and 518.

Vegetation and sediment samples

The results of the radiocarbon measured on the AMS from ten vegetation samples were consistently between $F^{14}C$ 1.02 to 1.03 ± 0.002. This included sample locations distributed from 200.8 m up gradient of the plume (310) to 68.4m down gradient of the contaminant plume (531). In general, the radiocarbon measured from the soil samples decrease with decreasing distance away from the center of the oil body .The highest $F^{14}C$ measured from soil samples was at location 310, 533 and 531 with $F^{14}C$ 1.051 ± 0.0029, 1.06 and 1.063 ± 0.0024, respectively. In the center of the plume at well 9017, 9015 and 9014 the radiocarbon values were more depleted with $F^{14}C$ 0.763± 0.0024, 0.896± 0.0034 and 0.874 ± 0.0023 respectively. Location 603, which lies 118.4m up gradient in the spray zone, also measured low radiocarbon $F^{14}C$ 0.67 ± 0.002. Location 9016 lies 12.16 m up gradient of the spill had $F^{14}C$ 0.965 ± 0.0025.

3.4. DISCUSSION

The results of the CO_2 efflux survey along the North Pool transect collected in the summer 2015 had similar magnitude of total J_{TSR} found in previous studies. The peak average J_{TSR} of 7.4μmol•$m^{-2}s^{-1}$ measured at location 9015, 2.0m up gradient from the proposed center of the contaminant plume were comparable to previous studies conducted by Sihota et al. (2011), which found a peak mean J_{TSR} of 7.1 μmol•$m^{-2}s^{-1}$

along the North Pool transect at location 9017, 23.3 m up gradient of the proposed center of the contaminant plume.

The $F^{14}C$ of gas samples collected across the Bemidji site deviates from a modern ^{14}C signature for sites overlying known residual oil using all four sampling methods. The results of all sampling methods had significantly lower mean $F^{14}C$ of the source zone (9017, 9016, 9015, 601, 301, 1302, 1212, 534) than the $F^{14}C$ of unaffected upgradient (310, 603, 604) and downgradient locations (518, 530, 531,532, 533, 9103, 9101). This mirrors findings of Sihota and Mayer (2012), which showed significant differences in CO_2 source between contaminated and background locations based on depleted ^{14}C signature.

Site location 9017 had high mean J_{TSR} and the lowest radiocarbon values in both the SP and SC method. At location 9017, the radiocarbon value increased with decreasing depth from $F^{14}C$ 0.351 ± 0.0026 at 50cm b.g.s, $F^{14}C$ 0.475 ± 0.0023 at 30cm b.g.s and $F^{14}C$ 0.572 ± 0.0031 at surface measured by the SC and $F^{14}C$ 0.900 ± 0.0134 measured at surface directly from the LI–8100A flux chamber. In general, there was a trend of decreased radiocarbon with depth with the exception of five locations where SP had higher $F^{14}C$ than the samples collected with SC (Figure 3.8). This reflects the findings of Sihota and Mayer 2012 where ^{14}C depletion increases with decreased proximity to the petroleum hydrocarbon source zone and confirms that the source of ^{14}C depletion is petroleum-derived.

The source of depleted radiocarbon in sediment samples can be attributed to residual oil in the subsurface as shown in Figure 3.7 (Delin et al, 1998). According to Trumbore 2000, the expected ^{14}C in SOM from natural soil respiration in temperate

climates would reflect short turnover times on the order of 3–16 years (Trumbore, 2000). Thus the source of depleted ^{14}C in soil is likely hydrocarbon derived.

Contaminant soil respiration CO_2 efflux (J_{CSR})

Radiocarbon results were used to calculate the quantity of CO_2 efflux derived from microbial degradation of petroleum hydrocarbons using the equations outlined in chapter 2. The J_{TSR} measurements were corrected using either F_{CSR}^{DCC} mass balance equation (2.6)(DCC $F^{14}C$ samples) or F_{CSR} simplification equation (2.10) ($F^{14}C$ samples obtained from SC, SP or MW methods). The results of the J_{CSR} for the simplification equation (SC,SP,MW) and mass balance equation (DCC) are quantified in tables 3.4 and 3.5 respectively. The J_{CSR} for background location 310, 200.8m up gradient of the source zone, was approximately 0.0 $\mu mol \cdot m^{-2}s^{-1}$ using SC,SP and MW methods. The maximum J_{CSR} calculated for DCC, SC, SP and MW were 1.6,2.0, 3.3, 5.4 $\mu mol \cdot m^{-2}s^{-1}$ respectively. The highest J_{CSR} using all four methods was obtained at location 9015, 1.98m up gradient from the center of the source zone. Location 9015 had the highest J_{TSR} but was not the location with the most depleted $F^{14}C$ samples. In the sources zone the average J_{CSR} was 1.4 1.4, 1.3, 3.2 $\mu mol \cdot m^{-2}s^{-1}$ for DCC, SC, SP and MW methods respectively.

In general, all four methods showed increased J_{CSR} in the source zone, which decreased with increased distance up and down gradient of the center of the oil plume.

Despite their close proximity to center of the oil body, up gradient locations 9016 (–12.2m) and 1212(–16.9m) had lower calculated J_{CSR} using simplification equation 2.10 for SC , SP and MW. These locations had reasonably elevated J_{TSR} (>4.0 $\mu mol \cdot m^{-2}s^{-1}$) but high measured $F^{14}C$ ratio, which indicates increased F_{NSR}

contribution to $J_{TSR.}$ The calculated J_{CSR} using the DCC mass balance equation 2.6 were smaller than other source zone locations but still higher than up or down gradient locations.

At five down gradient locations (9103, 9101, 532, 533 and 518) the calculated J_{CSR} calculated using the mass balance equation 2.6 for DCC method was negative. This is a result of the higher measured $F^{14}C$ in the sample collected after the CO_2 efflux measurement than prior to the survey CO_2 efflux measurement. These locations were recorded as BD in Table 3.3. The remaining 12 locations had a positive calculated J_{CSR} using the DCC method. The J_{CSR} calculated using the DCC calculation was the smallest average J_{CSR} along the North pool transect of all four techniques, however had comparable J_{CSR} results in the source zone.

Quantifying J_{CSR} and contaminant mass loss rates

Assuming a diffusion dominated system with dominantly vertical transport (Sihota and Mayer 2012, Molins et al 2010) and quasi steady state conditions (Sihota and Mayer 2012) the SZNA rates obtained at Bemidji can be determined from J_{CSR} using all four methods summarized in Table 3.4. The mean J_{CSR} rates for up gradient wells was greater than down gradient wells for all four methods, supporting the findings of Bekins et al. (2005) that found faster degradation of the up gradient plume. For consistency with Sihota and Mayer (2012), an average vadose zone thickness of 7m was assumed and an areal extent of the oil body is 2790m^2 (Sihota and Mayer, 2012). Using this area, a mass loss of carbon over the source zone can be determined in g/day for MW, SP, SC and DCC methods as 9260gC/day, 3760gC/day, 4050gC/day and 4050gC/day respectively. These rates are similar to the magnitude of SZNA rates reported by Sihota and Mayer (2012) which were sampled using only the MW method (Summarized in Table 3.5).

The results obtained from Bemidji, MN show that estimates of SZNA are significantly affected by the method used. The mass loss estimates obtained from MW in 2015 are nearly double those calculated using SP and SC data. This suggests that the MW method likely overestimates the contaminant degradation due to the depth of collection which is not representative of $F^{14}C$ emitted at surface. The different methods are compared more thoroughly in Chapter 5.

Chapter 3 Tables

Table 3. 1 The values of $F^{14}C$ measured on the accelerator mass spectrometer using air samples collected from Static chambers (SC), soil gas probes (SP) and soil gas monitoring wells (MW) from 20 locations along the north pool transect. Corresponding distance up–gradient (–) or down–gradient of the center of the oil plume are reported for each sampling location.

Location	Distance away from oil center	SC		SP		MW	
	(m)	($F^{14}C$)	±	($F^{14}C$)	±	($F^{14}C$)	±
310	–200.82	1.000	0.0061	0.948	0.0117	0.964	0.0070
603	–118.40	0.733	0.0072	0.848	0.0128	0.802	0.0095
604	–34.04	0.714	0.0040	0.539	0.0034	0.318	0.0018
1302	–23.90	0.650	0.0030	0.754	0.0062	0.300	0.0014
9017	–23.34	0.572	0.0031	0.475	0.0023	0.351	0.0026
1212	–16.92	0.809	0.0032	0.720	0.0047	0.506	0.0020
9016	–12.16	0.761	0.0042	0.788	0.0064	0.620	0.0024
301	–3.41	0.660	0.0030	0.597	0.0038	0.122	0.0008
9015	–1.98	0.724	0.0029	0.529	0.0021	0.271	0.0015
9014	11.75	0.799	0.0033	0.782	0.0043	0.319	0.0025
601	18.03	0.781	0.0035	0.848	0.0070	0.607	0.0025
534	24.73	0.716	0.0030	0.814	0.0106	0.569	0.0026
1402	26.66	0.833	0.0036	0.792	0.0082	–	–
9103	30.24	0.806	0.0046	0.825	0.0091	–	–
533	36.59	0.907	0.0037	0.858	0.0166	0.730	0.0029
9101	41.97	0.943	0.0093	0.836	0.0961	0.609	0.0024
532	47.12	0.926	0.0050	0.858	0.0050	0.655	0.0028
518	57.70	0.969	0.0050	0.966	0.0057	0.795	0.0032
531	68.40	1.036	0.0041	0.994	0.0052	0.907	0.0036
530	92.86	1.025	0.0041	0.978	0.0079	1.011	0.0046
Average		0.81	0.0042	0.78	0.0114	0.56	0.0029
Source zone average		0.73	0.00	0.71	0.01	0.41	0.00

Table 3. 2 The values of $F^{14}C$ measured on the accelerator mass spectrometer using air sample collected directly from LI–8100A dynamic closed chambers prior to chamber closure and the corresponding $F^{14}C$ collected after CO_2 efflux measurement. Results of 19 locations along the north pool transect are shown and their corresponding distances up-gradient (–) or down-gradient (+) of the center of the oil plume are reported for each sampling location.

Location	Distance away from oil center	Dynamic Closed Chamber prior to chamber closure		Dynamic Closed Chamber after chamber closure	
	(m)	($F^{14}C$)	±	($F^{14}C$)	±
310	–200.82	0.947	0.0015	_	_
603	–118.40	0.990	0.0139	0.985	0.0097
604	–34.04	0.995	0.0138	0.954	0.0121
1302	–23.90	0.970	0.0692	0.942	0.0122
9017	–23.34	0.965	0.0148	0.900	0.0134
1212	–16.92	0.981	0.0136	0.941	0.0127
9016	–12.16	1.022	0.0013	0.974	0.0017
301	–3.41	0.972	0.0134	0.905	0.0101
9015	–1.98	0.996	0.0014	0.898	0.0024
9014	11.75	_	_	0.940	0.0166
601	18.03	0.966	0.0182	0.951	0.0118
534	24.73	0.974	0.0110	0.948	0.0136
1402	26.66	0.930	0.0177	0.935	0.0129
9103	30.24	1.001	0.0121	1.005	0.0129
533	36.59	0.980	0.0137	0.990	0.0146
9101	41.97	0.957	0.0009	1.022	0.0010
532	47.12	0.951	0.0285	0.962	0.0115
518	57.70	0.980	0.0121	0.984	0.0117
531	68.40	0.979	0.0117	0.974	0.0141
530	92.86	_	_	_	_
Average		0.98	0.02	0.96	0.01
Source zone average		0.98	0.02	0.93	0.01

Table 3. 3 The petroleum derived contaminant soil respiration CO_2 efflux ($\mathbf{J_{CSR}}$) calculated using; Static chamber (SC) , soil gas probe (SP) , and soil gas monitoring wells (MW)

North Pool Transect Location	SC			SP			MW		
	F_{NSR}	F_{CSR}	J_{CSR}	F_{NSR}	F_{CSR}	J_{CSR}	F_{NSR}	F_{CSR}	J_{CSR}
			(μmol $m^{-2}s^{-1}$)			(μmol $m^{-2}s^{-1}$)			(μmol $m^{-2}s^{-1}$)
310	1.000	0.00	0.00	1.0000	0.0000	0.00	1.0000	0.0000	0.00
603	0.733	0.27	1.53	0.8945	0.1055	0.61	0.8315	0.1685	0.97
604	0.714	0.29	0.83	0.5687	0.4313	1.26	0.3117	0.6883	2.01
1302	0.650	0.35	1.83	0.7955	0.2045	1.07	0.2944	0.7056	3.69
9017	0.572	0.43	2.02	0.5004	0.4996	2.36	0.3440	0.6560	3.10
1212	0.809	0.19	0.77	0.7595	0.2405	0.98	0.4962	0.5038	2.04
9016	0.760	0.24	1.13	0.8305	0.1695	0.80	0.6082	0.3918	1.84
301	0.660	0.34	1.64	0.6299	0.3701	1.78	0.1196	0.8804	4.24
9015	0.723	0.28	2.04	0.5579	0.4421	3.27	0.2652	0.7348	5.43
9014	0.799	0.20	1.38	0.8246	0.1754	1.20	0.3128	0.6872	4.72
601	0.781	0.22	1.01	0.8940	0.1060	0.49	0.5949	0.4051	1.86
534	0.716	0.28	1.26	0.8583	0.1417	0.63	0.5574	0.4426	1.97
1402	0.833	0.17	0.81	0.8353	0.1647	0.80	-	-	-
9103	0.806	0.19	0.54	0.8701	0.1299	0.36	-	-	-
533	0.907	0.09	0.34	0.9053	0.0947	0.35	0.7161	0.2839	1.04
9101	0.942	0.06	0.22	0.8820	0.1180	0.44	0.5975	0.4025	1.51
532	0.926	0.07	0.35	0.9043	0.0957	0.45	0.6425	0.3575	1.67
518	0.968	0.03	0.11	1.0189	-0.0189	-0.06	0.7796	0.2204	0.74
531	1.035	-0.04	-0.14	1.0480	-0.0480	-0.19	0.8895	0.1105	0.44
530	1.025	-0.02	-0.13	1.0311	-0.0311	-0.16	0.9911	0.0089	0.05
North Pool Transect Average		0.19	0.9		0.18	0.9	0.55	0.45	2.2
Source zone average		0.27	1.4		0.25	1.3	0.40	0.60	3.2

Table 3. 4 The total soil respiration CO_2 efflux (J_{TSR}) compared to petroleum derived contaminant soil respiration CO_2 efflux ($\mathbf{J_{CSR}}$) calculated using back ground correction (BGC) and DCC methods.

North Pool Transect Location	Distance away from oil center	J_{TSR}	J_{CSR}	
			BGC	DCC
	(m)	(μmol $m^{-2}s^{-1}$)	(μmol $m^{-2}s^{-1}$)	(μmol $m^{-2}s^{-1}$)
310	-200.82	2.66	0.00	-
603	-118.40	5.74	3.08	0.23
604	-34.04	2.91	0.26	0.95
1302	-23.90	5.22	2.57	1.79
9017	-23.34	4.72	2.06	1.67
1212	-16.92	4.06	1.40	1.27
9016	-12.16	4.71	2.05	1.36
301	-3.41	4.82	2.16	1.86
9015	-1.98	7.39	4.73	3.17
9014	11.75	6.86	4.21	-
601	18.03	4.60	1.95	0.64
534	24.73	4.45	1.79	0.72
1402	26.66	4.87	2.21	0.22
9103	30.24	2.79	0.13	-0.09
533	36.59	3.68	1.02	-0.21
9101	41.97	3.74	1.08	-1.75
532	47.12	4.66	2.00	-0.15
518	57.70	3.38	0.72	-0.02
531	68.40	4.00	1.34	0.22
530	92.86	5.14	2.49	-
North Pool Transect Average		4.6	2.0	0.7
Source zone average		5.2	2.5	1.4

Table 3. 5 SZNA rates obtained using all four methods and previous studies at USGS Natural Attenuation Research Site Bemidji, MN.

Method	**Source Zone Natural Attenuation rate (As CO_2 efflux µmol· m^{-2} s^{-1}**		**Reference**
	All wells	**Source zone**	
MW ^{14}C	2.2	3.2	This study
SP ^{14}C	0.9	1.3	This Study
SC ^{14}C	0.9	1.4	This Study
DCC ^{14}C	0.7	1.4	This Study
MW ^{14}C	2.4	3.9	Sihota and Mayer 2012
BGC	2.6	–	Sihota et al 2011
Gradient method	1.6	6.2	Revesz et al 1995
Modelling	1.3–1.5	–	Chaplin et al 2002
Modelling	–	6.6	Molins et al 2010

Chapter 3 Figures

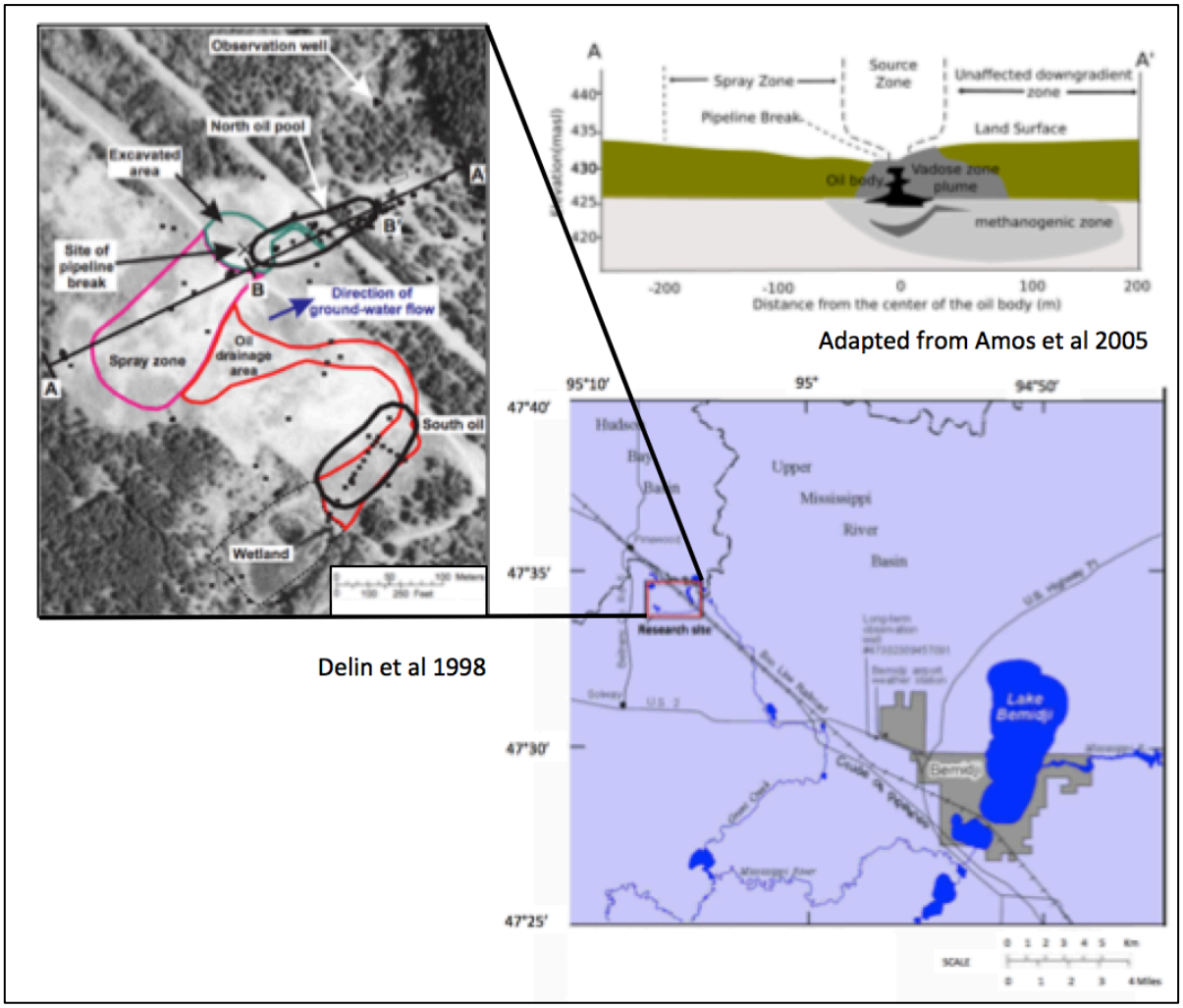

Figure 3. 1 Shows the site location of The National Crude Oil Spill Fate and Natural Attenuation Research Site located NW of Bemidji, MN. The site is outline by the red box (map obtained from the USGS Bemidji national crude oil spill website: (https://mn.water.usgs.gov/projects/bemidji/spatial/locatn-1.jpg) (Adapted from Delin et al, 1998, Amos et al 2005).

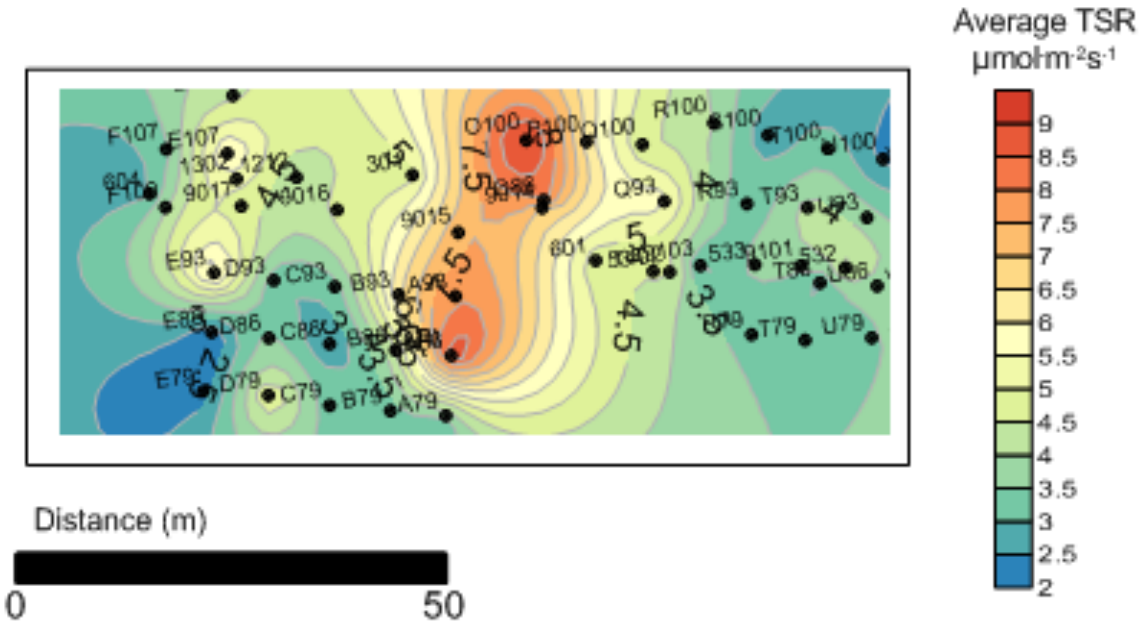

Figure 3. 2 Plan view of the spatial distribution of the average total CO_2 efflux (µmol•$m^{-2}s^{-1}$) measured across the USGS monitored toxicology site ranging from 1.9 µmol•$m^{-2}s^{-1}$ (shown in blue) to 9.1 µmol•$m^{-2}s^{-1}$ (shown in red). Measurements were taken from 60 collar locations from August 14 2015 to August 19 2015.

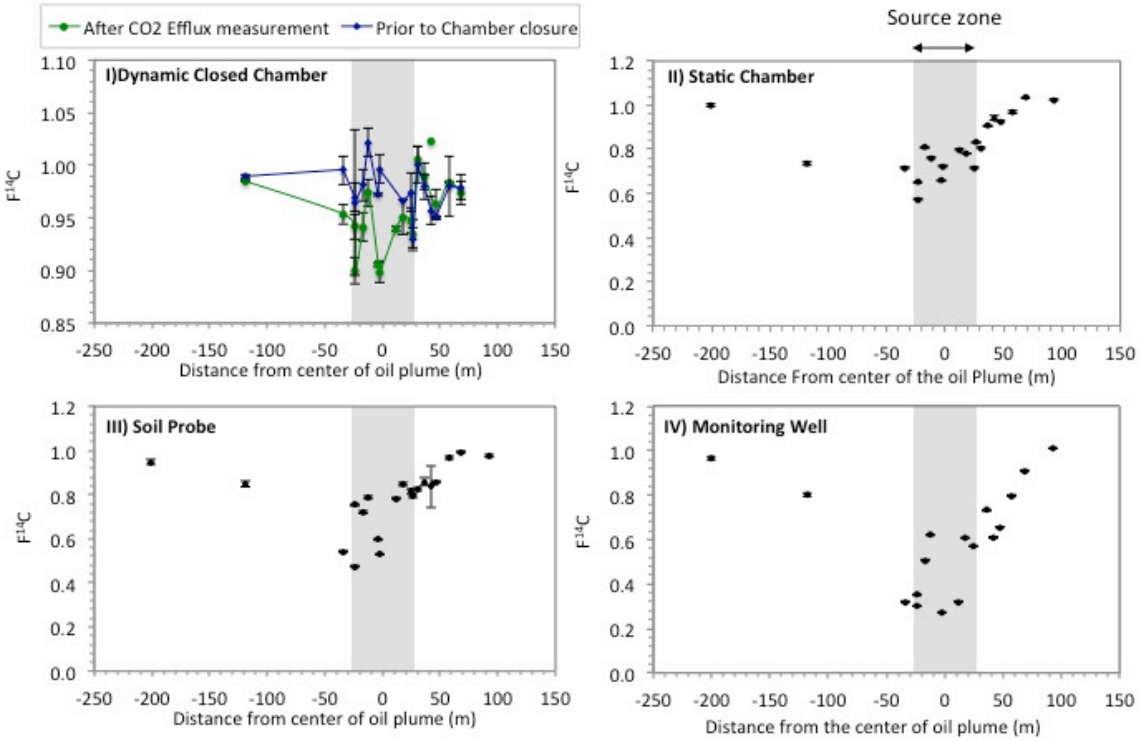

Figure 3. 3 The $F^{14}C$ measured on the accelerator mass spectrometer of samples collected from i) dynamic closed chambers *DCC* prior to chamber closure (blue) and after CO_2 efflux measurement (green) ii) Static chambers *SC* iii) Soil probes *SP* d) soil gas monitoring wells *MW* and their corresponding distance away from the center of the oil plume. The extent of the source zone 24m up gradient and 26m down gradient of the oil center is shaded in grey.

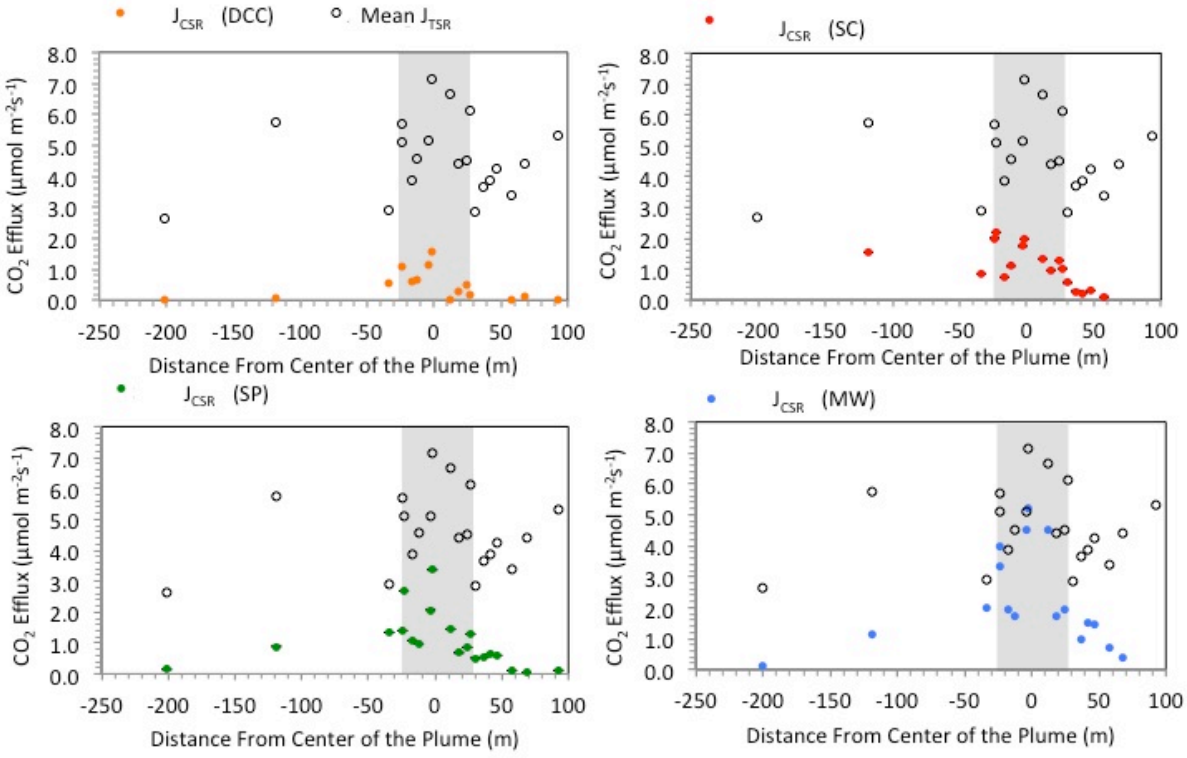

Figure 3. 4 The J_{TSR} compared to the J_{CSR} calculated using radiocarbon correction obtained from samples collected from and a) directly from dynamic closed chambers *DCC* (orange) b) Static chambers *SC* (red) c) Soil gas probes *SP* (green) d) soil gas monitoring wells *MW* (blue), at locations along the north pool transect in Bemidji, MN. The source zone area 24m up gradient and 26m down gradient is shaded in grey

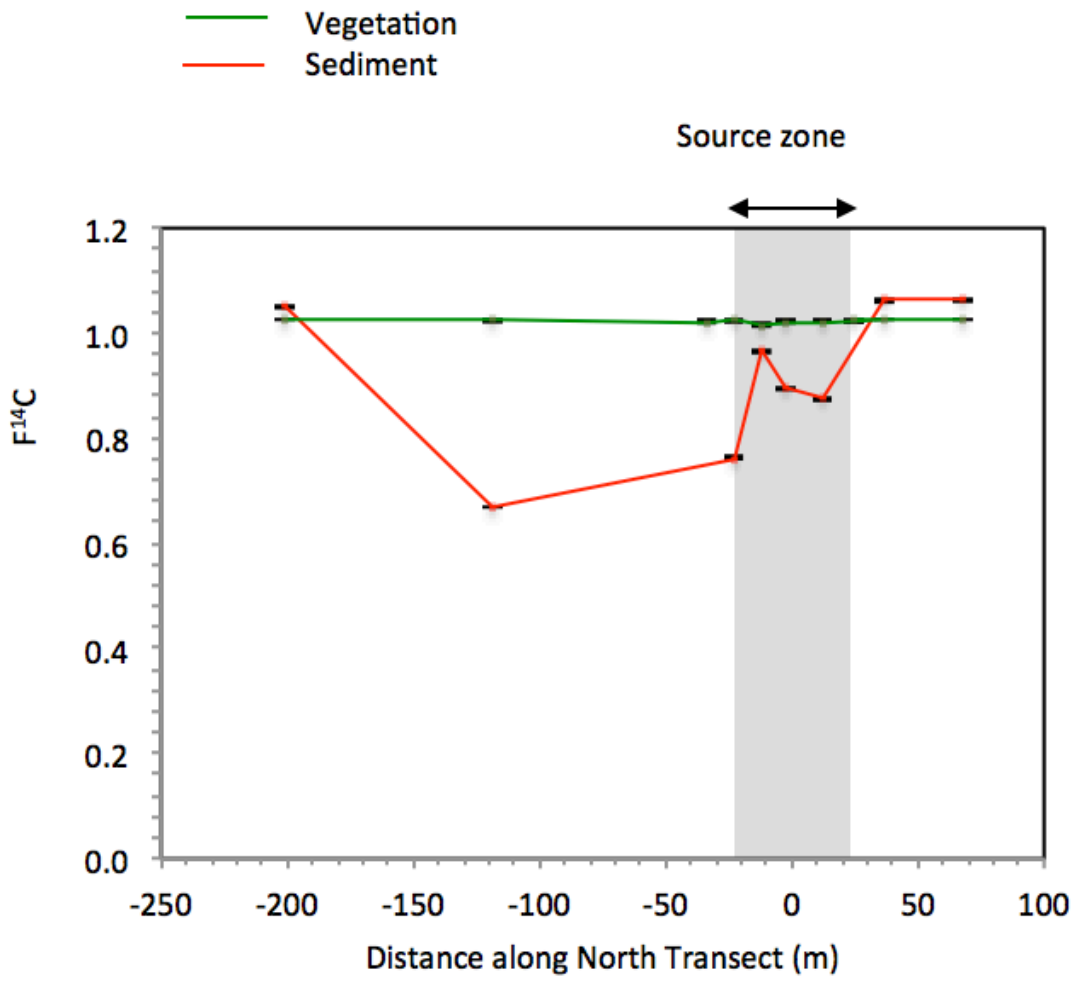

Figure 3. 5 Shows the $F^{14}C$ of 8 soil and 10 vegetation samples selected for radiocarbon analysis with distance along the north pool transect. Vegetation samples reflect modern $F^{14}C$ values, while soil samples $F^{14}C$ decrease near the center of the residual oil body.

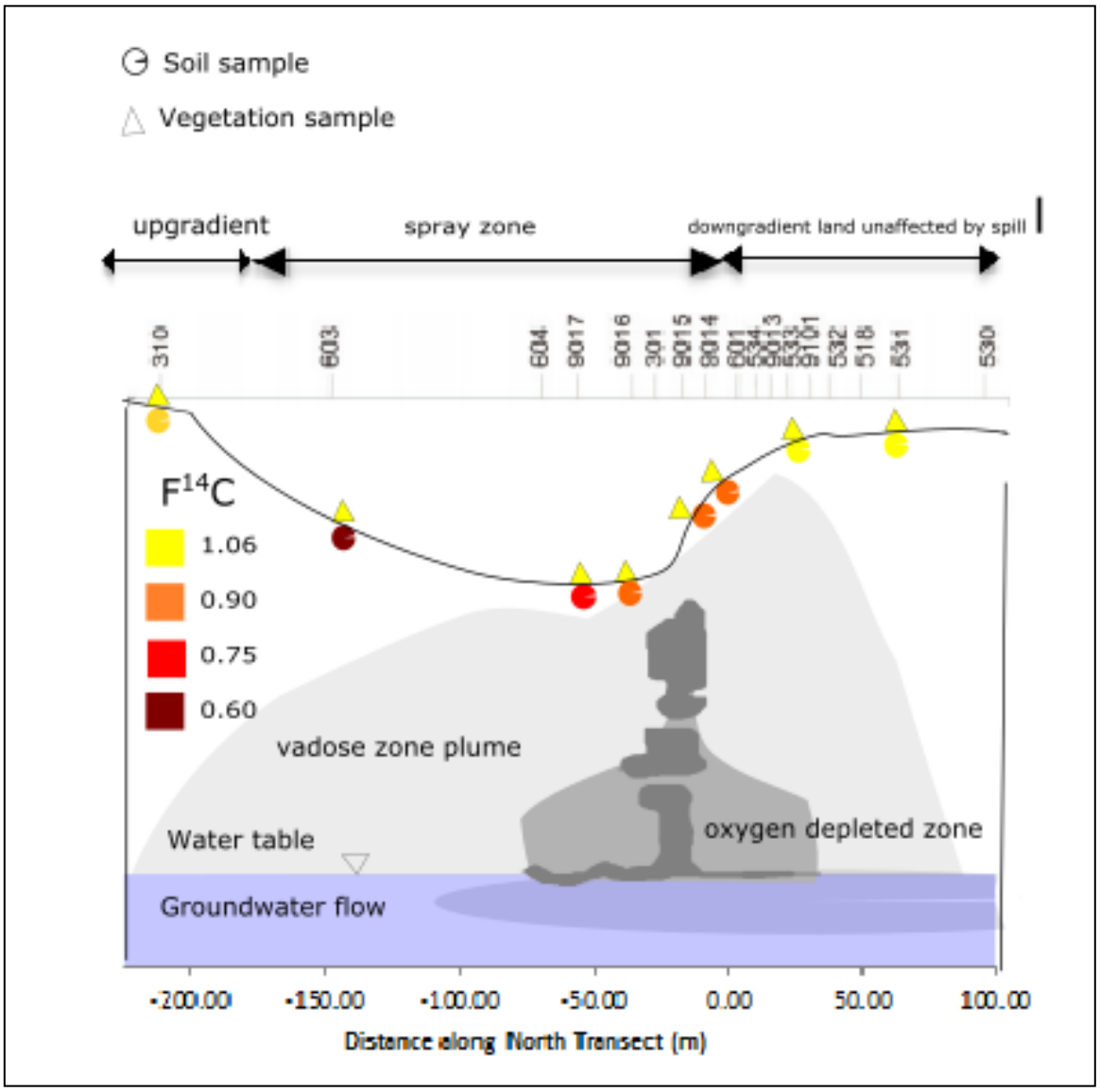

Figure 3. 6 Shows cross section of the $F^{14}C$ of 8 soil and 10 vegetation samples selected for radiocarbon analysis. Vegetation samples reflect modern $F^{14}C$ values, while soil samples $F^{14}C$ decrease near the center of the residual oil body. The subsurface data has been adapted from Sihota and Mayer, 2012 .

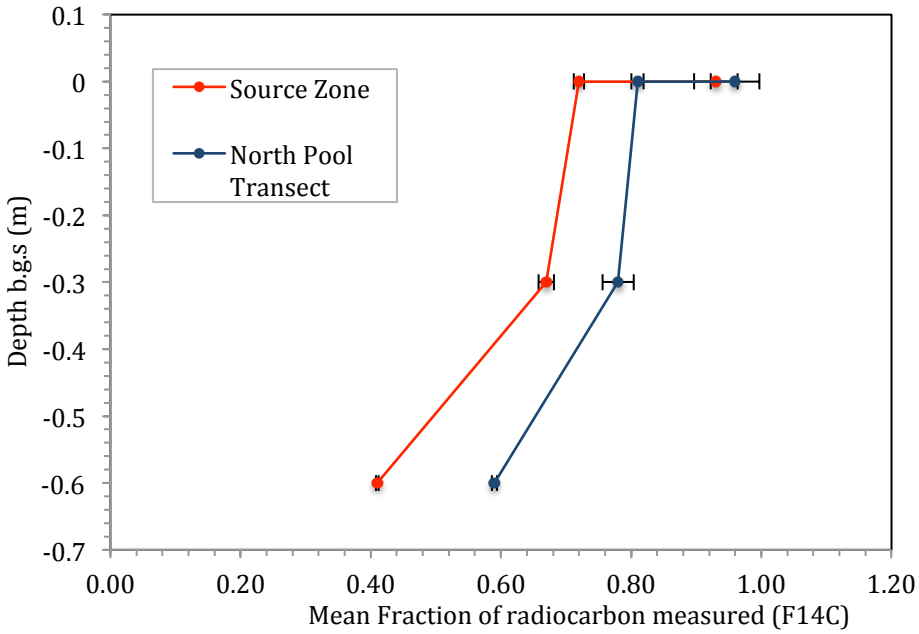

Figure 3. 7 Shows the mean Fraction of radiocarbon from gas samples decreases with depth for source zone area (red) and north pool transect locations (blue) .

Chapter 4

4. Radiocarbon Correction Method for Determining J_{CSR} at an Industrial Refinery Site

4.1. Introduction

At large scale industrial sites, the extent of hydrocarbon SZNA can be difficult to quantify due to site wide heterogeneities (of geology, contamination geometry etc.), scale and multiple contamination events (Sihota, 2014, Bekins et al, 2005). In the previous chapter, the source of contamination was restricted to a single large crude oil spill event. Alternatively, refining facilities may manage hydrocarbon products ranging from gasoline to crude oil, which contribute to multiple spill events across a site.

Implementing surface CO_2 efflux surveys at large scale oil refinery sites may help to i) identify hotspots for hydrocarbon degradation and delineate the extent of a hydrocarbon contaminant plume undergoing microbial biodegradation (Sihota et al. 2011) ii) be used to produce estimates of SZNA rates of subsurface hydrocarbons (Sihota, 2014). Previous work conducted by Sihota, 2014 used ^{14}C samples collected directly from the dynamic closed LI-8100A flux chamber to quantify SZNA rates across a large scale former refinery site. At sites where the extent of contamination is lesser understood, and an uncontaminated background site cannot be clearly identified, radiocarbon correction methods to CO_2 efflux surveys may provide greater local resolution of biodegradation processes than BGC methods (Sihota and Mayer, 2012, Sihota, 2014). High resolution (one sample per $1.2x\ 10^4\ m^2$) sampling was found to effectively constrain mass loss rates over the refinery site (Sihota, 2014). Sihota (2014) sampling suggested the importance of characterizing background ^{14}C overlying the

contaminant plume and advocated that increased cost and time required for ^{14}C sampling could inform remediation strategies and SZNA estimates.

The remaining challenges with this monitoring approach include understanding initial sources of background depletion at refinery sites and addressing the extent to which radiocarbon in plant physiology is affected at historically contaminated sites. Furthermore, a thorough method comparison is required to effectively sample for radiocarbon in CO_2 efflux surveys at industrial sites, in order to identify areas of petroleum biodegradation on–site and quantify contaminant loss rates. Therefore, gas samples were collected for radiocarbon analysis from three field sampling methods during a detailed CO_2 efflux survey at an industrial site in north–central Unites states. Plant and soil samples were collected for radiocarbon analysis to inform background $F^{14}C$. Results were compared to inform method development for radiocarbon correction during CO_2 efflux surveys for monitoring lesser characterized contaminated refinery sites with multiple spill history.

4.2. SITE DESCRIPTION

This study was conducted at a former industrial oil refinery in the north–central United States. The refinery was operational from 1923 to 1982 and processed gasoline, diesel, petroleum coke and asphalt. In 1996 the refinery was decommissioned and by 1999 subsurface piping, concrete foundations and structures used for plant operations were removed. The locations of known historical releases and previous infrastructure across the site are shown in Figure 4.1 (Sihota, 2014).

The subsurface geology has been characterized as an alluvial medium–coarse sand aquifer with inter–bedded silts and fine sands (Sihota, 2014). The groundwater ranges from 1.5 to 11 m b.g.s (Sihota, 2014). The south eastern part of the property contains the deepest aquifer, whereas the bedrock outcrops in the north eastern part of the south property and thus is devoid of the alluvial aquifer (Sihota, 2014).

Remedial efforts since 1999 have included the installation of a Waterloo Barrier in the south property to mitigate contamination of the North Platte River. Subsurface investigations since 1999 have confirmed LNAPL distribution across 4 ha of the site (Sihota, 2014). Aerobic and anaerobic degradation of hydrocarbons in the smear zone and vadose zone have been confirmed from previous soil gas data obtained from soil gas monitoring wells (Sihota, 2014).

.

4.3. RESULTS

Total soil respiration CO_2 efflux (J_{TSR}) *measurements*

The mean J_{TSR} across the site ranged from a maximum of 6.7 $\mu mol \cdot m^{-2}s^{-1}$ at location E3 to a minimum of 0.3 $\mu mol \cdot m^{-2}s^{-1}$ at NP7 (Table 4.1). Locations with high mean J_{TSR} (greater than 3.0 $\mu mol \cdot m^{-2}s^{-1}$) included E3, B7, L8, F4 and F6 with 6.7, 4.3, 3.7, 3.3 and 3.0 $\mu mol \cdot m^{-2}s^{-1}$ respectively. The average mean J_{TSR} for the south property collar locations was 2.7 $\mu mol \cdot m^{-2}s^{-1}$. The average mean J_{TSR} from north property locations was 1.2 $\mu mol \cdot m^{-2}s^{-1}$.

Radiocarbon Isotopes

Static Chamber (SC)

The ^{14}C collected from the SCs ranged from $F^{14}C$ 0.910±0.0081 at north property site NP6 to as low as $F^{14}C$ 0.245 ±0.0018 at location E3 (Table 4.1). The north property sites NP6 and NP7 show the highest fraction of radiocarbon across the site. The results from the SC show that despite C3's close proximity to other affected locations, it has a higher radiocarbon signature than the surrounding locations. The most depleted $F^{14}C$ locations are E3, L8, F6 and D2 with $F^{14}C$ 0.245±0.0018, $F^{14}C$ 0.314±0.0032, $F^{14}C$ 0.356 ±0.0027 and $F^{14}C$ 0.360 ±0.0006 respectively. These were also locations identified for elevated mean J_{TSR}. The north property locations; NP5, NP1 and NP4 had radiocarbon values less than modern of; 0.844 ± 0.0065, 0.824 ±0.0208 and 0.573 ±0.0094 respectively. While these sites were hypothesized to be unaffected background sites, the radiocarbon content indicates deviation from modern natural soil respiration radiocarbon signature.

Soil gas probe (SP)

The ^{14}C collected from the SP data ranged from youngest $F^{14}C$ 1.061 ± 0.0116 at north property site NP7 to the oldest of $F^{14}C$ 0.205 ±0.0017 at location D2 (Table 4.2). Similarly to the SC samples, E3 was depleted in radiocarbon and had $F^{14}C$ 0.315 ±0.0062. B7 had the second highest J_{TSR} and was also depleted ($F^{14}C$ 0.309 ±0.0025) but unfortunately the SC sample could not be run due to a suspected leak. Samples collected from NP4, NP6, NP5 and NP7 all had a close to modern signature, which ranged from $F^{14}C$ 0.966 ±0.0126 to 1.061 ±0.0116. Converse to the results of the SC,

samples taken from the SP suggest that north property locations are unaffected from contamination and can be used as background locations. The other north property site, NP1, had a slightly more depleted isotopic value of $F^{14}C$ 0.875 ±0.0.0119. Consistent with results from the SC, location I5 and C3 showed closer to modern radiocarbon values of 0.891 ±0.0.0091 and 0.879 ± 0.0029, respectively which indicate limited contamination at these sites.

Directly sampled from Dynamic Closed Chamber (DCC)

A sample for radiocarbon analysis was collected both prior to flux measurement and immediately after the survey measurement. The sample yields for both of these samples were less than 0.2mgC (the laboratory standard for AMS analysis). These measurements had the greatest error on the AMS which ranged from ±0.001 up to ±0.1724.

Table 4.3 summarizes the radiocarbon results collected directly from the dynamic closed chamber (DCC). The radiocarbon measured from initial DCC samples on the south property ranged from $F^{14}C$ 0.949 ±0.0023 at F6 to a minimum of 0.696 ±0.0127 at L8. The mean $F^{14}C_{initial}$ measured on the north and south property was 0.922± 0.02 and 0.866 ±0.01, respectively. Location C3 ($F^{14}C$ 1.174 ± 0.0587) and NP1 ($F^{14}C$ 0.517 ±0.1724) were considered outliers and not used for analysis of means. The samples collected immediately after the chamber measurement ranged from $F^{14}C$ 1.109 ±0.0158 site at NP7 to a minimum of $F^{14}C$ 0.624 ± 0.001 at B4. The mean $F^{14}C_{final}$ measured on the north and south property was 0.897± 0.03 and 0.838 ±0.01,

respectively. Contrary to hypothesis, samples collected after flux measurement were not consistently more depleted in ^{14}C than prior to flux measurement samples.

Vegetation and Sediment Samples

The radiocarbon results of the vegetation and sediment samples retrieved from the collar areas of ten selected locations (Figure 4.8) are summarized in Table 4.4. The results of the vegetation samples show a modern $F^{14}C$ signature, across the de-commissioned refinery site, regardless of sample location. The results of vegetation samples had a mean $F^{14}C$ 1.02 ± 0.002. The results of $F^{14}C$ from sediment samples show depleted signatures with mean $F^{14}C$ 0.29 ± 0.001. One sediment sample was analyzed from the north property sample site due to low % carbon (<0.01%), which had depleted $F^{14}C$ 0.12± 0.001. The results of the XRD analysis indicate no significant carbonate mineralogy, and consists of predominantly silicates including; quartz, microcline, sanidine, muscovite and albite.

Contaminant soil respiration CO_2 efflux (J_{CSR})

F_{CSR} was calculated using $F^{14}C$ samples collected from the SC and SP according to equation (2.9) and normalized to mean $F^{14}C$ of the 'background' north property sites, which had mean $F^{14}C$ 0.872 ±0.01 and 0.981 ±0.01 using SC and SP methods, respectively. F_{CSR} were used to correct average J_{TSR} values using equation (2.10) in chapter 2. The results of F_{CSR} and J_{CSR} for SC and SP methods are summarized in table (4.1) and (4.2). Using SC and SP methods the maximum J_{CSR} was calculated at site E3 which was 4.8 and 4.6 $\mu mol \cdot m^{-2}s^{-1}$, respectively. Locations of elevated J_{CSR} identified by

SC method include E3, L8, F6, D2, K8, F4 and N8, which were also identified along with location B7 as hotpots using SP method.

After normalization, the mean J_{CSR} on the north property site was 0.0 μmol·m^{-2}s^{-1} using both SC and SP methods. The mean J_{CSR} calculated on the south property was 1.4 and 1.3 μmol·m^{-2}s^{-1} for SC and SP methods, respectively.

The F_{CSR} for the DCC method was calculated using the mass balance equation (2.6) in chapter 2, where the $[CO_2]_{final}$ and $[CO_2]_{initial}$ were considered at 255 seconds when the gas samples were collected for radiocarbon analysis. The average $[CO_2]_{initial}$ on the north property was 411 ppm and $[CO_2]_{final}$ after 255 seconds was 453ppm, whereas the average $[CO_2]_{initial}$ on the south property was 408 ppm, and $[CO_2]_{final}$ after 255 seconds was 510ppm. The maximum CO_2 concentration after 255 seconds was 662ppm measured at location E3. On the south property 6 out of 14 locations had an increase in $F^{14}C$ ($F^{14}C_{final} > F^{14}C_{initial}$) over the measurement, which corresponded to a negative F_{CSR} correction for 4 out of 14 locations. The average F_{CSR} correction on the south property was 0.32. On the north property 3 out of 5 locations had ($F^{14}C_{final} > F^{14}C_{initial}$), which corresponded to negative $F_{CSR,}$ and an average F_{CSR} correction of -1.3. The corresponding average J_{CSR} was 0.8 μmol·m^{-2}s^{-1} on the south property and 0.3 μmol·m^{-2}s^{-1} on the north property 'background' sites. The maximum J_{CSR} calculated using DCC method was 4.3 μmol·m^{-2}s^{-1} at location K8. In contrast to the SC and SP methods, E3 was not identified as the highest J_{CSR} signal location using DCC method due to $F^{14}C_{final} > F^{14}C_{initial.}$ Similarly, other hotspot locations identified by SC and SP methods had negative J_{CSR} , including F4 and B7 in the northern western portion of the south property.

4.4. DISCUSSION

Total efflux compares to 2012/ 2014 data.

The results of the mean J_{TSR} on the south property was significantly lower than mean values measured in 2012 and 2014. These lower overall CO_2 concentrations compared to previous years, may have contributed to the lower J_{CSR} signal derived from radiocarbon analysis, especially for the DCC method which typically yields the smallest concentrations of CO_2 and thus susceptible to increased analytical error.

The $F^{14}C$ on the north property are significantly greater than those collected on the south property. If we assume that hydrocarbons are the only source of radiocarbon depletion, this is likely due to the historical refining activities that took place on the south property since the 1920s.

The collar locations on the north property (NP1, NP4, NP5, NP6 and NP7) were initially thought to be background locations. This was further supported by low average J_{TSR} 1.2 $\mu mol \cdot m^{-2}s^{-1}$ and modern $F^{14}C$ 0.98 collected using SP from soil gas at 30cm b.g.s. However, the mean radiocarbon from SCs (collected from surface air) was $F^{14}C$ 0.872 ±0.01 (excluding outlier NP4). Furthermore the mean $F^{14}C_{initial}$ 0.922± 0.02 from the DCC also deviate from a modern radiocarbon signature that would be expected from background air. It should be noted that the mean of the north property ambient air samples ($F^{14}C_{initial}$ 0.922± 0.02) was calculated without including location NP1 $F^{14}C$ 0.5172, which had an anomaly high analytical error on the AMS (±0.1724). These results indicate that either i) the north property sites should not be considered

as 'background,' which are unaffected from historical contamination ii) local depletion of $^{14}CO_2$ over this area exists due to local Seuss effect caused from nearby emissions of the industrial site or town (Seuss and Urey, 1956). It is likely that both factors contribute to depleted radiocarbon measured on the north property.

The first scenario is supported by a decrease in mean $F^{14}C_{initial}$ 0.922± 0.02 to $F^{14}C_{final}$ 0.897± 0.03 over the DCC measurement period. This suggests there may be a contribution, although small, of J_{CSR} at the north property locations, and a better background site should be identified in future site investigations.

The second scenario is supported by elevated average initial [CO_2] of ~411ppm and $F^{14}C_{initial}$ 0.922± 0.02 from DCC samples on the north property. The associated mass balance would suggests an initial depletion of $^{14}CO_2$ prior to chamber placement with approximately 378ppm of modern CO_2 diluted with approximately 33ppm of ancient carbon:

$$411 ppm CO_2 \cdot F^{14}C\ (0.92) = 378 ppm CO_2 \cdot F^{14}C(1.00) + 33 ppm CO_2 \cdot F^{14}C(0.0)$$

The initial dilution of surface samples contradicts the assumption of modern $^{14}CO_2$ when the surface chambers are placed. On the south property the mean $F^{14}C_{initial}$ 0.866 ±0.01 collected using DCC method indicated an ambient air radiocarbon depletion on the south property which mirrors previous research that measured average $F^{14}C$ 0.88 for initial carbon samples collected from prior to DCC measurements (Sihota, 2014). This suggests that an ambient air sample is important before determining F_{CSR} contribution to J_{TSR} .

On the south property areas identified as hot spots for biodegradation based on elevated J_{TSR} >2.8 μmol·m^{-2}s^{-1} (D2, K8 ,F6, F4, L8, B7 and E3) had the most depleted

$F^{14}C$ obtained from SP ranging from $F^{14}C$ 0.205± 0.0017 to 0.523 ±0.0015. Similarly, these sites were also the lowest $F^{14}C$ obtained from SCs which ranged from $F^{14}C$ 0.245 ±0.0018 to 0.484 ±0.0010. The contamination can be delineated using the elevated CO_2 efflux data together with both the SC and SP $F^{14}C$ results. These seven locations can be used to delineate the region with most active source zone biodegradation occurring at this site.

If a two source model is assumed where petroleum is the source of carbon with $F^{14}C = 0.00$ and modern soil respired carbon $F^{14}C = 1.00$, then source zone natural attenuation rates at the site can be estimated using the three different methods (Table 4.5). The SZNA rates calculated using SP compared to SC agree reasonably well. An average SZNA using the correction obtained by SP samples over the seven hotspot locations was 1.4 $\mu mol \cdot m^{-2}s^{-1}$, and using all 14 south property locations was 0.8 $\mu mol \cdot m^{-2}s^{-1}$. Comparably, the samples obtained from SC gave mean estimates of SZNA at the site of 1.4 $\mu mol \cdot m^{-2}s^{-1}$, and using all south property locations was 0.9 $\mu mol \cdot m^{-2}s^{-1}$. The SZNA calculated using DCC method were 0.8 $\mu mol \cdot m^{-2}s^{-1}$ over the 14 south property locations, with minor increase over the hotspot locations to 0.9 $\mu mol \cdot m^{-2}s^{-1}$. These estimates of SZNA are lower than previous observations where SZNA was 2.5±0.3 $\mu mol \cdot m^{-2}s^{-1}$ using BGC method and 2.0±0.4 $\mu mol \cdot m^{-2}s^{-1}$ using RCC method (Sihota, 2014).

Contaminant source zone geometry

The geometry of the contaminant source zone delineated using J_{CSR} calculated from the SC and SP corresponds well with the subsurface data reported by Sihota, 2014 (Figure 4.7d). The Mol fraction of LNAPL measured underlying the hotspots identified using radiocarbon corrected J_{CSR}, were $1e^{-4}$ – $1e^{-2}$ for benzene, $1e^{-2}$ – $1e^{-1}$ for toluene, $1e^{-3}$ – $1e^{-2}$ for naphthalene (Sihota, 2014). The J_{CSR} of hotpot areas identified, overly a smear zone 3–6m thick (Sihota, 2014). The DCC method had poorer spatial correlation to areas associated with high BTEX concentrations and where LNAPL had previously been mapped in the subsurface (Figure 4.7a,d) While the DCC method successfully identified location C3 for high J_{CSR}, it had poor CSR sensitivity at locations E3 and F4 which overly known contamination. Additionally, the DCC method identified high J_{CSR}efflux at location NP6 which was previously thought to be uncontaminated. Overall, the DCC method shows poor spatial correlation to subsurface data. Conversely, both the SP and SC J_{CSR} agree well with subsurface mapping of the contaminant source zone and therefore may be used to delineate the subsurface source zone. The results of the SP and SC show reasonable spatial agreement with subsurface data as well as similar magnitudes of $J_{CSR}$and thus can be used to provide reasonable estimates of SZNA at this site.

Chapter 4 Tables

Table 4. 1Radiocarbon isotope results for samples collected from Static chambers (SC) and corresponding calculated petroleum derived contaminant soil respiration CO_2 efflux (J_{CSR})*samples that were processed using luxfer addition

Location		Average J_{TSR}	Radiocarbon from Static Chamber		SC		J_{CSR}
		($\mu molm^{-2}s^{-1}$)	$F^{14}C$	±	F_{NSR}	F_{CSR}	($\mu molm^{-2}s^{-1}$)
	C3*	2.16	0.91	0.09	0.20	1.04	-0.04
	D2*	2.80	0.36	0.64	1.79	0.41	0.59
	E3*	6.73	0.24	0.76	5.09	0.28	0.72
	E6*	1.95	0.66	0.34	0.66	0.76	0.24
	F4*	3.25	0.48	0.52	1.68	0.55	0.45
	F6*	3.01	0.36	0.64	1.94	0.41	0.59
	I5	1.78	0.87	0.13	0.23	1.00	0.00
	J4	1.79	0.60	0.40	0.71	0.69	0.31
	K8	2.86	0.41	0.60	1.70	0.46	0.54
	L8	3.70	0.31	0.69	2.53	0.36	0.64
	N8	1.36	0.52	0.48	0.65	0.60	0.40
	NP1	0.44	0.82	0.18	0.08	0.95	0.05
	NP4	1.30	0.57	0.43	0.56	0.66	0.34
	NP5	1.68	0.84	0.16	0.26	0.97	0.03
	NP6	2.15	0.91	0.09	0.19	1.04	-0.04
	NP7	0.31	0.91	0.09	0.03	1.04	-0.04
	B4*	1.14					
	B7*	4.29					
	F7	0.35					
Average	South property	2.66	0.52	0.00	0.60	0.40	1.4
	Hotspots	3.71	0.44	0.00	0.51	0.49	2.0
	North property	1.18	0.87	0.01	1.00	0.00	-0.01

Table 4. 2 Radiocarbon isotope results for samples collected from soil gas probe (SP) and corresponding average total soil respiration CO_2 efflux (J_{TSR}) and calculated petroleum-derived contaminant soil respiration CO_2 efflux (J_{CSR}) .
*samples that were processed using luxfer addition

Location		Average J_{TSR}	Radiocarbon measured from SP		SP		
		($\mu molm^{-2}s^{-1}$)	$F^{14}C$	±	F_{NSR}	F_{CSR}	J_{CSR} ($\mu molm^{-2}s^{-1}$)
	NP7	0.31	1.0607	0.0116	1.08	-0.08	-0.03
	NP6	2.15	0.9776	0.0096	1.00	0.00	0.01
	NP5	1.68	1.0269	0.0118	1.05	-0.05	-0.08
	NP4	1.30	0.9662	0.0126	0.98	0.02	0.02
	NP1	0.44	0.8745	0.0119	0.89	0.11	0.05
	N8	1.36	0.7144	0.0129	0.73	0.27	0.37
	L8	3.70	-	-	-	-	-
	K8	2.86	0.4105	0.0028	0.42	0.58	1.66
	J4	1.79	0.5481	0.0053	0.56	0.44	0.79
	I5	1.78	0.8906	0.0091	0.91	0.09	0.16
	F7	0.35	0.7859	0.012	0.80	0.20	0.07
	F6*	3.01	0.5231	0.0015	0.53	0.47	1.41
	F4*	3.25	0.4271	0.0026	0.44	0.56	1.84
	E6*	1.95	0.5594	0.0036	0.57	0.43	0.84
	E3*	6.73	0.3146	0.0062	0.32	0.68	4.57
	D2*	2.80	0.2052	0.0017	0.21	0.79	2.21
	C3*	2.16	0.8785	0.0029	0.90	0.10	0.23
	B7*	4.29	0.3090	0.0025	0.31	0.69	2.94
	B4*	1.14	0.7121	0.0013	0.73	0.27	0.31
Average	North Property	1.18	0.98	0.01	1.00	0.00	-0.01
	South Property	2.66	0.56	0.00	0.53	0.47	1.5
	Hot spots	3.71	0.44	0.00	0.39	0.61	2.4

Table 4. 3 Radiocarbon isotope results for samples collected directly from dynamic closed chamber and corresponding average total soil respiration CO_2 efflux (J_{TSR}) and calculated petroleum-derived contaminant soil respiration CO_2 efflux (J_{CSR}).
*samples processed with luxfer addition

Location		Average J_{TSR}	Initial radiocarbo measured directl from closed chamber		Radiocarbon measurec directly from closed chamber after efflux measurement		F_{CSR} at t=255s	J_{CSR}
		($\mu molm^{-2}s^{-1}$)	$F^{14}C$	±	$F^{14}C$	±		($\mu molm^{-2}s^{-1}$)
North Property	NP7	0.31	0.935	0.0163	1.109	0.0158	-6.76	-2.1
	NP6	2.15	1.005	0.0087	0.7927	0.0852	1.21	2.6
	NP5	1.68	0.866	0.0111	0.8279	0.0213	0.43	0.7
	NP4	1.30	0.881	0.0245	0.8936	0.0213	-0.04	-0.1
	NP1	0.44	0.517	0.1724	0.8633	0.0244	-7.49	-3.3
South Property	N8	1.36	0.908	0.007	0.8161	0.0097	0.89	1.2
	L8	3.70	0.695	0.0127	0.7445	0.0079	0.17	0.6
	K8	2.86	0.927	0.0085	0.7961	0.012	1.49	4.3
	J4	1.79	0.911	0.0097	0.9183	0.014	0.04	0.1
	I5	1.78	0.867	0.0198	0.9108	0.0094	0.13	0.2
	F7	0.35	0.782	0.0264	0.9043	0.0141	-4.24	-1.5
	F6*	3.01	0.948	0.0023	0.8856	0.0011	0.33	1.0
	F4*	3.25	0.877	0.0016	0.9178	0.002	-0.04	-0.1
	E6*	1.95	0.941	0.0021	0.8754	0.0011	0.50	1.0
	E3*	6.73	0.616	0.0052	0.8297	0.0025	-0.18	-1.2
	D2*	2.80	0.889	0.0017	0.7909	0.0058	0.62	1.7
	C3*	2.16	1.173	0.0587	0.8679	0.0056	1.90	4.1
	B7*	4.29	0.761	0.002	0.8521	0.0011	-0.07	-0.3
	B4*	1.14	0.877	0.0039	0.6239	0.001	2.90	3.3
Mean North Property		1.18	0.92	0.01	0.91	0.04	-1.29	0.3
Mean South Property		2.66	0.87	0.02	0.84	0.01	0.32	0.8
Hot spots		3.71	0.85	0.03	0.84	0.01	0.39	0.8

Table 4. 4 Radiocarbon measured from vegetation and soil samples from ten select locations across the refinery site.

Sample location	Vegetation		Soil	
	$F^{14}C$	Error	$F^{14}C$	Error
E3	1.0215	0.0024	0.1018	0.0007
F5	1.0146	0.0022	0.2039	0.0009
C3	1.0193	0.0023	0.2879	0.0013
F4	0.9967	0.0024	0.2312	0.0013
J4	1.0192	0.0022	0.8309	0.0034
D2	1.0114	0.0022	0.2526	0.0013
K8	1.0134	0.0022	0.1485	0.0011
NP1	1.025	0.0023	–	–
NP5	1.022	0.0024	0.1243	0.0009
NP7	1.0225	0.0028	–	–

Table 4. 5 SZNA estimates using methods for quantifying average J_{CSR} at the northern USA- decommission refinery site

Method	**Source Zone Natural Attenuation rate (As CO_2 efflux µmol· m^{-2} s^{-1}**		**Reference**
	South Property	**Hot spots**	
SP ^{14}C	1.5	2.4	This study
SC ^{14}C	1.4	2.0	This study
DCC ^{14}C	0.79	0.83	This study
BGC	1.5	2.5	This study
DCC ^{14}C	1.8	-	Sihota 2014
BGC	2.9	-	Sihota 2014

Chapter 4 Figures

Figure 4. 1 Shows the locations of previous site buildings (orange), extent of smear zone (grey) and historical releases (pink) of the USA refinery site modified from Sihota, 2014.

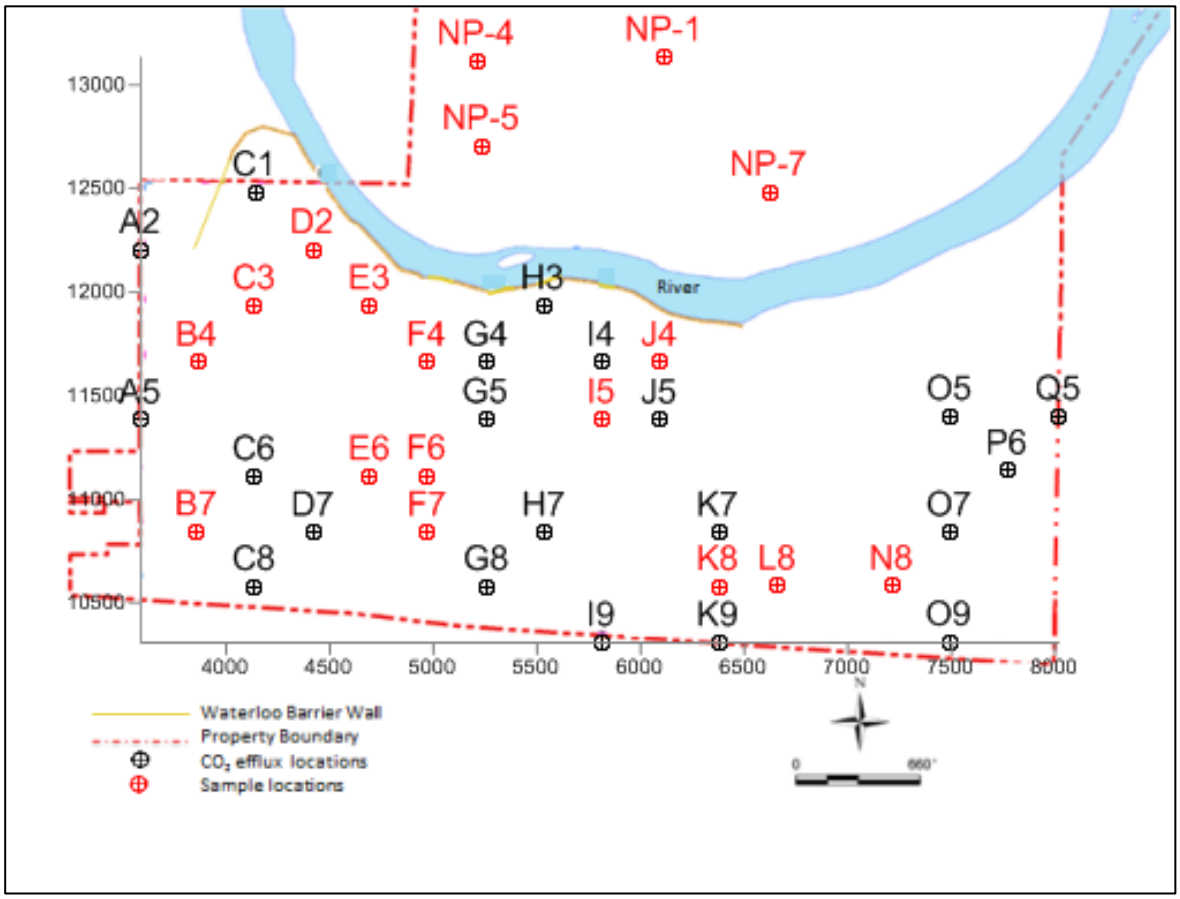

Figure 4. 2 A map of the 40 locations at the USA refinery site for CO_2 efflux measurement using the LI–8100A. The selected locations for ^{14}C sampling are shown in red.

I)

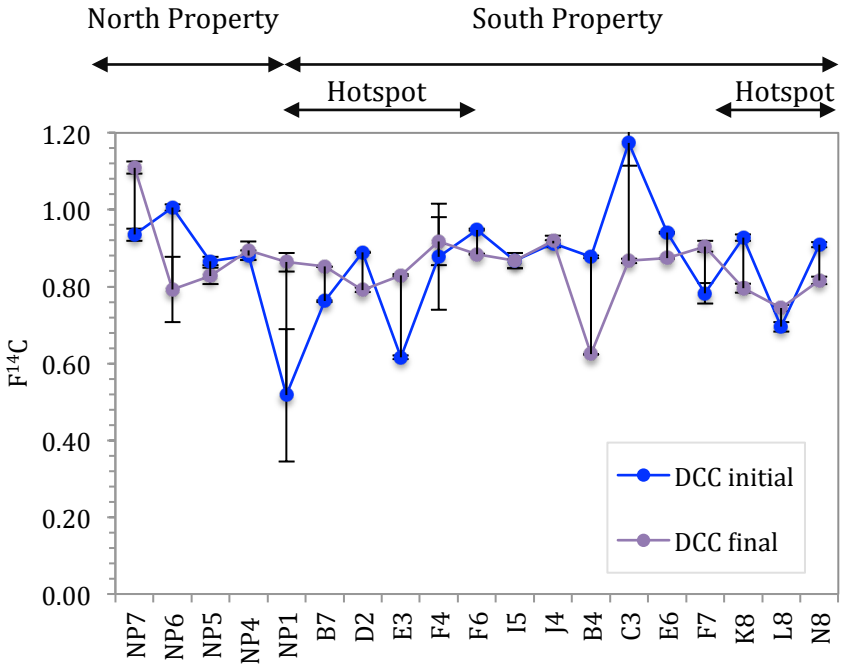

II)

Figure 4. 3 Radiocarbon ($F^{14}C$) measured using I) SP (green) and SC (red) samples agree well with more modern north property sites and significantly depleted areas on the south property (at L8 and E3) compared to II) $DCC_{initial}$ (blue) taken prior to CO_2 efflux measurement and DCC_{final} (purple) samples taken after the 90s CO_2 efflux measurement period. DCC samples did not always decrease between $DCC_{initial}$ to $DCC_{final.}$ samples.

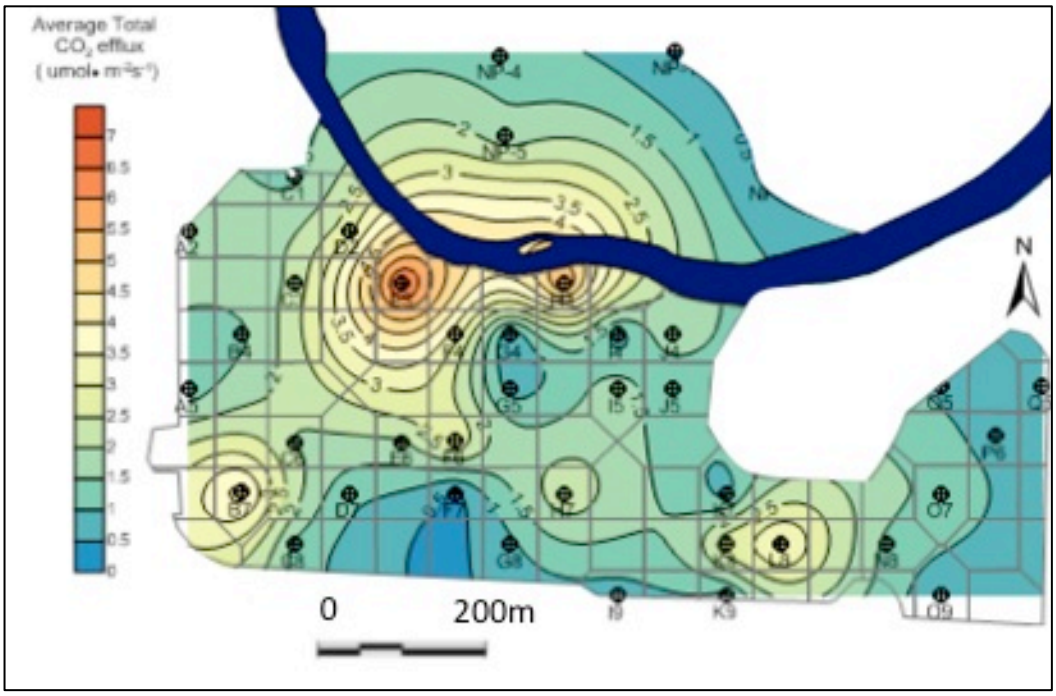

Figure 4. 4 The average J_{CSR} across the site using LI– 8100A efflux measurements at all 40 CO_2 efflux locations ranging from 6.7 µmol• $m^{-2}s^{-1}$ at E3 to 0.3 µmol• $m^{-2}s^{-1}$ at NP7.

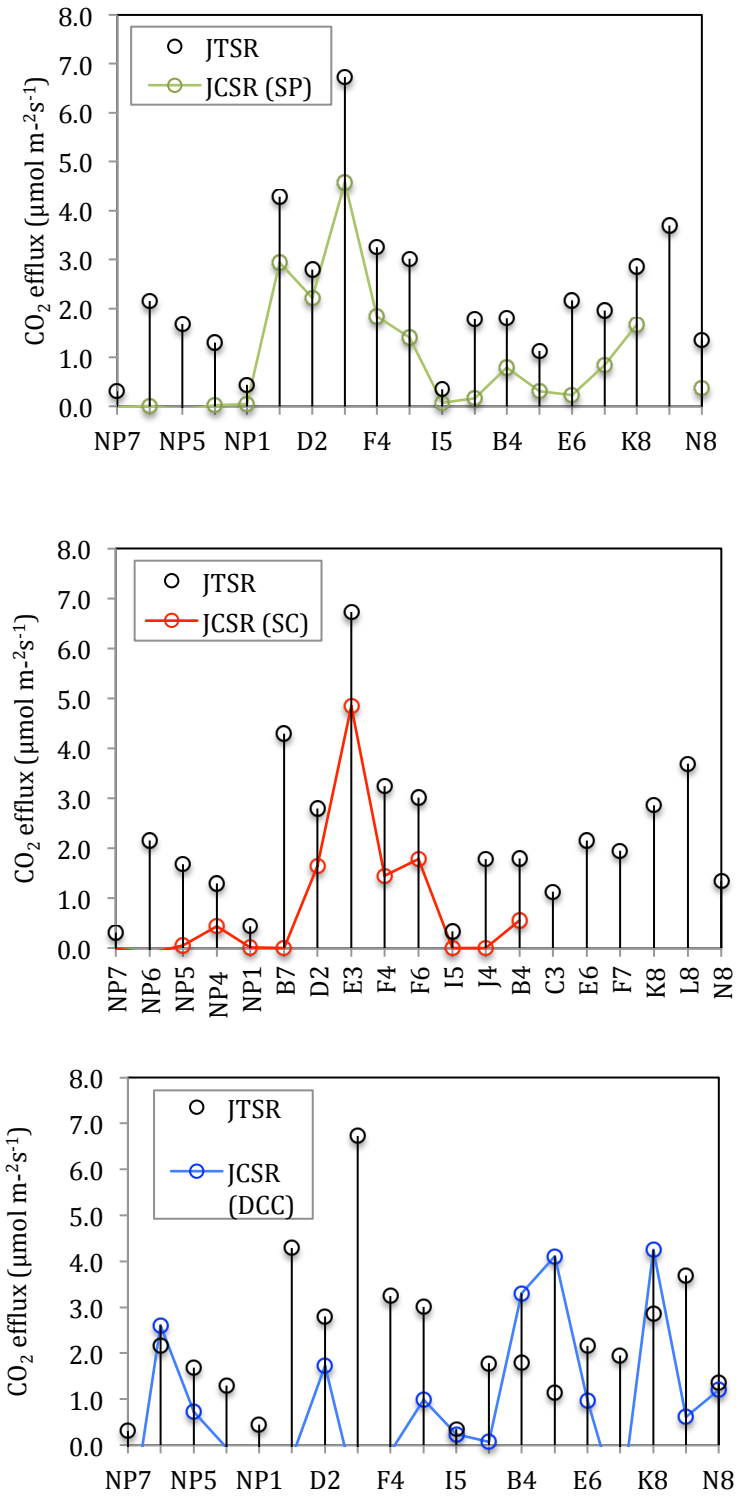

Figure 4. 5 The mean total soil respiration CO_2 efflux (J_{TSR})(black) compared to corrected J_{CSR} quantified using soil gas probe (SP) (green) Static chambers (SC) and dynamic closed chamber (DCC) (blue) methods.

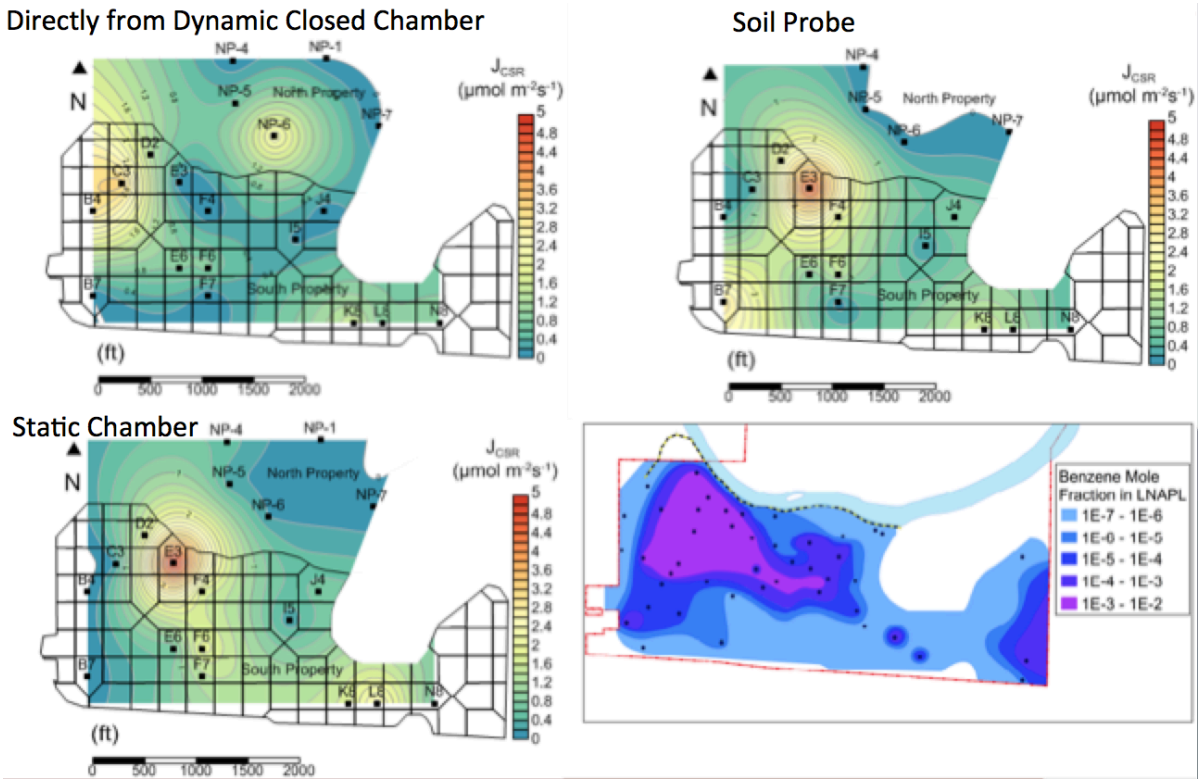

Figure 4. 6 Shows the J_{CSR} calculated in this study using a) dynamic closed chamber samples (DCC) b) Static chamber samples (SC) and c) soil gas probe samples (SP) compared to the d) Benzene Mol Fraction data compiled by Sihota, 2014 from data measured in 2002.

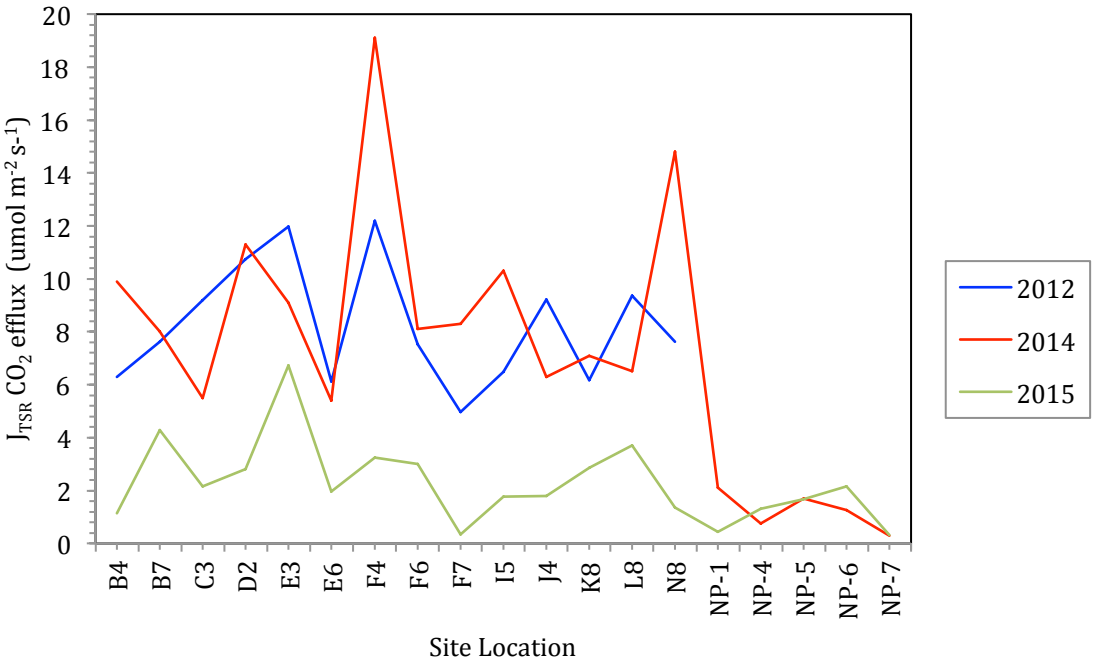

Figure 4. 7 Shows the average J_{TSR} measured in September 2012, 2014 and 2015.

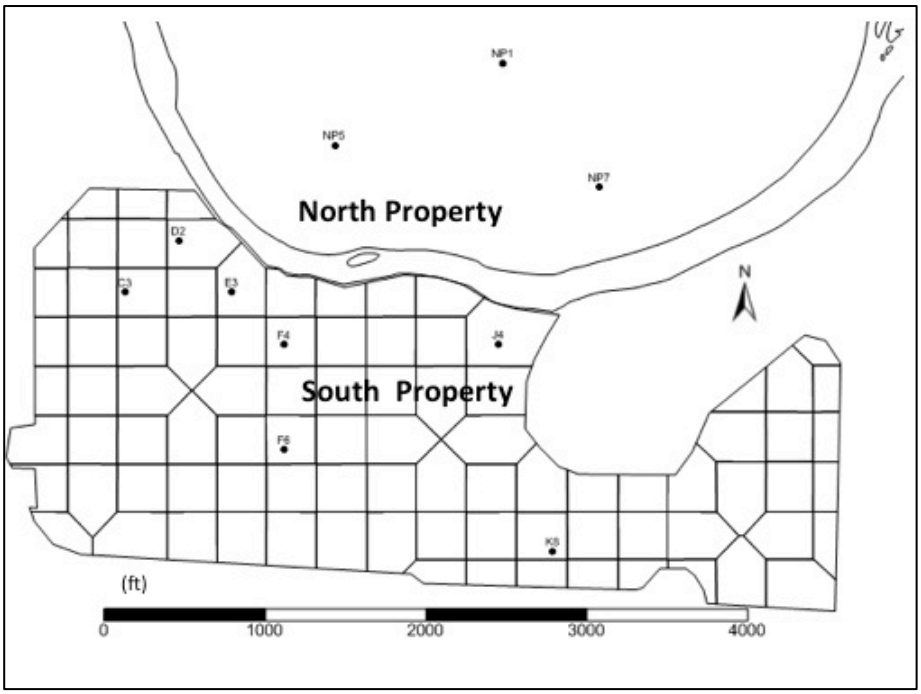

Figure 4. 8 Ten selected locations for $F^{14}C$ analysis in plants and soils.

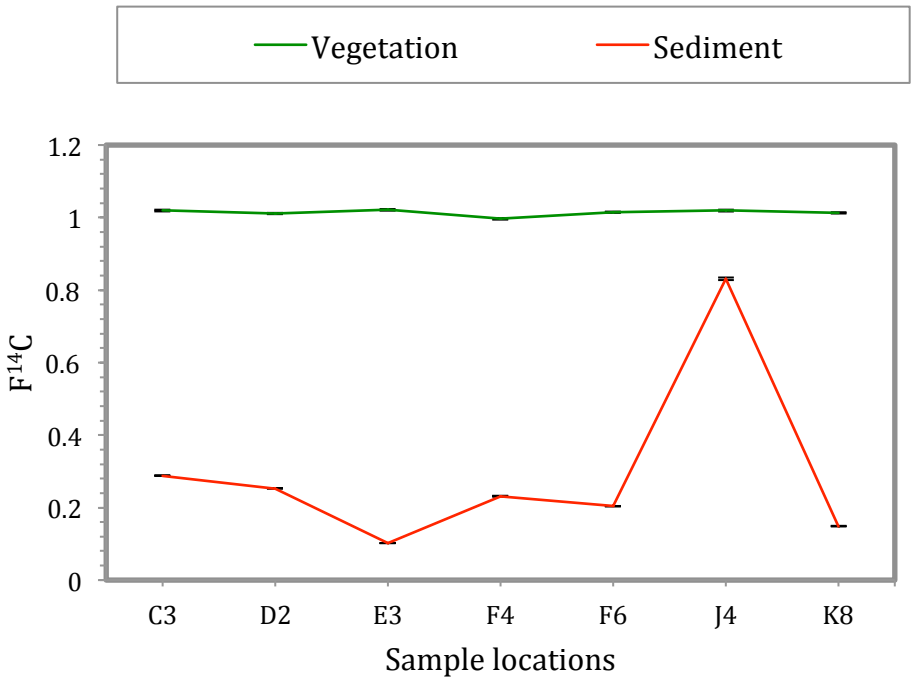

Figure 4. 9 The $F^{14}C$ of the vegetation shows a modern signature, while the $F^{14}C$ of the sediment shows depleted signature suggested to be attributed to residual oil in the subsurface.

Chapter 5

5. METHOD COMPARISON AND VALIDATION OF RADIOCARBON CORRECTION FOR DETERMINING J_{CSR} AND PRACTICAL IMPLICATIONS FOR MONITORING AT HYDROCARBON BIODEGRADATION SITES

Developing a protocol for field sampling of soil gas CO_2 for radiocarbon analysis and using this data to correct J_{TSR} measurements at ground surface may be analyzed through comparison of the four different sampling methods described in chapter 2 at the two different field sites described in chapter 3 and 4. These methods were used to quantify the contribution of subsurface petroleum degradation to total CO_2 efflux measured at surface using an LI–8100A dynamic closed chamber flux system. The results of each method are compared below.

5.1. U.S.G.S NATIONAL CRUDE OIL SPILL FATE AND NATURAL ATTENUATION RESEARCH SITE IN BEMIDJI, MN

At the National Crude Oil Spill Fate and Natural Attenuation Research Site in Bemidji, MN the mean source zone $F^{14}C$ for SC, SP, MW and DCC methods were 0.73, 0.71, 0.41 and 0.93 respectively. The respective F_{CSR} for each method are shown in Table 5.1, and are used as the correction for J_{TSR} to determine J_{CSR}. Analysis of variance (ANOVA) on the log percent modern carbon (pMC= $F^{14}C \cdot 100$) values for each method demonstrated significant variance $F(3,56)=7.92$ $p<0.005$ among the sampling methods used. A post hoc Tukey test showed that while DCC and MW methods were significantly different from one another, neither method was significantly different than SP and SC methods, which showed good agreement with each other.

Soil gas Monitoring wells

F_{CSR} calculated from radiocarbon samples collected from MW along the north pool transect had the highest mean F_{CSR}. The higher F_{CSR} can be attributed to collecting MW from greater depth (~0.6m) as compared to the other methods. This F_{CSR} value collected using MW reflect the radiocarbon signature at 0.6m b.g.s and thus when this correction is applied to J_{TSR} measured at surface, it is likely to overestimate the contribution of J_{CSR} and carbon mineralization rate. Consequently, the highest rates of J_{CSR} were calculated using ^{14}C samples collected from soil gas monitoring wells. They contained the highest carbon content per volume, which made analytical processing easier, and allowed for low radiocarbon measurement error of $F^{14}C$ ± 0.0008 to 0.0095.

Soil gas probe (SP) and Static chamber (SC)

The mean F_{CSR} SP (0.18) shows good agreement with F_{CSR} collected from SC (0.19). Despite the spatial differences (0.3 m b.g.s) in sample collection depth, the means were not significantly different (see appendix Figure 5.4). The SC method is more spatially representative of the CO_2 efflux measured at surface, while the SP method reflects the radiocarbon signature of shallow subsurface soil gas. However, the initial 14C signature when the SC chamber is placed is not considered and assumed negligible. At Bemidji, background site (310) values were modern ($F^{14}C$ 1.000 ± 0.0061) in SC samples suggesting the surface background does not deviate from modern radiocarbon values. Conversely, background SP samples had initial depletion ($F^{14}C$ 0.948 ± 0.0117), perhaps affected by a deeper source of depleted soil gas. Overall, our findings indicate these difference were insignificant suggesting both SP and SC method agree well and can be used to represent $J_{CSR.}$

Dynamic Closed Chamber

Both the SC and DCC samples were collected at surface. However, the DCC method differs from the SC both in time and number of samples required. A DCC sample was collected immediately before and after the CO_2 efflux measurement while SC were left to collect soil gas for a 24 hour period. The samples obtained directly from the dynamic closed chamber LI–8100A system accounts for the initial ^{14}C signature directly before the measurement was taken as well as directly after, and thus should be reflective of the difference in ^{14}C collected over the CO_2 efflux measurement time span. However there are many practical difficulties with taking the measurement over this short time interval. The physical sampling time interval over which a 300mL gas sample was extracted for the DCC method was ~210s at the USGS site and ~330s at the USA refinery site. This was initiated after the 90s CO_2 flux measurement. Therefore there is ambiguity in the representative concentration and time used in equation (2.6). To account for this, the F_{CSR} was calculated where final concentration is considered at t=195 seconds. This is the concentration half way through sample extraction and therefore this method assumes this is the most representative of the concentration over the sampling time required. This assumption suggests that the mean F_{CSR} calculated along the north pool transect using samples collected directly from the LI–8100A (DCC method) should be reported as a range with the mean F_{CSR} 0.12 (t_{final}=300s) to mean F_{CSR} 0.23 (t_{final} =90s), which corresponds to the time required for sample extraction in the field. The ambiguity of the sampling time interval creates uncertainty of this measurement approach. However, it can be noted that both the mean F_{CSR} calculated using SP (0.18)and SC (0.19) at Bemidji, MN fall within the range for mean F_{CSR} (0.12–0.23) calculated using the DCC method.

The average error for ambient and post measurement concentrations was $F^{14}C \pm 0.02$. This error is greater than the analytical precision measured using radiocarbon samples taken

from all other methods. Finally, the analytical costs for quantifying J_{CSR} using the DCC method is doubled, by requiring a second $F^{14}C$ value (both $F^{14}C_{initial}$ and $F^{14}C_{final}$) at each sampling location.

5.2. USA REFINERY SITE

The two surface chamber methods (DCC and SC) and the SP method were used at the USA refinery site to compare F_{CSR} contribution to J_{TSR}. The F_{CSR} results on the south property overlay areas of known subsurface contamination and are therefore the most suitable locations for comparison. Analysis of variance (ANOVA) on the log percent modern carbon (pMC) values for each method demonstrated significant variance $F(2,43)=23.24$ $p<0.005$ among the sampling methods used. A post hoc Tukey test showed that while the mean of the radiocarbon collected using SP and SC methods were not significantly different $p<0.05$, both methods had significantly more depleted radiocarbon than mean DCC method. However, the average F_{CSR} across the south property was found to be equal using the DCC to the average F_{CSR} using the other SC and SP methods. The findings of this study indicate the difference in F_{CSR} was found over the hotspots locations, where there was no change in calculated J_{CSR} using DCC method, and there was an increased J_{CSR} calculated using SC and SP methods over the hotspot areas.

SP and SC methods

Similar to the results at Bemidji, the mean $F^{14}C$ collected from SPs and SCs across the refinery site are not significantly different. On the south property. Of fourteen south property locations sampled, only ten locations had data from both SP and SC that could be compared. The average F_{CSR} of these ten locations (N8, K8, J4, I5, F6, F4, E6, E3, D2 and C3) were 0.44 and 0.38 for SP and SC respectively. The F_{CSR} was determined from F_{NSR} that was normalized to the average $F^{14}C$ from the north property sites, which were considered 'background'. However, while the mean $F^{14}C$ at the north property was ~ modern ($F^{14}C$ 0.981 ± 0.01) using SP methods, the SC had an average initial depletion (excluding outlier NP4) in radiocarbon signature ($F^{14}C$ 0.871 ± 0.01). Therefore normalizing SC radiocarbon samples to the background (north property) does not address that initial depleted radiocarbon is present at what has historically been considered background sites. The difference in F_{CSR} for non-normalized data at those sites is 0.45, and 0.46 for SP and SC respectively. This suggests that the susceptibility of the SC method to initial depletion of surface air, causes uncertainty of the method in areas where background air is not modern. The initial depleted radiocarbon signature of SC at the background site may be a result of a 'Seuss effect' where increased fossil fuels in the atmospheric air at surface deplete the background $F^{14}C$ (Seus and Urey, 1956).

The sample yield from 250mL sample for SC and SP were 0.25mgC and 0.20 mgC respectively (Figure 5.2b), which are the within the lower recommended limits for analytical measurement on the AMS (Crann et al. 2016). Both methods had a low mean average radiocarbon error of ± 0.003 and 0.004 for SC and SP respectively.

DCC method

The DCC method depends on the concentration difference over the CO_2 efflux measurement interval where change in radiocarbon is weighted according to the fraction of radiocarbon. Contrary to hypothesis, 6 out of 14 south property sampling locations had an increased, rather than a decreased radiocarbon fraction over the 90s CO_2 efflux measurement interval (Table 4.3). Of these samples all had error greater than $F^{14}C$ ±0.001 on either the prior or post flux radiocarbon sample. Sihota, (2014) found depending on the magnitude of flux, a positive SZNA could still be derived from samples that had increased ^{14}C over the sampling interval (Sihota, 2014). In this study, J_{CSR} at four out of 14 south property locations had a negative F_{CSR} over the measurement interval.

The mean sample yields for the DCC method were the lowest out of the compared methods, and differed significantly from the other two methods. Mean sample yield was 0.13mgC for 500mL initial sample and 0.06mgC for sample collected after the CO_2 efflux measurement. During laboratory processing, sixteen out of the DCC radiocarbon before/after samples had a dead carbon addition (Luxfer G–stor cyclinder) to increase the sample volume to ~0.5 mgC and thus reduce the analytical error. The remaining 22 samples were analyzed without dead carbon addition and ranged from 0.06–0.08 mg C. Three of the sixteen dead carbon addition samples (19%) had analytical error greater than ±0.01 on the AMS where 16 out of 22 (73%) of the samples processed without dead carbon addition had error greater than ±0.01, with a mean error of ±0.02 and maximum error ±0.17. However, while dead carbon addition

reduces the analytical error of the AMS itself, the precision of the dead carbon addition process is another source of error that is less easily quantified. In general, the increased cost of second radiocarbon sample prior to chamber measurement, and reduced accuracy as a result of small sample sizes limits the practicality of the DCC method. Furthermore, the sensitivity of this method to accurately quantify F_{CSR} is not supported by subsurface data in all cases, as it was unable to identify known hot spots (ex. E3) at the de–commissioned refinery site (Sihota 2014). The susceptibility of this method to error makes it a less reliable method for collection of radiocarbon in the field.

5.3. Assumptions of Radiocarbon Simplification

The results of the plant data at both sites clearly supports that the radiocarbon signature of plants is modern with mean $F^{14}C$ 1.02 ± 0.002. This does not support the initial hypothesis that plants overlying hydrocarbon contamination may incorporate ancient radiocarbon into their biological respiration processes. Therefore the assumption that natural soil respiration contributes a modern radiocarbon $F^{14}C \sim 1.00$ is valid.

The radiocarbon simplification ($F_{CSR} = 1 – F^{14}C$) assumes that the initial radiocarbon concentration in the surface chambers is modern, with negligible effect of initial ambient CO_2 concentration on the measured radiocarbon fraction. This assumption was hypothesized to be valid if the concentrations in SCs were significantly higher than

ambient CO_2 concentrations. Results showed that the average concentration in the SCs over 24 hours ranged from 5000– 10 000ppm at Bemidji site and 1000–6000 ppm at the USA refinery site. These concentrations were lower than hypothesized, thus the $F^{14}C$ of ambient air should be considered. The F_{CSR} using SC samples can be re–calculated using equation (2.6) from Chapter 2, which includes the average initial concentration and change in radiocarbon signature (Table 5.6.) This re–calculated average F_{CSR} along the North Pool transect at Bemidji increases from 0.19 to 0.21, and similarly increased from 0.40 to 0.47 across the USA refinery site. The increase F_{CSR} is likely a reflection of initial depleted radiocarbon CO_2 signature which averaged $F^{14}C$ 0.98±0.02 at Bemidji and 0.87±0.02 at the USA refinery. Since the $F^{14}C$ of the CO_2 present before the chamber was placed was near modern at Bemidji, the F_{CSR} varied little after the re–calculation. However, the initial depleted ^{14}C signature of CO_2 overlying the USA refinery site had a more significant increased F_{CSR} calculated using equation (2.6) rather than equation (2.8) radiocarbon simplification. This implies that in cases where background radiocarbon is depleted (<0.9), the radiocarbon simplification may not be valid and initial radiocarbon signature should be accounted for (Sihota, 2014). Based on the results of this study, collecting a background sample ~30cm above ground surface to characterize a site's background signature, may guide if the radiocarbon simplification equation (2.8) can be used prior to a field program.

Using radiocarbon as a tracer for petroleum source assumes that all other sources of ancient ^{14}C in the system are negligible. This assumption is supported by reactive transport models conducted by Molins et al. (2010) where reactive (O_2, CO_2, CH_4) and stagnant gas (Ar, N_2), water flow (infiltration rates, soil hydraulic

parameters), aerobic respiration, Fe and Mn, reduction and methanogenesis data was integrated by previous researchers to model transport in the vadose zone (Molins et al 2010, Dillard et al 1997, Amos et al, 2006). By assuming 4–6% carbonate composition of the aquifer calcite dissolution was modeled under quasi steady state conditions and modeled the contribution of calcite dissolution to carbon flux was negligible (0.2%)(Molins et al 2010 Bennet et al. 1997, Sihota, 2014). Using these simulations, the carbon balance at the Bemidji, Minnesota research site were quantified by Sihota et al. (2011) and determined 98% of carbon mineralized by biodegradation corresponded to CO_2 efflux measured at the ground surface (Sihota et al 2011, Molins et al 2010). The remaining carbon recharged to the saturated zone (Sihota et al 2011, Molins et al 2010).

The results of XRD of shallow soils indicate that the carbon analyzed in soil samples was devoid of carbonate minerals(Table 5.6). The XRD analysis concluded that soil samples consisted of predominantly quartz, albite, sanidine and anorthite at Bemidji, MN and at USA refinery site; quartz, albite, sanidine, anorthite, muscovite and microcline. Thus there does not appear to be an ancient carbonate source in the system.

5.4. Strengths and Limitations

The radiocarbon correction (RCC) method has improved local sensitivity to quantify F_{CSR} as compared to BGC method (Sihota and Mayer 2012, Sihota, 2014). The use of radiocarbon as a tracer is more resistant to fractionation, especially under anaerobic conditions, during microbial degradation processes as compared to stable

carbon isotopes (Conrad et al. 1997, Sihota and Mayer 2012). Furthermore, the $F^{14}C$ signature of NSR is distinct from CSR derived from petroleum products by reflecting two end–member sources of $F^{14}C$ depleted petroleum sources ($F^{14}C$ =0.00) and $F^{14}C$ rich natural soil respiration sources ($F^{14}C$=1.00) (Conrad et al. 1997, Cowie et al. 2010, Sihota and Mayer 2012). The F_{CSR} simplification requires only one radiocarbon isotope measurement, rather than a before and after sample, to identify contribution of petroleum sources to overall J_{TSR}. This reduces analytical costs. As well, the findings of this study determined the three F_{CSR} simplification methods compared (MW, SP and SC) allow for sufficient CO_2 sample for a reliable radiocarbon analysis.

In cases where the background radiocarbon signature is approximately modern the simplified equation (2.8) may be considered representative of the $F^{14}C$ signature of the surface efflux measurement. Alternatively, if the background air at the surface has an initial depleted radiocarbon signature, sampling shallow soil gas may be more representative of the soil efflux from the subsurface. Therefore, in cases where the background air signature at surface is depleted, SP sampling is recommended.

The limitations of using radiocarbon to quantify F_{CSR} of CO_2 efflux measured using an LI–8100A dynamic closed chamber, are increased analytical costs as compared to stable carbon isotopes or BGC method due to required precision of trace concentrations on the AMS. The analytical constraints of this method required increased concentrations of CO_2 for laboratory measurement (Crann et al. 2015). This tracing tool is not effective where significant additional sources of ancient radiocarbon exist, such as in peatlands or carbonate/limestone bedrock (Clark, 2015). However, the

RCC method provides increased precision and a decisive trace for contaminant soil respiration as compared to BGC and stable isotope analysis.

This study can be used to inform methods for correcting CO_2 flux measurements at future CO_2 efflux surveys. The radiocarbon sampling methods described can be used to quantify J_{CSR} that may be used to constrain current models of biodegradation in the subsurface (Molins et al. 2010). Previous methods (Sihota and Mayer, 2012) used for quantifying J_{CSR} using radiocarbon correction method are likely to have overestimated the $F_{CSR.}$ The surface and shallow soil probes methods described may give more representative radiocarbon samples for quantifying F_{CSR} in CO_2 efflux surveys.

Chapter 5 Tables

Table 5. 1 Fraction of contaminant soil respiration (F_{CSR}) for four methods at Bemidji, MN. Averages FCSR is shown for North pool transect and source zone locations.

Well Location	Distance away from oil center (m)	F_{CSR}					
		MW	SP	SC	DCC		
					(90s)	(195s)	(300s)
310	–200.82	0.00	0.00	0.00	–	–	–
603	–118.4	0.17	0.11	0.27	0.10	0.04	0.03
604	–34.04	0.69	0.43	0.29	0.63	0.32	0.23
1302	–23.9	0.71	0.20	0.35	0.47	0.34	0.56
9017	–23.34	0.66	0.50	0.43	0.65	0.35	0.27
1212	–16.92	0.50	0.24	0.19	0.58	0.31	0.23
9016	–12.16	0.39	0.17	0.24	0.60	0.29	0.20
301	–3.41	0.88	0.37	0.34	0.72	0.39	0.29
9015	–1.98	0.73	0.44	0.28	0.78	0.43	0.32
9014	11.75	0.69	0.18	0.20	–	–	–
601	18.03	0.41	0.11	0.22	0.24	0.14	0.11
534	24.73	0.44	0.14	0.28	0.28	0.16	0.13
1402	26.66	-	0.16	0.17	0.02	0.04	0.05
9103	30.24	-	0.13	0.19	ND	ND	ND
533	36.59	0.28	0.09	0.09	ND	ND	ND
9101	41.97	0.40	0.12	0.06	ND	ND	ND
532	47.12	0.36	0.10	0.07	ND	ND	ND
518	57.7	0.22	ND	0.03	ND	ND	0.00
531	68.4	0.11	ND	ND	0.09	0.06	0.05
530	92.86	0.01	ND	ND	–	–	–
Mean	North Pool Transect	0.45	0.18	0.19	0.23	0.13	0.12
	Source Zone	0.60	0.25	0.27	0.48	0.27	0.24

Table 5. 2 Comparison of average F_{CSR} percent difference at Bemidji,MN from F_{CSR} calculated directly from the LI–8100A system at t= 90s, 195s and 300s.

		FCSR					
		MW	SP	SC	DCC		
					(90s)	(195s)	(300s)
North Pool Transect	Average Source zone Mean	0.41	0.22	0.19	0.24	0.13	0.11
		0.56	0.29	0.27	0.47	0.27	0.21
	% difference (90s)	0.53	–0.08	–0.23	0.00	–0.57	–0.76
	% difference (195s)	1.02	0.49	0.36	0.57	0.00	–0.21
	% difference (300s)	1.17	0.69	0.56	0.76	0.21	0.00
Source Zone	% difference (90s)	0.08	–0.24	–0.27	0.00	–0.27	–0.38
	% difference (195s)	0.34	0.03	0.00	0.27	0.00	–0.12
	% difference (300s)	0.45	0.15	0.12	0.38	0.12	0.00

Table 5. 3 Fraction of contaminant soil respiration (FCSR) for four methods at USA refinery site. Averages FCSR is shown for the south property locations

Location		F_{CSR}				
				DCC		
		SP	SC	90 s	225 s	420 s
North Property Site	NP7	ND	ND	-16.41	-6.76	-4.32
	NP6	0.00	ND	2.34	1.21	0.89
	NP5	ND	0.03	0.71	0.43	0.35
	NP4	0.02	0.34	-0.22	-0.04	0.01
	NP1	0.11	0.05	-15.01	-7.49	-5.08
	N8	0.27	0.40	3.41	0.89	0.65
	L8	-	0.64	-0.01	0.17	0.20
	K8	0.58	0.54	3.27	1.49	1.09
	J4	0.44	0.31	0.00	0.04	0.05
	I5	0.09	0.00	0.13	0.13	0.13
South Property Site	F7	0.20	-	-13.11	-4.24	-2.47
	F6*	0.47	0.59	0.63	0.33	0.26
	F4*	0.56	0.45	-0.24	-0.04	0.00
	E6*	0.43	0.24	1.09	0.50	0.37
	E3*	0.68	0.72	-0.71	-0.18	-0.05
	D2*	0.79	0.59	1.23	0.62	0.48
	C3*	0.10	ND	4.84	1.90	1.26
	B7*	0.69	-	-0.37	-0.07	0.00
	B4*	0.27	-	6.89	2.90	1.97
Mean	North property	0.0	0.00	-3.39	-1.29	-0.77
	South Property	0.43	0.40	0.50	0.32	0.28

Table 5. 4 Comparison of average F_{CSR} percent difference at USA refinery site from F_{CSR} calculated directly from the LI–8100A system at t= 90s, 225s and 420s.

		F_{CSR}				
		SP	SC	DCC		
				(90 s)	(225 s)	(420 s)
Mean	South Property	0.44	0.48	0.50	0.32	0.28
% Difference	(90s)	0.13	0.05	0.00	0.45	0.56
	(225s)	0.33	0.41	0.45	0.00	0.12
	(420s)	0.44	0.52	0.56	0.12	0.00

Table 5. 5 Re–calculation of of SC methods using Equation (2.6) in chapter 2. The results from Bemidji are shown in table A) and results from USA refinery site are shown in table B).

A)

Well Location	SC Radiocarbon ($F^{14}C$)	Error (±)	Initial Radiocarbon ($F^{14}C$)	Error (±)	Average Initial CO_2 concentration (ppm)	Final CO_2 concentration (ppm)	F_{CSR}
310	1.000	0.0061	0.947	0.0015	388.2461	10016	0.0038
603	0.733	0.0072	0.990	0.0139	388.2461	7330	0.2813
604	0.714	0.0040	0.995	0.0138	388.2461	7137	0.3024
1302	0.650	0.0030	0.970	0.0692	388.2461	6499	0.3702
9017	0.572	0.0031	0.965	0.0148	388.2461	5717	0.4569
1212	0.809	0.0032	0.981	0.0136	388.2461	8086	0.2000
9016	0.761	0.0042	1.022	0.0013	388.2461		
301	0.660	0.0030	0.972	0.0134	388.2461	6592	0.3603
9015	0.724	0.0029	0.996	0.0014	388.2461	7230	0.2925
9014	0.799	0.0033	-	-	388.2461	7982	
601	0.781	0.0035	0.966	0.0182	388.2461	7800	0.2297
534	0.716	0.0030	0.974	0.0110	388.2461	7157	0.2991
1402	0.833	0.0036	0.930	0.0177	388.2461	8327	0.1720
9103	0.806	0.0046	1.001	0.0121	388.2461	8056	0.2042
533	0.907	0.0037	0.980	0.0137	388.2461	9067	0.0965
9101	0.943	0.0093	0.957	0.0009	388.2461	9418	0.0588
532	0.926	0.0050	0.951	0.0285	388.2461	9254	0.0757
518	0.969	0.0050	0.980	0.0121	388.2461	9679	0.0325
531	1.036	0.0041	0.979	0.0117	388.2461	10347	–0.0369
530	1.025	0.0041	-	-	388.2461	10239	
Mean North Pool Transect	0.81	0.0094	0.98	0.0764	388.2461	8106	0.21
Mean Source Zone	0.72	0.0074	0.98	0.1022	388.2461	7132.8750	0.32

B)

Well Location	SC Radiocarbon ($F^{14}C$)	Error	Initial Radiocarbon ($F^{14}C$)	Error	Initial CO_2 concentration (ppm)	Final CO_2 concentration (ppm)	FCSR
NP7	0.9088	0.0119	0.9351	0.0163	399.8500	1023	0.1081
NP6	0.9098	0.0081	1.0054	0.0087	395.2600	1012	0.1515
NP5	0.8441	0.0065	0.8662	0.0111	420.8800	802	0.1803
NP4	0.5728	0.0094	0.8814	0.0119	418.33	1442	0.5533
NP1	0.8241	0.0208	0.5172	0.1724	413.8800	873	–0.1008
N8	0.5229	0.0062	0.9087	0.0070	398.9700	1762	0.5900
L8	0.3144	0.0032	0.6956	0.0127	411.4500	6232	0.7125
K8	0.405	0.0049	0.9277	0.0085	392.5600	4844	0.6411
J4	0.6026	0.0047	0.9116	0.0097	409.1300	848	0.6857
I5	0.8681	0.0052	0.8676	0.0198	399.1300	4419	0.1319
F7			0.7823	0.0264	400.4300	823	
F6	0.3563	0.0027	0.9481	0.0023	404.5600	1217	0.9382
F4	0.4837	0.001	0.8777	0.1380	417.6200	1239	0.7166
E6	0.6618	0.0014	0.9402	0.0021	405.6400		
E3	0.2447	0.0018	0.6166	0.0052	411.7700	13455	0.7670
D2	0.36	0.0006	0.8890	0.0017	403.6400	2651	0.7350
C3	0.9055	0.0029	1.17329	0.0587	413.3500		
B7			0.7617	0.0020	406.9000	1248	
B4			0.8773	0.0039	399.0000	1462	
Mean North Property	0.76	0.01	0.85	0.04	407.86	1152.30	0.25
Mean South property	0.52	0.00	0.87	0.02	405.30	3349.98	0.66
Mean hot spots	0.46	0.00	0.86	0.04	411.75	5535.94	0.78

Table 5. 6 The $F^{14}C$ and associated mineralogy determined using X–ray diffraction analysis for sediment samples at CO_2 efflux locations.

Site	Sampling Location	Sediment Fraction of Radiocarbon		Mineralogy
		$F^{14}C$	±	
Bemidji,MN	310	1.051	0.0029	Albite, Quartz
	603	0.668	0.0021	Albite, Quartz, Sanidine
	604	–	–	Albite, Quartz
	9017	0.7631	0.0024	Calcian Albite (Na(0.75) Ca (0.25), Quartz
	9016	0.9653	0.0025	Calcian Albite (Na(0.75) Ca (0.25), Quartz
	9015	0.8959	0.0034	Quartz, Albite
	9014	0.8742	0.0023	Albite, Anorthoclase, Quartz
	533	1.0625	0.0036	Sodian Anorthite, Calcian Albite, Quartz
	534	–	–	Albite, quartz
	531	1.0629	0.0024	Sodian Anothite (Na(0.45) Ca0.55), Quartz
USA Refinery	E3	0.1018	0.0007	Quartz, Anorthite, Albite
	F6	0.2039	0.0009	Quartz, Albite, Quartz HP, Alpha Ca SO4, Sanididne, Muscovite
	C3	0.2879	0.0013	Quartz, Albite, Sanidine
	F4	0.2312	0.0013	Quartz, Sanididine, Albite, Montmorillonite, Muscovite,
	J4	0.8309	0.0034	Quartz, Anorthite sodian, microcline intermdiate
	D2	0.2526	0.0013	Quartz, microcline
	K8	0.1485	0.0011	Quartz, Albite, Muscovite
	NP5	0.1243	0.0009	Silicon Dioxide (Quartz) , Muscovite, Albite

Table 5. 7 A comparison of positives and negatives of each method for correcting surface efflux surveys for contribution of petroleum derived contaminant soil respiration CO_2 efflux (J_{CSR}).

Method	*Pros*	*Cons*
MW	Increased sample yield for easy lab processing, used previously	Expensive, involves drilling or existing soil gas monitoring network, overestimates contribution of FCSR to surface efflux
SP	statistically similar to other methods, representative of shallow subsurface soil gas, sample yield within recommended limits, allows for sample collection on same day	Spatial discrepancy between surface flux and sample
SC	statistically similar to other methods, spatially representative to surface efflux	Susceptible to initial dilution of ambient air, requires 24 hour collection time
DCC	Spatially representative, considers initial local 14C signature	Low sample yields are below recommended limits for processing, increased error in analytical processing, discrepancy between sampled CO2 concentration and time obtained
BGC	Cheaper, less analytical processing	Does not consider variations in background across site, cannot identify CSR below background threshold

Chapter 5 Figures

a)

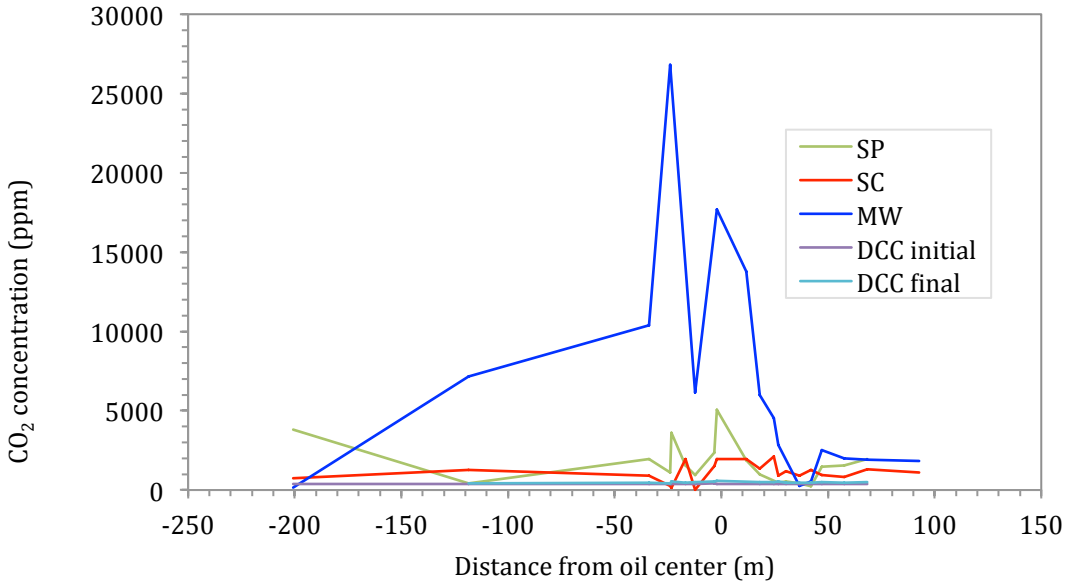

b)

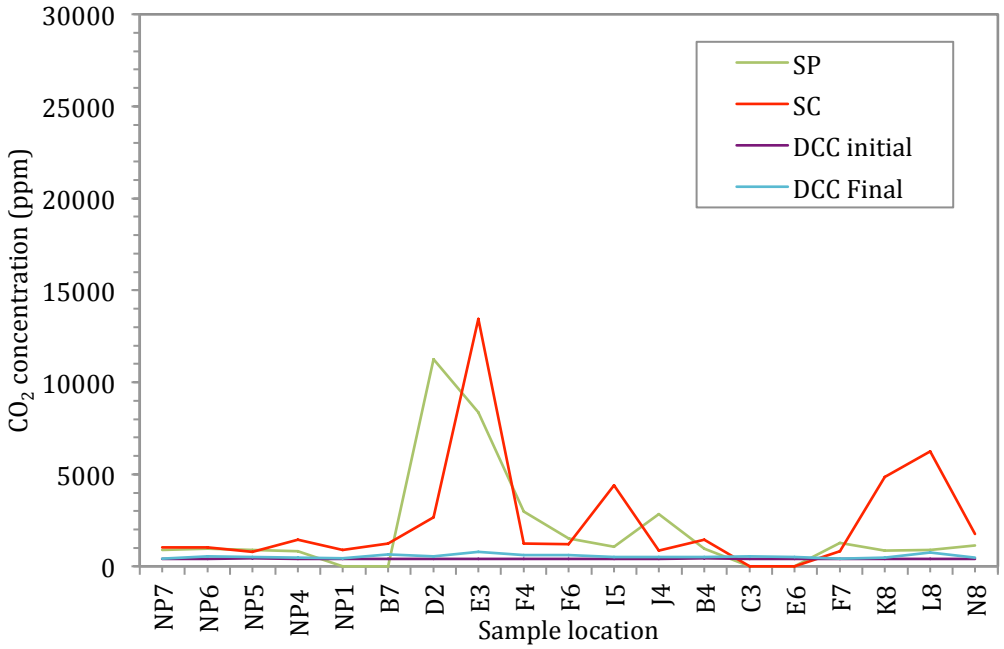

Figure 5. 1 Shows the concentration of CO_2 collected using MW, SP, SC and DCC methods at a) Bemidji National Crude oil spill research site and b) USA refinery site.

a)

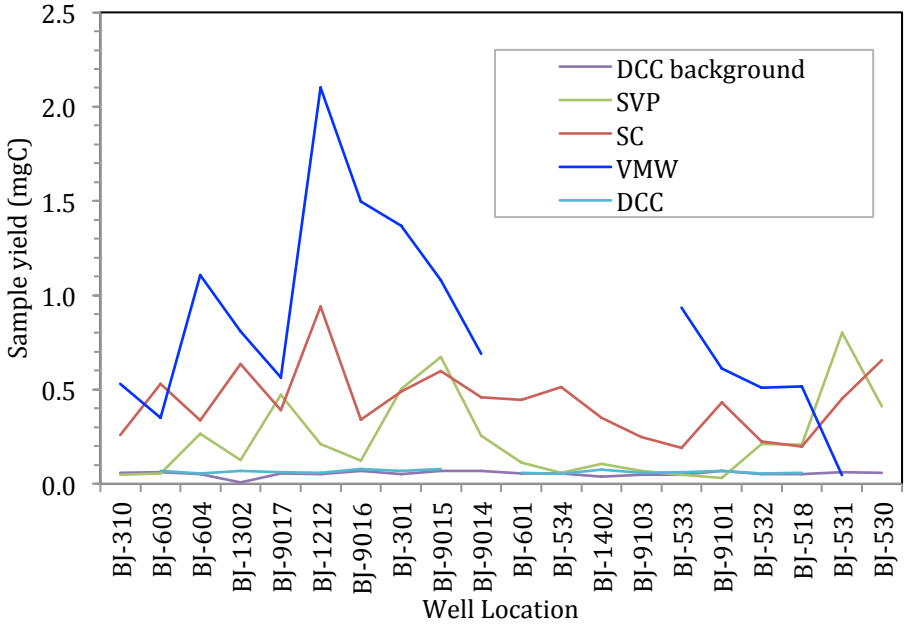

b)

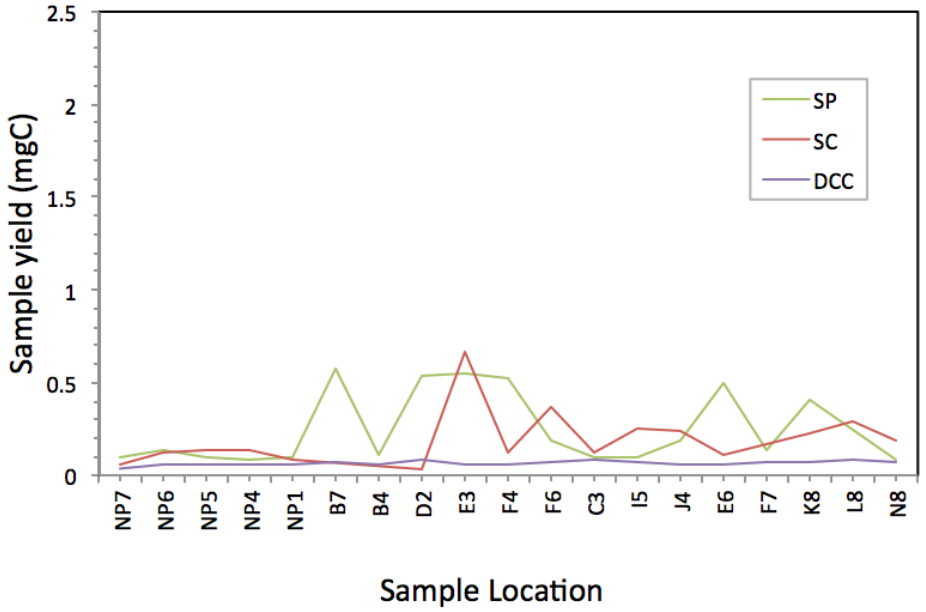

Figure 5. 2 Shows the sample yields using MW, SP, SC and DCC field sampling at a) Bemidji National Crude oil spill research site b) USA refinery site. The amount recommended for analytical analysis is 0.2– 0.5 mgC.

A)

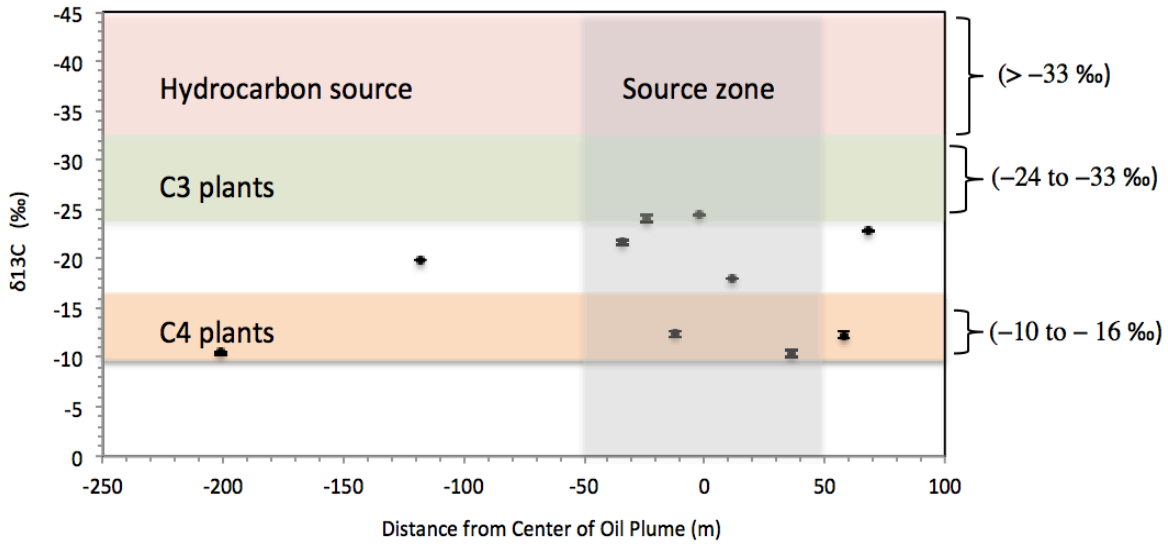

B)

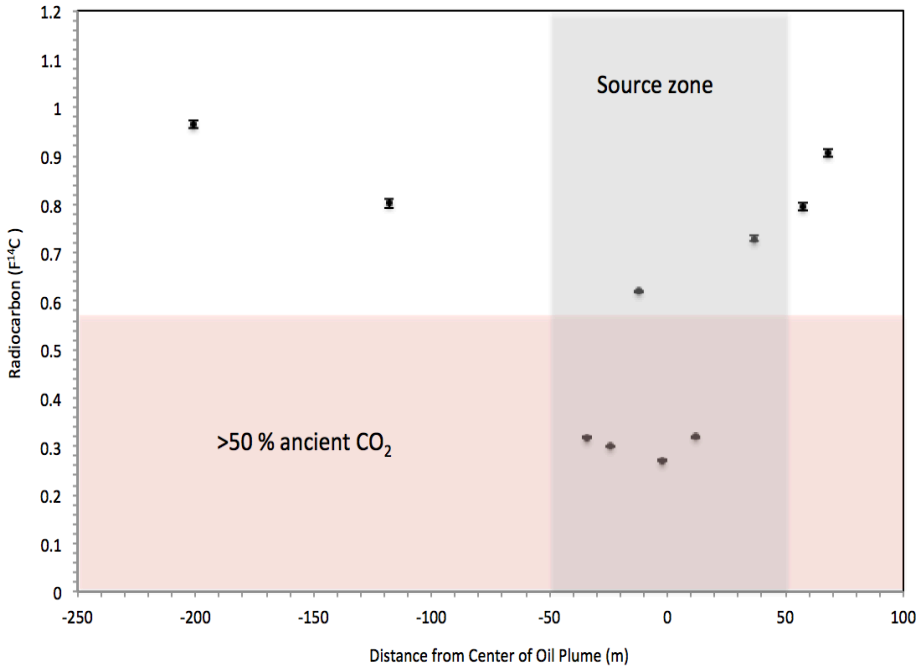

Figure 5. 3 A) The δ13C (‰) compared to B) the $F^{14}C$ of radiocarbon collected from MW from ten locations along the North Pool Transect at Bemidji, MN.

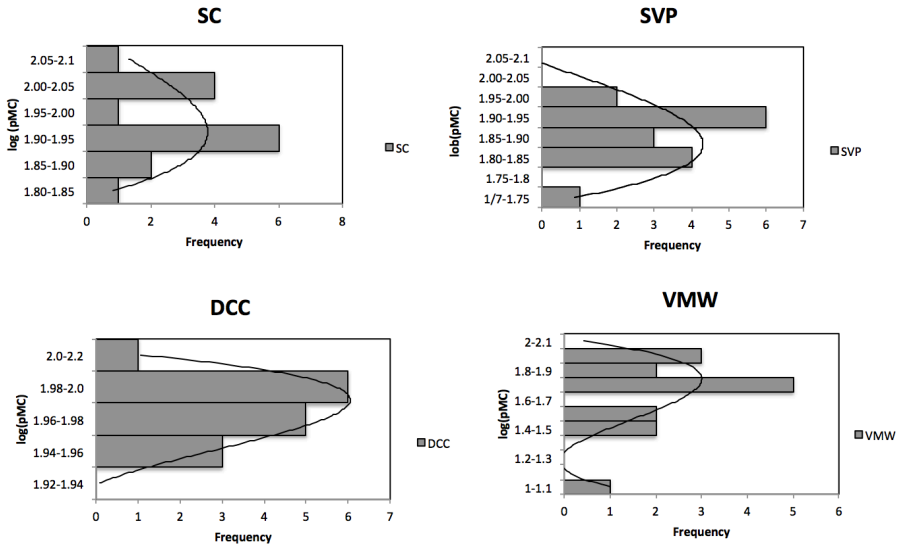

SUMMARY

Groups	*Count*	*SUM*	*Average*	*Variance*	*SD*
SC	15	28.405	1.894	0.005	0.073
SP	15	28.078	1.872	0.010	0.099
MW	15	25.305	1.687	0.055	0.235
DCC	15	29.698	1.980	0.000	0.016

ANOVA

Source of Variation	*SS*	*df*	*MS*	*F*	*P-value*	*F-crit*
Between Groups	-1.94114553	3	-0.64704851	-7.92	<0.005	4.73
Within Groups	4.575412216	56	0.08170379			
Total	2.634266686	59				

TUKEY POST HOC TEST

Groups	*Q-value*	*Tukey Statistic*	*Mean*	*Difference*	*Difference*	*Difference*
	3.74	0.276		SP	MW	DCC
SC			1.894	0.022	0.207	0.086
SP			1.872		0.185	0.108
MW			1.687			0.293
DCC			1.980			

Figure 5. 4 Shows the log–normal distribution of the four methods analyzed at Bemidji, MN. The results show a near– normal distribution for groups used in the ANOVA mean variance analysis tests.

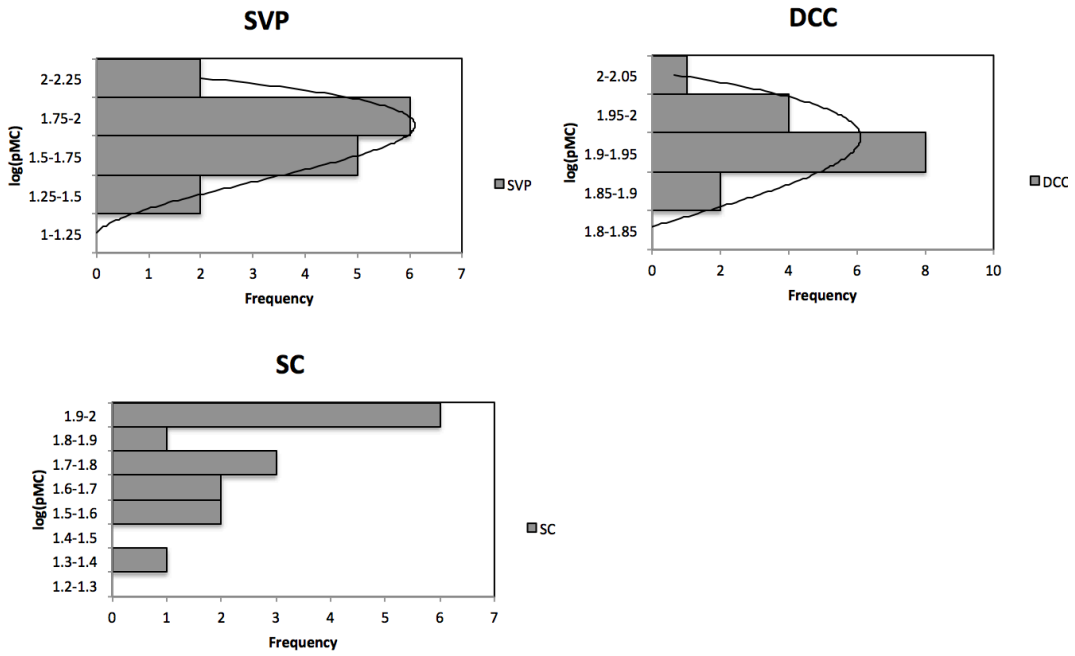

SUMMARY

Groups	*Count*	*SUM*	*Average*	*Variance*	*SD*
SC	15	26.521	1.768	0.033	0.181
SP	15	26.960	1.797	0.046	0.213
DCC	15	29.092	1.939	0.001	0.037

ANOVA

Source of Variation	*SS*	*df*	*MS*	*F*	*P-value*	*F-crit*
Between Groups	0.71	2	0.36	23.24	0.005	6.07
Within Groups	0.66	43	0.02			
Total	2.634266686	59				

TUKEY POST HOC TEST

Groups	*Q-value*	*Tukey Statistic*	*Mean*	*Difference*	*Difference*
	3.44	0.110		SP	DCC
SC			1.768	0.029	0.171
SP			1.797		0.142
DCC			1.939		

Figure 5. 5 Shows the log–normal distribution of the four methods analyzed at USA de-commisioned refinery site. The results show a near– normal distribution for groups used in the ANOVA mean variance analysis tests.

Chapter 6

6. SUMMARY AND CONCLUSIONS

6.1. SUMMARY

Surface CO_2 efflux surveys are a non–invasive and inexpensive method for initial site investigation and ongoing monitoring of subsurface biological activity at degradation sites. It is a useful and practical surface tool for assessment of natural attenuation as a remediation strategy of hydrocarbons in the subsurface. This study supports findings of Sihota and Mayer (2012), that radiocarbon is an effective tool for quantifying J_{CSR} with an evaluation of four sampling methods. The key findings of this comparison of the four methods are summarized below.

1. Vapor Monitoring Wells (MW):

Gas samples obtained from soil gas monitoring wells (which are at greater depth compared to surface measurements) have the highest CO_2 yields and the most depleted radiocarbon values, compared to samples from other techniques. The increased sample yields from MW leads to easier processing and graphitization for analysis on the accelerator mass spectrometer. However, because these samples are collected at ~0.6m depth, the MW samples overestimate the proportion of radiocarbon that reaches the surface, compared to gas samples collected closer to the surface. Therefore, sampling MW samples over-represent the true proportion of ancient radiocarbon present in the efflux arriving at the surface.

2. LICOR LI–8100A Dynamic Closed Chamber (DCC):

In contrast, the radiocarbon sampling method directly from the LI–8100A Dynamic Closed Chamber attempts to reflect the proportion of J_{CSR} at the surface, both temporally and spatially, by considering the change of ancient $^{14}CO_2$ over the time interval. However, because this sampling method is dominated with low-concentration atmospheric CO_2 the sample yields in the laboratory are below recommended limits required for graphitization and analysis on the accelerator mass spectrometer. Despite experimentation with lower analytical limits of the accelerator mass spectrometer, the results still showed increased analytical error for the radiocarbon value measured on the accelerator mass spectrometer, as well as increased process error. These practical limits of the radiocarbon laboratory process reduce the consistency of the results. Analysis suggested that this decreases the DCC method's ability to clearly identify and quantify the contribution of J_{CSR} to J_{TSR} measurements.

Increasing the sample size with a dead carbon addition was done in an attempt to reduce analytical error on the AMS . This effectively reduced analytical error, however it increased the process error. If this dead carbon addition method is implemented in the future, it is recommended that further work be done to quantify the process error of dead carbon addition to samples.

The results obtained in this study show that sampling radiocarbon directly from the LI–8100A dynamic closed chamber provides the lowest estimates of the contribution of petroleum–degradation derived efflux. We suggest this is a result of the

practical limitations of analytical processing and thus the time interval that provides optimal estimates of J_{TSR} is believed to be too small to adequately sample ^{14}C and make a radiocarbon correction that is representative of the subsurface processes. Furthermore, practical sampling limitations lead to ambiguities between the appropriate concentration and flux time interval to use.

3. Soil Gas Probes (SP) and Static Chamber (SC) Methods:

The study found that the results of radiocarbon samples obtained from SP and SC methods were in relatively close agreement in many cases. Both methods had sample yields within the recommended limits required for analysis on the AMS. The SCs are spatially representative of the LI–8100A dynamic closed chamber CO_2 efflux measurement. The SC sampling requires a 24 hour accumulation period prior to sampling in contrast with 90s CO_2 efflux measurements, adding a temporal variable to the radiocarbon correction of CO_2 efflux measurements. However, we argue that this would reflect the proportion of radiocarbon representative of the fraction of J_{CSR} to the average J_{TSR}. In contrast the SP samples are collected from 30cm b.g.s and thus show both temporal and spatial deviation when correcting the survey LI8100A– efflux measurement.

Therefore, the SC radiocarbon collection method for J_{CSR} contribution provides an inexpensive, spatially representative method with sufficient sample yield for effective radiocarbon correction for J_{CSR} contribution to total CO_2 efflux in surface surveys. Similarly, SPs provide representative radiocarbon samples despite spatial discrepancies. Furthermore, this method may avoid initial dilution of $F^{14}C$ at sites

where modern background location does not exist. Either SP or SC methods may be implemented during CO_2 efflux surveys to delineate source zones at lesser–understood contaminated sites prior to subsurface sampling. These radiocarbon methods may increase resolution of CO_2 efflux surveys used as an initial tool to identify hot spots and guide further site investigation. Pairing repeat surface LI–8100A CO_2 efflux measurements with radiocarbon isotopic analyses allows for quantification of the contribution of petroleum degradation to total CO_2 efflux at site locations. These values can be used to constrain models of subsurface transport and aid in estimating source zone depletion rates.

6.2. CONCLUSION

After analyzing radiocarbon samples obtained from soil gas monitoring wells, SPs, SCs and directly from LI-8100A DCC, and comparing the associated correction for petroleum source contribution in CO_2 efflux surveys, results show that radiocarbon simplification using shallow SPs (<30cm b.g.s) and surface SCs are sufficient to quantify the contribution of petroleum degradation to total surface CO_2 efflux. The results of soil gas monitoring wells collected at 0.6m b.g.s appear to over-estimate the J_{CSR} reaches the surface. Alternatively, samples collected directly from DCC do not meet laboratory processing standards and are likely to under-represent the contribution of derived CO_2 due to significant dilution with atmospheric CO_2. While the SC is spatially representative of surface efflux values, the SP avoids radiocarbon depletion signature from outside surface sources. This thesis demonstrated that previous methods of

radiocarbon correction from soil gas monitoring wells may be subject to overestimate the contribution of J_{CSR} to total measured CO_2 efflux overlying hydrocarbon source zones. Both SP and SC methods were found to obtain representative radiocarbon samples and provide reasonable estimates of source zone natural attenuation at hydrocarbon bioremediation sites.

7. REFERENCES

[1] Aelion, M., P. Höhener, D. Hunkeler, and R. Aravena, editors (2010). Environmental isotopes in biodegradation and bioremediation. Taylor and Francis, Boca Raton, FL.

[2] Aggarwal, P. and Hinchee, R (1991) Monitoring Insitu Biodegredation using Stable Carbon Isotopes. *Enviornmental Science Technology* **25:** 1178– 1180

[3] Amos, R.T., K.U. Mayer, B.A. Bekins, G.N. Delin, and R.L. Williams (2005) Use of dissolved and vapor–phase gases to investigate methanogenic degradation of petroleum hydrocarbon contamination in the subsurface. Water Resour. Res. **41**: W02001.

[4] Amos, R. Bekins, B., Delin, G. Cozzarelli, I., Blowes, D. And Kirshtein, J. (2011) Methane oxidation in a crude oil contaminated aquifer: Delineation of aerobic reactions at the plume fringes *Journal of Contaminant Hydrology* **125:** 13–25

[5] Anderson and Libby (1947) Natural Radiocarbon from Cosmic Radiation *Physical Review* **72:** 931–934

[6] Bekins, B. Godsy, E. ,and Warren, E. (1999) Distribution of microbial physiologic types in an aquifer contaminated by crude oil. Microb. Ecol. **37**:263 – 275.

[7] Bekins, B., Cozzarelli, E. Godsy, E. Warren, E. Essaid, H. and Tucillo, M. (2001). Progression of Natural attenuation processes at a crude oil spill site II. Controls on spatial distribution of microbial populations. *Journal of Contaminant Hydrology.* **53:**387–406

[8] Bekins, B.A., F.D. Hostettler, W.N. Herkelrath, G.N. Delin, E. Warren, and H.I. Essaid (2005) Progression of methanogenic degradation of crude oil in the subsurface. Environ. Geosci. **12**: 139–152

[9] Baedecker, M., Cozzarelli, I., Eganhouse, P., Siegel, D. and Bennet, P. (1993) Crude oil in a shallow sand and gravel aquifer– III. Biogeochemical reactions and mass balance modeling in anoxic groundwater. *Applied Geochemsitry* **8:** 569 – 586.

[10] Brock, F., Higham, T., Ditchfield, P. and Ramsey, C. (2010) Current pre–treatment methods for AMS Radiocarbon dating at the oxford radiocarbon accelerator Unite (ORAU) *Radiocarbon* **52:** 103– 112

[11] CCME (2008) Soil, petroleum hydrocarons PHC in *Canada–wide standard for petroleum hydrocarbon (PHC) in soil technical report*

[12] Clark, I. and Fritz, P. (1997) *Environmental Isotopes in hydrogeology,* 1st ed. Boca Raton, Fl: CRC Press.

[13] Clark, I. (2015). *Groundwater Geochemistry and Isotopes*. CRC Press.

[14] Chaplin, B., Delin, G., Baker, R. and Lahvis, M. (2002)Long–Term Evolution of Biodegradation and Volatilization Rates in a Crude Oil–Contaminated Aquifer *Bioremediation Journal* **6:** 237– 255

[15] Crann, C.A., Murseli, S., St–Jean, G., Zhao, X., Clark, I.D. and Kieser, W.E. (2016) First status Report on Radiocarbon Sample Preparation Techniques at the A.E. Lalonde AMS Laboratory (Ottawa, Canada),*Radiocarbon*, , pp. 1–10. doi: 10.1017/RDC.2016.55

[16] Conrad, M. Templeton, A. Dalye, P. and Alvarez–Cohen, L. (1999). Isotopic evidence for biological controls on migrations of petroleum hydrocarbon. *Organic Geochemistry.* **30**: 843– 859

[17] Conrad, M. Daley, P. Fischer, M., Buchanan, B., Leighton, T. and Kashgarian, M (1997). Combined 14C and 13C Monitoring of in Situ Biodegradation of petroleum hydrocarbons. *Environ. Sci. Technol.* **31:** 1463– 1469

[18] Coffin, R., Pohlman, J., Grabowski, K., Knies, D., Plummer, R., Magee, R., and Boyd, T. (2008) Radiocarbon and stable Carbon Isotope Analysis to Confirm Petroleum Natural Attenuation in the Vadose Zone *Enviornmental Forensics* **9:** 75– 84

[19] Cowie, B . Greenberg, B. and Slater, G. (2010). Determination of microbial carbon sources and cycling during remediation of petroleum hydrocarbon impacted soil using natural abundance 14C analysis of PLFA. *Environ. Sci Techno.* **44:**2322–2327

[20] Cozzarelli, I.M., B.A. Bekins, M.J. Baedecker, G.R. Aiken, R.P. Eganhouse, and M.E. Tuccillo (2001) Progression of natural attenuation processes at a crude–oil spill site: I. Geochemical evolution of the plume. J. Contam. Hydrol. **53**: 369–385

[21] Delin, G. N., Essaid, H. I., Cozzarelli, I. M., Lahvis, M. H., & Bekins, B. A. (1998). Ground water contamination by crude oil near Bemidji, Minnesota *US Geological Survey* No. 084–98

[22] Dillard. L., Essaid, H., Herklrath,W. (1997). Multi–phase flow modeling of crude–oil spill site with bimodal permeability distribution. *Water Resources* **33:** 1617–1632

[23] Dörr, H., and Münnich, K. (1986) Annual variations of the 14C content of soil CO2 *Radiocarbon* **28**:338– 345

[24] Etkin, D. (2009) Environmental Research Consulting: Analysis of U.S Oil Spillage *American Petroleum Institute* **356:** 1– 71

[25] Franzi, D. (1988) Surficial and subsurface distribution of aquifer sediments at the Bemidji, Minnesota, research site. In: ragone, S.E. (ed.) US geological Survey program of toxic water–Groundwater Contaminantion– Procedding of the second technical meeting, Cape Cod MA 21– 25 October, 1985 U.S. Geological Survey Open–File Report 86–481 pp. C5– C10

[26] Godwin, H. (1962) Half–life of radiocarbon *Nature* **195:** 984– 984.

[27] Hult, M. and Grabbe, R. (1988). Distribution of gases and hydrocarbon vapours in the unsaturated zone. *US Geological Survey program on toxic waste–groundwater contamination–Proceedings of the second technical meeting, Cape Cod, MA 21–25 October 1985* U.S Geological Survey Open–File Report 86–481 p. C17– C20

[28] Johnson, P. Lundegard p. and Liu, Z (2006)) Source Zone Natural Attenuation at Petroleum hydrocarbon spill sites I Site specific assessment approach *Groundwater Monitoring and Remediation* **4:** 82–92

[29] Landmeyer, J., Vroblesky, D. and Chapelle, F. (1996). stable carbon isotope evidence of biodegradation zonation in a shallow jet–fuel contaminated aquifer *Environ. Sci. Technol.* **30:** 1120–1128

[30] Libby, W., Arnold, E. and Anderson J. (1949) Age determination by radiocarbon content: World wide assay of natural radiocarbon *Science.* **109:** 227– 228

[31] LI–COR, 2007. Automated Soil CO2 Flux System & LI–8150 Multiplexer Instruction Manual, 2nd Ed. [Online]; LI–COR Inc.: Lincoln, Nebraska, p. 60

[32] Lundengard and Johnson (2006) Source Zone Natural Attenuation at Petroleum hydrocarbon spill sites II. Application to former oil field. *Groundwater Monitoring and Remediation* **4:** 93–106

[33] Molins, S., K.U. Mayer, R.T. Amos, and B.A. Bekins (2010) Vadose zone attenuation of organic compounds at a crude oil spill site – Interactions between biogeochemical reactions and multicomponent gas transport. J. Contam. Hydrol. **112** :15–29

[34] Mulligan, C. and Yong, R. (2004). Natural attenuation of contaminated Soils. *Environ. Int.* **30:** 587– 601

[35] National Research Council, Alternatives for Groundwater Cleanup, 315 pp., National Academy Press, Washington, D.C., 1994.

[36] Kieser WE, Zhao X–L, Clark ID, Cornett RJ, Litherland AE, Klein M, Mous DJW, Alary J–F. 2015. The André E. Lalonde AMS Laboratory – the new accelerator mass spectrometry facility at the University of Ottawa. Nuclear Instruments and Methods in Physics Research B **361**:110–4

[37] Olsson, I. (1970). The use of oxalic acid as a standard. *Radiocarbon variations and absolute chronology*, **17:** 10– 17

[38] Plastra, S and Meijer, A. (2014). Biogenic Fraction of biogas and natural gas fuel mixture determined with 14C *Radiocarbon* **56:** 7– 28

[39] Reimer, P., Vardm E. Bayliss, A., Beck, J. Blackwell, P., Ramsey, C., Grootes, P., Guilderson, T., Haflidason, H., Hajdas, I., Hatte, C. Heaton, T., Hoffman, D. Hogg, A., Hughen, K. Kaiser, K., Kromer, B., Manning, S., Niu, M., Reimer, R., Richards, D., Scott, E., Southon, J., Staff, R., Turner, C and van de Plicht, J. (2013) Intcal 13 and marine 13 radiocarbon age calibration curves 0– 50 000 years Cal BP. *Radiocarbon* **55:** 1869– 1887

[40] Seuss, H. and Urey, H. (1956) Abundances of elements *Review of Modern Physics* **28:** doi:10.1103/RevModPhys.28.53.

[41] Stuiver, M., Reimer, P.J., Bard, E., Beck, J., Burr, G., Hughen, K., Kromer, B., McCormac, G., van der Plicht, J., and Spurk, M. (1998) INTCAL98 radiocarbon age calibration, 24,000–0 cal BP. *Radiocarbon* **40**: 1041– 1083.

[42] Sihota , N. Singurindy, O. and Mayer, K.U. (2011) CO2–effluc measurements for evaluating source zone natural attenuation rates in a petroleum hydrocarbon contaminated aquifer *Environ. Sci and Technology* **45:** 482 –488

[43] Sihota, N. and Mayer, U. (2012) Characterizing vadose zone hydrocarbon biodegradation using carbon dioxide effluxes, isotopes and reactive transport modelling. *Vadose Zone Journ*. **11:** doi:10.2136/vzj2011.0204

[44] Sihota, N. and Mayer K.U (2015). Comparison of Source Zone Natural Attenuation Rates at Crude oil and Ethanol–Blended Fuel Release Sites. *Bioremediation* **19:** 218 –230

[45] Sihota, N., Trost, J., Bekins, B. Berg, A. Mason, B. Warren, E and Mayer, K.U (2016) Seasonal variability in vadose zone biodegradation at a crude oil pipeline rupture site. *Vadose Zone Journal* **15**

doi:10.2136/vzj2015.09.0125

[46] Sihota, N. (2014). Novel approaches for quantifying source zone natural attenuation of fossil and alternative fuels. *University of British Columbia* DOI: 10.14288/1.0166025

[47] Stenström K, Skog G, Georgiadou E, Genberg J, Johansson A.(2011) A guide to radiocarbon units and calculations. LUNFD6 NFFR-**3111**:1-17

[48] St–Jean, G., Kieser, W.E., Crann, C.A. and Murseli, S. (2016) Semi–Automated Equipment for CO_2 Purification and Graphitization at the A.E. Lalonde AMS Laboratory (Ottawa, Canada), *Radiocarbon*, , pp. 1–16. doi: 10.1017/RDC.2016.57.

[49] Suchomel, K Kreamer, D. Long, A.(1990) Production and Transport of Carbon Dioxide in a Contaminated Vadose Zone: A Stable and Radioactive Carbon Isotope Study *Environ. Sci. Tech* **24:** 1824 – 1831

[50] Tuccillo, M. Cozarelli, I. and Herman, J. (1999) Iron reduction in the sediments of a hydrocarboncontaminated aquifer *Applied Geochemistry* **14:** 655–667

[51] Trumbore, S. (2000). Age of Soil organic matter and soil respiration: Radiocarbon Constraints on Belowground C dynamics. *Ecological Applications* **10:**399 –411.

[52] Revesz,K. Coplen, T. Baedecker, M. and Glynn,P. (1995) Methand production and consumpito monitored by Stable H and C isotope ratios at a crude oil spill site, Bemidji, Minnesota*. Applied Geochemsitry***10:**505 –516

[53] Warren, E. Sihota, N. Hostettler, F. and Bekins, B. (2014). Comparison of surficial CO_2 efflux to other measures of subsurface crude oil degradation **184:** 275 –284

[54] Wigley, T., Plummer L., and Pearson F. (1978) Mass transfer and carbon isotopes evolution in natural water systems *Geochimica et Cosmochimica Acta* **42:** 1117 –1139

8. APPENDIX

Table A. 1 Well information for North Pool Transect at Bemidji, MN

Well	Distance from Oil center (m)	Longitude NAD 83	Latitude NAD 83		Elevation NAV D 88 (m ASL)	DATE CONSTR UCTED	Number of Screens	Screen Material	DIAMETER OF DRILL HOLE (INCHES)	Casing Diame ter (INCH ES)	Casing material	Botto m of Screen m ASL	top of scre en m AS L	total well depth Ft BSL
BJ–310	–200.82	342603.2	5270956.58	BACK GROUND	433.681	NA		STAINL ESS STEEL	7.25	2.04"	STAINL ESS STEEL			
BJ–603	–118.40	342679.87	5270987.01	SPRAY ZONE	431.363	NA		STAINL ESS STEEL	7.25	2.04"	STAINL ESS STEEL			
BJ–604	–34.04	342753.23	5271029.69	NWT	430.473	JUNE 1986		STAINL ESS STEEL	7.25	2.04"	STAINL ESS STEEL			
BJ–1302	–23.90	342761.78	5271035.42	SOURCE ZONE	430.178	MAY 2013		STAINL ESS STEEL	8.25	2.04"	PVC THREAD ED	7.22	6.5 6	17.22
BJ–9017	–23.34	342763.57	5271032.76	SOURCE ZONE	430.136	JULY 2004		STAINL ESS STEEL	7.25	2.04"	PVC THREAD ED			
BJ–1212	–16.92	342768.07	5271038.45	SOURCE ZONE	430.215	JUNE 2012	10 1"	STAINL ESS STEEL	7.25	2.04"	PVC	428.65 4	424 .48 5	18.8
BJ–9016	–12.16	342773.94	5271036.96	SOURCE ZONE	430.229	JULY 2004		STAINL ESS STEEL	7.25	2.04"	PVC THREAD ED			
BJ–301	–3.41	342780.28	5271044.25	SOURCE ZONE	430.621	NA		STAINL ESS STEEL	7.25	2.04"	STAINL ESS STEEL			
BJ–9015	–1.98	342787.9	5271040.35	SOURCE ZONE	430.789	JULY 2004		STAINL ESS STEEL	7.25	2.04"	PVC THREAD ED			
BJ–9014	11.75	342795.65	5271046.99	SOURCE ZONE	431.892	JULY 2000		STAINL ESS STEEL	7.25	2.04"	PVC THREAD ED			
BJ–601	18.03	342803.85	5271043.98	SOURCE ZONE	432.65	NA		STAINL ESS STEEL	7.25	2.04"	STAINL ESS STEEL			
BJ–534	24.73	342810.46	5271045.59	SOURCE ZONE	432.14	NA		STAINL ESS STEEL	7.25	2.04"	STAINL ESS STEEL			
BJ–1402	26.66	342812.26	5271046.3	SOURCE ZONE	432.822	MAY 2014	11 1"		8.25	2.04"	PVC THREAD ED	425.82 1	432 .32 2	22.97
BJ–9103	30.24	342815.22	5271048.46	NWT	432.85	OCT 1991	8 1"	STAINL ESS STEEL	7.25	2.04"	PVC THREAD ED	426.35 2	482 .35	21.32
BJ–533	36.59	342820.96	5271051.17	NWT	432.944	NA		STAINL ESS STEEL	7.25	2.04"	STAINL ESS STEEL			
BJ–9101	41.97	342825.92	5271053.26	NWT	432,776	MAY 1990		STAINL ESS STEEL	7.25	2.04"	STAINL ESS STEEL			
BJ–532	47.12	342830.71	5271055.16	NWT	433.072	NA		STAINL ESS STEEL	7.25	2.04"	STAINL ESS STEEL			
BJ–518	57.70	342840.39	5271059.45	NWT	433.117	NA		STAINL ESS STEEL	7.25	2.04"	STAINL ESS STEEL			
BJ–531	68.40	342849.7	5271064.85	NWT	433.014	NA		STAINL ESS STEEL	7.25	2.04"	STAINL ESS STEEL			
BJ–530	92.86	342870.99	5271077.16	NWT	433.293	NA		STAINL ESS STEEL	7.25	2.04"	STAINL ESS STEEL	NA	NA	NA

Table A. 2 Radiocarbon results from Bemijdi, MN samples measured on the AMS.

Lab ID	Submitter ID	Material	^{14}C age BP	±	F^{14}C	±	mgC
*UOC–1258	BJ–0310–DCC–0815–A	Gas	17169	105	0.118	0.0015	0.26
Sample lost	*BJ–0310–DCC–0815–B*	*Gas*	——	——	——	——	
UOC–1260	BJ–0310–SC–0815	Gas	–13	119	1.0016	0.0148	0.31
UOC–1261	BJ–0310–SP–0815	Gas	439	465	0.9468	0.0548	<0.10
UOC–1262	BJ–0310–MW–0815	Gas	291	59	0.9644	0.007	0.53
UOC–1263	BJ–0603–DCC–0815–A	Gas	93	392	0.9885	0.0483	<0.10
UOC–1264	BJ–0603–DCC–0815–B	Gas	129	313	0.984	0.0383	<0.11
*UOC–1265	BJ–0603– SC–0815	Gas	6666	133	0.4361	0.0072	0.54
UOC–1266	BJ–0603–SP–0815	Gas	1337	400	0.8467	0.0422	<0.10
UOC–1267	BJ–0603–MW–0815	Gas	1774	95	0.8019	0.0095	0.35
UOC–1268	BJ–9103–SC–0815	Gas	1737	117	0.8056	0.0118	0.25
UOC–1269	BJ–9103–SP–0815	Gas	1559	320	0.8236	0.0328	<0.10
Removed	*BJ–9103–MW–0815*	*Gas*	——	——	——	——	
Removed	*BJ–0530–DCC–0815–A*	*Gas*	——	——	——	——	
Removed	*BJ–0530–DCC–0815–B*	*Gas*	——	——	——	——	
UOC–1273	BJ–0530–SC–0815	Gas	–190	84	1.0239	0.0107	0.41
UOC–1274	BJ–0530–SP–0815	Gas	190	204	0.9766	0.0248	0.11
UOC–1275	BJ–0530–MW–0815	Gas	–87	36	1.0109	0.0046	0.7
UOC–1276	BJ–1402–DCC–0815–A	Gas	596	643	0.9285	0.0743	<0.10
UOC–1277	BJ–1402–DCC–0815–B	Gas	551	307	0.9337	0.0357	<0.10
UOC–1278	BJ–1402–SC–0815	Gas	1470	91	0.8327	0.0095	0.35
UOC–1279	BJ–1402–SP–0815	Gas	1886	222	0.7908	0.0219	0.11
Sample lost	*BJ–1402–MW–0815*	*Gas*	——	——	——	——	
UOC–1281	BJ–1302–DCC–0815–A	Gas	276	4615	0.9662	0.555	<0.10

UOC–1282	BJ–1302–DCC–0815–B	Gas	492	334	0.9406	0.0391	<0.10
UOC–1283	BJ–1302–SC–0815	Gas	3462	80	0.6499	0.0065	0.63
UOC–1284	BJ–1302–SP–0815	Gas	2278	184	0.753	0.0172	0.12
UOC–1285	BJ–1302–MW–0815	Gas	9664	38	0.3003	0.0014	2.09
UOC–1286	BJ–9015–SC–0815	Gas	2605	72	0.723	0.0065	0.59
UOC–1287	BJ–9015–SP–0815	Gas	5121	73	0.5286	0.0048	0.67
UOC–1288	BJ–9015–MW–0815	Gas	10503	45	0.2705	0.0015	1.08
Sample lost	*BJ–9014–DCC–0815–A*	*Gas*	—	—	—	—	
UOC–1290	BJ–9014–DCC–0815–B	Gas	510	373	0.9385	0.0435	<0.10
UOC–1291	BJ–9014–SC–0815	Gas	1810	82	0.7982	0.0081	0.46
UOC–1292	BJ–9014–SP–0815	Gas	1983	114	0.7813	0.0111	0.25
UOC–1293	BJ–9014–MW–0815	Gas	9175	64	0.3191	0.0025	0.69
UOC–1294	BJ–9017–DCC–0815–A	Gas	298	402	0.9636	0.0482	<0.10
UOC–1295	BJ–9017–DCC–0815–B	Gas	862	398	0.8982	0.0446	<0.10
UOC–1296	BJ–9017– SC–0815	Gas	4491	100	0.5717	0.0071	0.39
UOC–1297	BJ–9017–SP–0815	Gas	5994	89	0.4742	0.0053	0.47
UOC–1298	BJ–9017–MW–0815	Gas	8413	60	0.3509	0.0026	0.57
UOC–1299	BJ–9016–SC–0815	Gas	2206	104	0.7599	0.0099	0.34
UOC–1300	BJ–9016–SP–0815	Gas	1931	192	0.7863	0.0188	0.12
UOC–1301	BJ–9016–MW–0815	Gas	3834	31	0.6204	0.0024	1.5
UOC–1302	Luxfer Background	Gas	62379	1606	0.0004	0.0001	0.87
UOC–1303	Luxfer Background	Gas	60049	2034	0.0006	0.0001	0.62
UOC–1304	Luxfer +AgCo+Ag	Gas	54512	1055	0.0011	0.0001	0.64
UOC–1305	Luxfer +AgCo+Ag	Gas	60124	2337	0.0006	0.0002	0.62
UOC–1585	Luxfer Background	Gas	63056	1846	0.0004	0.0001	0.44
UOC–1586	Luxfer Background	Gas	>65000	2113	<0.0004	0.0001	<0.10

UOC–1587	Luxfer +AgCo+Ag	Gas	57112	1149	0.0008	0.0001	0.5
UOC–1588	Luxfer +AgCo+Ag	Gas	44235	1802	0.0041	0.0009	<0.10
UOC–1386	BJ–0604–DCC–0815–A	Gas	48	473	0.994	0.0585	<0.10
UOC–1387	BJ–0604–DCC–0815–B	Gas	391	383	0.9525	0.0455	<0.10
UOC–1388	BJ–0604–SC–0815	Gas	2709	105	0.7137	0.0093	0.34
UOC–1389	BJ–0604–SP–0815	Gas	4968	119	0.5388	0.008	0.27
UOC–1390	BJ–0604–MW–0815	Gas	9205	44	0.3179	0.0018	1.1
UOC–1391	BJ–0601–DCC–0815–A	Gas	286	430	0.965	0.0516	<0.10
UOC–1392	BJ–0601–DCC–0815–B	Gas	416	382	0.9495	0.0451	<0.10
UOC–1393	BJ–0601–SC–0815	Gas	1996	86	0.78	0.0084	0.44
UOC–1394	BJ–0601–SP–0815	Gas	1339	205	0.8465	0.0216	0.11
UOC–1395	BJ–0601–MW–0815	Gas	4012	34	0.6068	0.0025	1.4
UOC–1396	BJ–0534–DCC–0815–A	Gas	219	375	0.9731	0.0455	<0.10
UOC–1397	BJ–0534–DCC–0815–B	Gas	443	476	0.9463	0.0561	<0.10
UOC–1398	BJ–0534–SC–0815	Gas	2687	81	0.7157	0.0072	0.51
UOC–1399	BJ–0534–SP–0815	Gas	1671	386	0.8122	0.039	<0.10
UOC–1400	BJ–0534–MW–0815	Gas	4537	36	0.5685	0.0026	1.39
UOC–1401	BJ–0533–DCC–0815–A	Gas	176	474	0.9784	0.0577	<0.10
UOC–1402	BJ–0533–DCC–0815–B	Gas	91	397	0.9888	0.0489	1.39
UOC–1403	BJ–0533–SC–0815	Gas	787	156	0.9067	0.0176	0.19
UOC–1404	BJ–0533–SP–0815	Gas	1243	467	0.8567	0.0498	<0.10
UOC–1405	BJ–0533–MW–0815	Gas	2531	60	0.7298	0.0055	0.94
UOC–1406	BJ–9103–DCC–0815–A	Gas	3	464	0.9997	0.0577	<0.10
UOC–1407	BJ–9103–DCC–0815–B	Gas	–31	384	1.0039	0.048	<0.10
UOC–1408	BJ–9101– SC–0815	Gas	482	80	0.9418	0.0093	0.43
UOC–1409	BJ–9101– SP–0815	Gas	1459	926	0.8339	0.0961	<0.10

UOC–1410	BJ–9101– MW–0815	Gas	3984	70	0.609	0.0053	0.61
UOC–1411	BJ–0532–DCC–0815–A	Gas	415	600	0.9497	0.0709	<0.10
UOC–1412	BJ–0532–DCC–0815–B	Gas	318	379	0.9612	0.0454	<0.10
UOC–1413	BJ–0532–SC–0815	Gas	623	118	0.9254	0.0136	0.226
UOC–1414	BJ–0532–SP–0815	Gas	1241	127	0.8569	0.0135	0.21
UOC–1415	BJ–0532–MW–0815	Gas	3402	80	0.6548	0.0065	0.51
UOC–1416	BJ–0518–DCC–0815–A	Gas	175	465	0.9784	0.0566	<0.10
UOC–1417	BJ–0518–DCC–0815–B	Gas	142	378	0.9825	0.0463	<0.10
UOC–1418	BJ–0518–SC–0815	Gas	262	124	0.9679	0.0149	0.2
UOC–1419	BJ–0518–SP–0815	Gas	284	128	0.9653	0.0153	0.21
UOC–1420	BJ–0518–MW–0815	Gas	1848	78	0.7945	0.0077	0.52
UOC–1421	BJ–0531–DCC–0815–A	Gas	179	463	0.9779	0.0564	<0.10
UOC–1422	BJ–0531–DCC–0815–B	Gas	222	396	0.9728	0.0479	<0.10
UOC–1423	BJ–0531–SC–0815	Gas	–274	63	1.0347	0.0081	0.8
UOC–1424	BJ–0531–SP–0815	Gas	58	108	0.9929	0.0134	0.28
UOC–1425	BJ–0531–MW–0815	Gas	789	79	0.9065	0.009	0.45
UOC–1426	BJ–1212–DCC–0815–A	Gas	164	473	0.9798	0.0577	<0.10
UOC–1427	BJ–1212–DCC–0815–B	Gas	496	389	0.9401	0.0455	<0.10
UOC–1428	BJ–1212–SC–0815	Gas	1706	60	0.8086	0.0061	0.94
UOC–1429	BJ–1212–SP–0815	Gas	2642	134	0.7197	0.012	0.21
UOC–1430	BJ–1212–MW–0815	Gas	5477	53	0.5057	0.0033	2.1
UOC–1431	BJ–0301–DCC–0815–A	Gas	235	473	0.9711	0.0572	<0.10
UOC–1432	BJ–0301–DCC–0815–B	Gas	811	321	0.904	0.0361	<0.10
UOC–1433	BJ–0301–SC–0815	Gas	3347	85	0.6592	0.007	0.49
UOC–1434	BJ–0301–SP–0815	Gas	4146	115	0.5968	0.0085	0.32
UOC–1435	BJ–0301–MW–0815	Gas	16902	101	0.122	0.0015	1.37

Table A. 3 Radiocarbon results from USA former refinery site samples measured on the AMS.

Submitter ID	Lab ID	Material	$F^{14}C$	±	mg CO2 sample	mgCO2 LUX	total CO2	Calculated $F^{14}C$
B4–DCC–A	*UOC–1454	Gas	0.1514	0.0039	0.0959	0.4616	0.5575	0.876049426
B4–DCC–B	*UOC–1455	Gas	0.0731	0.001	**0.062**	0.4727	0.5347	**0.623947984**
B4–SP	*UOC–1457	Gas	0.1371	0.0013	0.1035	0.4368	0.5403	0.712114493
B7–DCC–A	*UOC–1458	Gas	0.22	0.002	0.1663	0.4106	0.5769	0.761088334
B7–DCC–B	*UOC–1459	Gas	0.1033	0.0011	0.0669	0.4878	0.5547	0.850312108
B7–SP	UOC–1461	Gas	0.309	0.0025	0.5693	0	0.5693	0.309
C3–DCC–A	*UOC–1462	Gas	0.39	0.0587	0.1635	0.3291	0.4926	1.173298257
C3–DCC–B	*UOC–1463	Gas	0.1568	0.0056	0.0876	0.3988	0.4864	0.866764155
C3–SC	*UOC–1464	Gas	0.2011	0.0029	0.1194	0.4195	0.5389	0.904658417
C3–SP	*UOC–1465	Gas	0.176	0.0029	0.1001	0.4009	0.501	0.877474875
D2–DCC–A	*UOC–1466	Gas	0.1688	0.0017	0.1104	0.4727	0.5831	0.887912002
D2–DCC–B	*UOC–1467	Gas	0.1236	0.0058	0.0842	0.4568	0.541	0.789540618
D2–SC	*UOC–1468	Gas	0.0231	0.0006	0.0324	0.4851	0.5175	0.356231944
D2–SP	UOC–1469	Gas	0.2052	0.0017	0.532	0	0.532	0.2052
E3–DCC–A	*UOC–1470	Gas	0.1495	0.0052	0.1221	0.383	0.5051	0.615781327
E3–DCC–B	*UOC–1471	Gas	0.103	0.0025	0.0628	0.4457	0.5085	0.827972213
E3–SC	UOC–1472	Gas	0.2447	0.0018	0.6645	0	0.6645	0.2447
E3–SP	UOC–1473	Gas	0.3146	0.0062	0.5541	0	0.5541	0.3146
E6–DCC–A	*UOC–1474	Gas	0.2103	0.0021	0.1194	0.4161	0.5355	0.940217462
E6–DCC–B	*UOC–1475	Gas	0.1018	0.0011	0.0593	0.4533	0.5126	0.873480185
E6–SC	*UOC–1476	Gas	0.1431	0.0014	0.1145	0.4168	0.5313	0.660914847
E6–SP	UOC–1477	Gas	0.5594	0.0036	0.4961	0	0.4961	0.5594
F4–DCC–A	*UOC–1478	Gas	0.2255	0.0016	0.138	0.4002	0.5382	0.876985
F4–DCC–B	*UOC–1479	Gas	0.112	0.002	0.0621	0.4492	0.5113	0.916002899
F4–SC	*UOC–1480	Gas	0.0951	0.001	0.1173	0.4823	0.5996	0.482625789
F4–SP	UOC–	Gas	0.4271	0.0026	0.5285	0	0.5285	0.4271

	1481							
F6–DCC–A	*UOC –1482	Gas	0.2469	0.0023	0.1339	0.3816	0.5155	0.948114937
F6–DCC–B	*UOC –1483	Gas	0.1186	0.0011	0.0656	0.4264	0.492	0.883975
F6–SC	UOC–1484	Gas	0.3563	0.0027	0.3657	0	0.3657	0.3563
F6–SP	*UOC –1485	Gas	0.2074	0.0015	0.1925	0.2939	0.4864	0.522750883
F7–DCC–A	UOC–1486	Gas	0.7823	0.0264	0.1477	0	0.1477	0.7823
F7–DCC–B	UOC–1487	Gas	0.9043	0.0141	0.0676	0	0.0676	0.9043
F7–SP	UOC–1489	Gas	0.7859	0.012	0.1311	0	0.1311	0.7859
I5–DCC–A	UOC–1494	Gas	0.8676	0.0198	0.1587	0	0.1587	0.8676
I5–DCC–B	UOC–1495	Gas	0.8676	0.0198	0.0649	0	0.0649	0.8676
I5–SC	UOC–1496	Gas	0.8681	0.0052	0.256	0	0.256	0.8681
I5–SP	UOC–1497	Gas	0.8906	0.0091	0.0938	0	0.0938	0.8906
J4–DCC–A	UOC–1498	Gas	0.9116	0.0097	0.1035	0	0.1035	0.9116
J4–DCC–B	UOC–1499	Gas	0.9183	0.014	0.0531	0	0.0531	0.9183
J4–SC	UOC–1500	Gas	0.6026	0.0047	0.2422	0	0.2422	0.6026
J4–SP	UOC–1501	Gas	0.5481	0.0053	0.1815	0	0.1815	0.5481
K8–DCC–A	UOC–1502	Gas	0.9277	0.0085	0.1297	0	0.1297	0.9277
K8–DCC–B	UOC–1503	Gas	0.7961	0.012	0.0759	0	0.0759	0.7961
K8–SC	UOC–1504	Gas	0.405	0.0049	0.2256	0	0.2256	0.405
K8–SP	UOC–1505	Gas	0.4105	0.0028	0.4078	0	0.4078	0.4105
L8–DCC–A	UOC–1506	Gas	0.6956	0.0127	0.1891	0	0.1891	0.6956
L8–DCC–B	UOC–1507	Gas	0.7445	0.0079	0.0869	0	0.0869	0.7445
L8–SC	UOC–1508	Gas	0.3144	0.0032	0.2926	0	0.2926	0.3144
N8–DCC–A	UOC–1510	Gas	0.9087	0.007	0.1325	0	0.1325	0.9087
N8–DCC–B	UOC–1511	Gas	0.8161	0.0097	0.0704	0	0.0704	0.8161
N8–SC	UOC–1512	Gas	0.5229	0.0062	0.1911	0	0.1911	0.5229
N8–SP	UOC–1513	Gas	0.7144	0.0129	0.0787	0	0.0787	0.7144
NP1–DCCA	UOC–1514	Gas	0.5172	0.1724	0.1628	0	0.1628	0.5172
NP1–DCC–B	UOC–1515	Gas	0.8633	0.0244	0.0628	0	0.0628	0.8633
NP1–SC	UOC–1516	Gas	0.8241	0.0208	0.0807	0	0.0807	0.8241
NP1–SP	UOC–1517	Gas	0.8745	0.0119	0.0911	0	0.0911	0.8745
NP4–DCCA	UOC–1518	Gas	0.8814	0.0245	0.0704	0	0.0704	0.8814
NP4–DCC–B	UOC–1519	Gas	0.8936	0.0213	0.0559	0	0.0559	0.8936
NP4–SC	UOC–1520	Gas	0.5728	0.0094	0.1318	0	0.1318	0.5728
NP4–SP	UOC–1521	Gas	0.9662	0.0126	0.0904	0	0.0904	0.9662

NP5–DCCA	UOC–1522	Gas	0.8662	0.0111	0.1311	0	0.1311	0.8662
NP5–DCC–B	UOC–1523	Gas	0.8279	0.0213	0.0621	0	0.0621	0.8279
NP5–SC	UOC–1524	Gas	0.8441	0.0065	0.1311	0	0.1311	0.8441
NP5–SP	UOC–1525	Gas	1.0269	0.0118	0.1001	0	0.1001	1.0269
NP6–DCCA	UOC–1526	Gas	1.0054	0.0087	0.109	0	0.109	1.0054
NP6–DCC–B	UOC–1527	Gas	0.7927	0.0852	0.0635	0	0.0635	0.7927
NP6–SC	UOC–1528	Gas	0.9098	0.0081	0.1256	0	0.1256	0.9098
NP6–SP	UOC–1529	Gas	0.9776	0.0096	0.1297	0	0.1297	0.9776
NP7–DCCA	UOC–1530	Gas	0.9351	0.0163	0.0966	0	0.0966	0.9351
NP7–DCC–B	UOC–1531	Gas	1.109	0.0158	0.0359	0	0.0359	1.109
NP7–SC	UOC–1532	Gas	0.9088	0.0119	0.0587	0	0.0587	0.9088
NP7–SP	UOC–1533	Gas	1.0607	0.0116	0.0939	0	0.0939	1.0607
Luxfer Background	UOC–1302	Gas	0.0004	0.0001				
Luxfer Background	UOC–1303	Gas	0.0006	0.0001				
Luxfer +AgCo	UOC–1304	Gas	0.0011	0.0001				
Luxfer +AgCo	UOC–1305	Gas	0.0006	0.0002				

* Samples which ^{14}C- free CO_2 (Luxfer) addition

Table A. 4 Exponential efflux data measured by LI–8100A Dynamic closed CO_2 chamber taken from Bemidji, MN August 2015

Location	Exponential Efflux Measurement(μmol $m^{-2}s^{-1}$)											Average CO_2 Efflux (μmol $m^{-2}s^{-1}$)
	1	2	3	4	5	6	7	8	9	10	11	
A79	3.37	3.35	3.42	3.42								3.39
A86	9.08	4.55	12.16	10.62								9.10
A93	7.63	6.23	8.45	9.24								7.89
B79	3.01	3.25	3.48									3.25
B86	3.71	4.25	4.91									4.29
B93	6.50	6.52	6.35									6.46
C79	2.21	4.99	2.41									3.20
C86	2.48	2.33	2.74									2.52
C93	2.25	3.83	3.68									3.25
D79	4.43	5.08	5.88									5.13
D86	3.71	3.94	3.15									3.60
D93	2.56	3.50	3.21									3.09
E79	2.18	2.41	12.05									5.55
E86	1.76	2.05	2.19									2.00
E93	6.11	7.13	6.21									6.48
E107	5.75	6.10	6.69									6.18
E114	4.18	4.18	4.73									4.36
F100	3.83	4.07	4.06									3.99
F107	3.21	3.48										3.35
O86	7.80	8.62	8.14									8.19
O93	6.29	6.29	6.22									6.27
O100	9.27	9.41	9.31									9.33
P100	6.33	5.44										5.89
Q93	3.66	7.87										5.77
Q100	4.86	4.15										4.51
R79	3.21	3.22	3.70									3.38
R93	3.18	3.28	2.77									3.08
R100	4.49	4.22	3.69	3.77								4.04
S100	2.52	2.70	2.51									2.58
T79	3.61	3.15										3.38
T86	3.41	1.66	3.33									2.80
T93	4.18	4.29	4.22									4.23
T100	3.28	3.56	3.22									3.35
U79	3.40	3.19										3.30
U86	3.75	3.70	3.71									3.72
U93	3.89	3.70	3.63									3.74
U100	2.21	2.29	2.36									2.29

V86	5.42	5.29	5.42									5.38
V100	2.86	2.88	2.91									2.88
W86	3.45	2.99	3.16									3.20
W93	3.77	3.62	3.69									3.69
W100	1.94	2.03	1.73									1.90
310	2.86	2.59	2.49	3.35	3.49	1.16						2.66
603	7.88	5.88	6.12	5.79	5.8	5.52	3.19					5.74
604	3.74	3.31	2.89	3.38	2.52	2.12	2.43					2.91
1302	5.10	5.04	5.84	5.33	4.6	5.43						5.22
9017	4.90	4.67	5.11	4.23	4.69							4.72
1212	4.26	3.69	6.01	3.96	2.93	3.48						4.06
9016	5.36	4.53	4.72	4.94	4.17	4.51						4.71
301	5.32	4.69	5.07	4.8	4.5	4.51						4.82
9015	7.99	8.04	7.77	7.24	7.82	6.3	6.58					7.39
9014	8.97	7.26	6.88	7.54	6.13	6.83	6.83	6.32	6.31	6.51	5.92	6.86
601	5.28	3.69	6.3	3.91	3.71	4.73						4.60
534	4.57	4.53	4.52	4.16								4.45
9103	3.93	2.86	2.85	2.65	2.25	2.62	2.37					2.79
533	5.67	3.76	3.67	3.64	2.87	3.38	2.74					3.68
9101	6.75	3.28	3.42	3.48	2.37	3.14						3.74
532	7.50	6.95	3.83	4.08	4.23	3.63	4.03	3.03				4.66
518	4.64	3.82	3.20	3.02	2.95	3.07	2.96					3.38
531	5.62	3.66	3.53	4.17	3.43	4.22	3.37					4.00
530	4.59	6.78	6.26	4.64	3.92	4.67						5.14
1402	6.68	4.94	4.28	5.19	4.15	4.93	3.90					4.87

Table A. 5 The exponential CO_2 efflux measured using LI–8100A at former refinery site in September 2015.

	CO_2 Efflux (umol/m^2–s)				
Location	Measurement 1 Exponential	Measurement 2 Exponential	Measurement 3 Exponential	Measurement 4 Exponential	Average CO_2 Efflux
A1	0.41				0.41
A2	2.17	1.42	2.62		2.07
A3		0.63			0.63
A4	1.85				1.85
A5	1.09	1.45	1.08		1.21
A6	0.82				0.82
A7	0.78				0.78
A8	2.16	1.88			2.02
B1		1.18			1.18
B2	2.14				2.14
B3	1.99				1.99
B4	1.22	1.07	1.12		1.14
B5	0.28				0.28
B6	0.58				0.58
B7	4.40	3.87	4.60		4.29
B8	0.94				0.94
C1	1.11		1.20	1.81	1.37
C2	0.33	0.51	1.31		0.72
C3	2.17	2.37	1.95		2.16
C4	2.04				2.04
C5	0.65				0.65
C6	1.50	2.15	2.23		1.96
C7	4.13				4.13
C8	1.49	1.41	1.24		1.38
D1	2.22	0.70	0.89		1.27
D2	2.84	3.02	2.54		2.80
D3	1.92				1.92
D4	2.02				2.02
D5	2.34				2.34
D6	5.42				5.42
D7	1.06	1.97	0.45		1.16
D8	3.90				3.90
E3	6.21	7.19	6.80		6.73
E4	18.52				18.52
E5	2.92				2.92

E6	1.96	1.98	1.92		1.95
E7	0.63				0.63
E8	1.44				1.44
F3	2.68				2.68
F4	3.05	3.24	3.46		3.25
F5	1.90				1.90
F6	2.64	2.98	3.42		3.01
F7		0.45		0.24	0.35
F8	2.60				2.60
G3	2.73				2.73
G4	0.33	0.50	0.61		0.48
G5	0.36	0.69	1.32		0.79
G6	3.92				3.92
G7	1.68				1.68
G8	0.40	1.68	0.66		0.91
H3	5.69	5.21			5.45
H4	0.57	5.93			3.25
H5	0.89				0.89
H6	3.15				3.15
H7	2.29	2.40	2.61		2.43
H8	0.26				0.26
I3	3.44				3.44
I4	0.49	0.76	0.99		0.75
I5	1.96	1.83	1.55		1.78
I6	3.02	2.38	2.67		2.69
I7	3.73				3.73
I8	0.20				0.20
I9	0.29	1.27	1.17		0.91
J4	1.73	1.64	2.01		1.79
J5	0.18	1.54	1.92	2.00	1.41
J6	1.77				1.77
J7	0.59				0.59
J8	0.54	0.39	0.34		0.42
J9	0.11				0.11
K7		0.62	1.27	0.49	0.79
K8	3.34	3.76	1.17	3.17	2.86
K9	0.85				0.85
L7	1.19				1.19
L8	3.37	3.02	4.70		3.70
L9	1.67				1.67
M7	1.15	1.62	0.73		1.17
M8	1.39				1.39
M9	0.66				0.66
N7	0.09				0.09
N8	1.02	1.65	1.40		1.36
N9	1.13				1.13
NP1	0.28	0.45	0.60		0.44
NP10	0.89				0.89
NP2	0.54				0.54
NP3	1.12				1.12
NP4	1.30	1.44	1.13	1.46	1.30
NP5	1.30	1.60	2.15		1.68
NP6	2.26	1.32	2.00	2.40	2.15

NP7		0.37	0.20	0.37	0.31
NP8	0.71				0.71
NP9	0.40				0.40
O5	0.84	1.14	0.71	0.86	0.87
O6	2.20				2.20
O7	1.11	1.87	1.36		1.45
O8	1.94				1.94
O9	0.57	0.46	0.96		0.66
P5	1.63				1.63
P6		0.54	1.40	0.39	0.78
P7	1.47				1.47
P8	0.95				0.95
P9	1.58				1.58
Q4	0.48				0.48
Q5	0.44	1.10	1.15		0.90
Q6	1.06				1.06
Q7	0.84				0.84
Q8	0.98				0.98